
Evapotranspiration and Floodplain Aquifer Storage Capacity in Yakima Tributaries



A Report for Washington State Department of Ecology Project #IAA C2200177
and the Groundwater Subcommittee of the Yakima Basin Integrated Plan

February, 2024

Lisa L. Ely, Carey A. Gazis, Lindsay Henning, Emily Polizzi, Edward Vlasenko

Department of Geological Sciences
Central Washington University



TABLE OF CONTENTS

Executive Summary	6
1. Floodplain Aquifer Storage Capacity in North Fork Teanaway River and Taneum Creek	9
INTRODUCTION	9
Teanaway River Study Site	10
Taneum Creek Study Site.....	14
Glacial History and Sedimentary Deposits	16
METHODS	17
Stratigraphy and Sediment Analysis.....	17
Piezometer Pump Tests.....	17
Floodplain Mapping.....	18
Aquifer Storage Volume Calculations.....	20
FLOODPLAIN STRATIGRAPHY AND SEDIMENT CHARACTERISTICS.....	21
Teanaway River Stratigraphy.....	22
Taneum Creek Stratigraphy	25
Relative Permeability of Stratigraphic Layers	29
Summary of Floodplain Stratigraphy	32
FLOODPLAIN GEOMORPHOLOGY AND MAPPING	32
North Fork Teanaway Floodplain Mapping.....	32
Taneum Creek Floodplain Mapping	38
CALCULATION OF FLOODPLAIN AREA	41
Effective Storage Volume of Floodplain Aquifers.....	41
CHAPTER 1 CONCLUSIONS.....	46
REFERENCES.....	47
2. Using MODFLOW to Assess Groundwater Storage in the Teanaway River Floodplain Aquifer	48
INTRODUCTION	48
Overview and Purpose	48
Site Description	49
WATER BALANCE: STEADY-STATE ANALYTICAL MODEL	52
GROUNDWATER FLOW MODEL	55
Model Domain and Initial Conditions	55
Boundary Conditions	58
Unsaturated Zone Flow.....	63
Model Calibration.....	64
Model Scenarios	66

Limitations of the Model.....	72
CHAPTER 2 CONCLUSIONS.....	73
REFERENCES.....	75
3. Evaluation of Soil Moisture and Evapotranspiration at a site on Taneum Creek, Central Washington.....	79
INTRODUCTION.....	79
Overview and Purpose.....	79
Measuring Evapotranspiration.....	80
Study Site.....	81
METHODS.....	84
Environmental Monitoring Field Methods.....	84
Calculation of Evapotranspiration using Penman-Monteith Method.....	88
Stable Isotope Sampling and Analysis.....	89
QUALITATIVE AERIAL IMAGERY ANALYSIS.....	90
SOLAR RADIATION.....	91
VARIATION IN SOIL PROPERTIES IN TANEUM STUDY AREA.....	91
EVAPORATION TRENDS.....	95
SOIL-HEAT-FLUX BASED DETERMINATIONS OF EVAPOTRANSPIRATION AND COMPARISON WITH SATELLITE-BASED ESTIMATES.....	96
STABLE ISOTOPE EVIDENCE FOR EVAPORATION AND GROUNDWATER INPUT.....	99
CHAPTER 3 CONCLUSIONS.....	100
REFERENCES.....	103
Appendix A. Composite Aerial Imagery of Taneum Creek.....	105
Appendix B. Environmental Measurements and Weather Data for Taneum Creek Study Area.....	107

LIST OF TABLES

Table 1. Study area boundaries.....	10
Table 2. LiDAR metadata.....	19
Table 3. North Fork Teanaway Watershed incised floodplain area.....	41
Table 4. Taneum Creek floodplain area.....	41
Table 5. Potential aquifer storage capacity in the North Fork Teanaway Watershed.....	42
Table 6. Potential aquifer storage capacity comparison of methods.....	43
Table 7. Potential aquifer storage capacity in the Taneum Creek Watershed.....	44
Table 8. Volumetric Amounts for the TVFF Annual Steady-State Water Balance.....	54

Table 9. Initial Flow and Storage Parameters Used in the Model	58
Table 10. Extinction Depth (cm) for a Given Soil and Land Cover Type.....	63
Table 11. Flow and Storage Parameters in the Calibrated Model.	64
Table 12. Average Increase in Water Elevation in April.....	69
Table 13. Average Monthly Leakage from the Aquifer into the Streamflow Routing Network..	71
Table 14. Yearly Steady-state Inflows and Outflows from the TVFF Site.	73
Table 15. Summary of Penman-Monteith equation input parameters	88
Table 16. Summary of Aerial Imagery Interpretations.....	90
Table 17. Calculated moisture lost from upper 20 cm of soil at Taneum sites.....	94
Table 18. Estimates of Water Budget Components for Taneum Floodplain Aquifer	101

LIST OF FIGURES

Figure 1. Upper Yakima River study area map.	10
Figure 2. North Fork Teanaway River Watershed study area.	11
Figure 3. North Fork Teanaway River Watershed 100k surface geology map.	12
Figure 4. Incised floodplain of the Teanaway River at the confluence with Indian Creek.	13
Figure 5. Taneum Creek study area map.	14
Figure 6. Taneum Creek 100k surface geology map.	15
Figure 7. Taneum Creek lower reach map.....	15
Figure 8. Glacial gray silt layer.....	16
Figure 9. North Fork Teanaway River and Dickey Creek confluence.	21
Figure 10. Correlation of stratigraphic profiles in the North Fork Teanaway watershed.....	22
Figure 11. Stratigraphy and grain-size distribution of the incised floodplain of the North Fork Teanaway at Indian Creek.	24
Figure 12. Stratigraphy and grain-size distribution from Middle Reach Taneum Creek, Site 2..	26
Figure 13. Correlation of stratigraphic profiles in the Middle Reach of Taneum Creek.....	27
Figure 14. Taneum Creek lower reach meadow transect.....	28
Figure 15. Photographs of the gray silt.....	30
Figure 16. Surface water flow over the gray silt layer at Teanaway River and Taneum Creek...	31

Figure 17. Grain-size distribution within gray silt layers	32
Figure 18. Valley cross section at confluence of North Fork Teanaway River and Indian Creek	33
Figure 19. North Fork Teanaway watershed geomorphic map.....	34
Figure 20. North Fork Teanaway watershed relative elevation model map.....	35
Figure 21. North Fork Teanaway watershed incised floodplain map from relative elevation model.....	36
Figure 22. North Fork Teanaway comparison of geomorphic and REM maps.....	37
Figure 23. Taneum Creek geomorphic map	38
Figure 24. Taneum Creek relative elevation map.....	39
Figure 25. Taneum Creek floodplain map from relative elevation model.....	39
Figure 26. Taneum Creek comparison of geomorphic and REM maps	40
Figure 27. Indian Creek piezometer data.....	45
Figure 28. General location of the Teanaway River and the research site, Teanaway Valley Family Farm (TVFF).	49
Figure 29. The Teanaway Valley Family Farm (TVFF) site along the Teanaway River.....	50
Figure 30. Precipitation, observation-well water levels, and Teanaway River stage.	51
Figure 31. Hydrologic balance equation (2) and schematic of control volume for the analytical water balance model.	53
Figure 32. The model domain with its boundary conditions.	56
Figure 33. Cross section along the line of Wells 2 through 8 at TVFF.	57
Figure 34. Schematic diagram of the river boundary condition (RIV).....	59
Figure 35. Catchments that contribute runoff to the model domain.....	61
Figure 36. Mass balance.	65
Figure 37. Modeled vs. observed head elevations	65
Figure 38. Head elevations calculated by groundwater flow model over the model time frame .	66
Figure 39. Map of model scenarios.....	67
Figure 41. Modeled discharge to the Teanaway River.	68
Figure 40. Volume of water input and output for each model scenario	68
Figure 42. Water elevation contours for different models in April and September of simulation Year 4.....	70

Figure 43. Average monthly actual evapotranspiration (AET), potential evapotranspiration (PET) and evapotranspiration (ET) for the different model scenarios over the model domain (floodplain) at TVFF.....	72
Figure 44. Taneum Creek Watershed Map.....	82
Figure 45. Taneum Creek 100-yr flood on May 15th, 2011.....	83
Figure 46. Map of environmental monitoring sites at Taneum Creek study area.....	85
Figure 47. Equipment schematic.....	85
Figure 48. Evaporation pan and precipitation gage.....	86
Figure 49. Lower Taneum Creek Isotope Sampling Sites.....	89
Figure 50. Net solar radiation measured at the Taneum Meadow site and at an AgWeather station in Thorp, WA (AgWeatherNet, 2023).....	91
Figure 51. Daily average soil temperatures at two Taneum sites and daily mean temperatures at Thorp AgWeatherNet station.....	92
Figure 52. Soil moisture measurements at two Taneum sites.....	93
Figure 53. Daily soil heat flux averages at two Taneum sites.....	95
Figure 54. Daily evaporation rates at the Taneum study area.....	95
Figure 55. Calculated ET and evaporation rates at Taneum site.....	96
Figure 57. Box and whisker plots showing distributions of ET values for OpenET and field-measurement-based estimates.....	97
Figure 58. Comparison of ET values for OpenET and two modified soil-heat-flux calculations.....	98
Figure 56. Difference in calculated ET methods vs. daily temperature.....	98
Figure 59. Oxygen isotope compositions of Taneum site water samples.....	99
Figure 60. Difference in hydrogen isotope composition between beaver ponds and Taneum Creek samples.....	100
Figure 61. Magnitude of fluxes and available storage at Taneum Creek site.....	102

Executive Summary

The Yakima Basin is home to a robust agricultural economy, essential natural resources, the Confederated Tribes of the Yakama Nation, and several municipalities that rely on the consistent quality and supply of water from the Yakima River. Climate change is predicted to bring changing precipitation patterns, which could alter the seasonal distribution of the water supply within the basin. The Yakima Basin Integrated Plan (YBIP) is taking preemptive measures to anticipate these changes and secure water resources through investments in irrigation, conservation, and water storage (YBIP, 2021). Enhancing groundwater storage during the spring high-flow season is one practical strategy to increase late-summer water supplies within the Yakima River watershed. Floodplain aquifers could store infiltrating snowmelt and diverted river water during peak spring flows and naturally release that groundwater as baseflow through the dry summer.

In recent decades, large wood (LW) restoration projects have been implemented in several Yakima River tributaries. Logging and management practices of the early 20th century stripped Upper Yakima River tributaries of large wood. Returning streams to their natural state through instream LW installations has the potential to increase floodplain groundwater storage by decreasing channel incision, increasing floodplain-channel connectivity, and raising the water table elevation. The Teanaway River and Taneum Creek watersheds contain multiple established LW projects. If these or other restoration projects function to reconnect the channel and floodplain, those sites could be candidates for future floodplain aquifer storage.

The degree to which floodplain aquifer storage from channel overbank inundation can augment summer water supplies to the Yakima River watershed depends on several factors, including 1) the connectivity of the channel and floodplain and ability of water from the channel to inundate the floodplain; 2) the capacity of the floodplain aquifer to store additional groundwater, taking into account both the stratigraphy and the preexisting groundwater; 3) the groundwater transmission rate and how it affects the duration of groundwater storage; and 4) the loss of water to evapotranspiration. These factors are addressed in this report, using examples from the North Fork Teanaway River and Taneum Creek watersheds in the upper Yakima Basin.

Chapter 1. Aquifer storage capacity and stratigraphy.

The floodplain sediment composition plays a key role in how water will be transmitted and stored in the shallow aquifer. Calculations taking into account the stratigraphy and geomorphology of the floodplain indicate a potential floodplain aquifer capacity of 1040-1990 acre-feet in the North Fork Teanaway watershed and 350-1120 acre-feet in Taneum Creek. In both cases, the minimum value in the range excludes the fine-grained stratigraphic layers that we interpreted as less effective aquifers, and the maximum value assumes a uniform stratigraphy and greater porosity. Widespread fine-grained gray silt and clay layers could impede vertical movement of groundwater or create confined aquifers within the floodplains, as indicated by pump tests, perched surface water and elevated piezometric surfaces in wells that penetrate the clay. Due to their lower permeability and transmissivity, these layers may not function effectively for seasonal groundwater recharge and storage. Details of the aquifer stratigraphy and floodplain mapping are in the M.S. thesis by Emily Polizzi (2023).

Under current conditions, Taneum Creek is more conducive to additional groundwater storage from channel overbank flow than the North Fork Teanaway River. The effective capability of the floodplain aquifer in the North Fork Teanaway watershed to store groundwater from the spring into the summer dry season is potentially limited by the presence of low-permeability stratigraphic layers, the disconnection between the elevation of the floodplain above the incised channel, and the rapid draining of the aquifer (see Chapter 2) into the incised channel. Unless the channels of the North Fork Teanaway River and its tributaries aggrade at least 2 meters, significant overbank inundation of the incised floodplain is unlikely to occur during peak spring discharges. Taneum Creek is not as deeply incised below the elevation of the floodplain in the study reaches. Large wood restoration followed by a flood in 2011 created multiple side channels connecting the creek to the floodplain. However, the stratigraphy at Taneum Creek also contains low-permeability layers that could limit the effective aquifer storage volume. Calculations of NDVI greenness indicate that in the years after the channel restoration and 2011 flood, the Taneum Creek floodplain might retain groundwater longer into the summer than before. The extent to which this groundwater augments later return flow to the channel depends partly on the amount that is lost to evapotranspiration from the increased vegetation growth (see Chapter 3). In both study areas, the height of the preexisting groundwater table during the spring could limit the additional accommodation space, depending on the timing of the recharge.

Chapter 2. Using MODFLOW to assess groundwater storage in the Teanaway River floodplain aquifer.

One possible method for enhancing groundwater storage is managed aquifer recharge (MAR). A numerical model of the Teanaway Valley Family Farm (TVFF) was created to investigate the potential for MAR on the floodplain of the Teanaway River. The approach involved modeling the effects of an infiltration pond on groundwater storage in the shallow alluvial aquifer. A groundwater flow model was created using the United States Geological Survey (USGS) numerical modeling code MODFLOW and calibrated with observed physical parameters. A theoretical pond was then added to the calibrated model to evaluate its influence on the existing groundwater regime. A steady-state water balance determination for the site was used to inform the inputs to the model and validate model results. Details of the model inputs and the model development are in the M.S. thesis by Lindsay Henning (2023).

The analytical model provides a first-order estimate of the magnitude of flows into and out of the groundwater. Precipitation is the largest inflow, roughly equal to the sum of inputs from upland runoff and flow from the Teanaway into the groundwater. The inflow from irrigation on the hay farm upgradient from TVFF is small in comparison. The largest outflow is baseflow to the river. Total annual baseflow outflow is approximately 20% greater than the annual outflow from evapotranspiration. Evapotranspiration increases with larger pond sizes, but not appreciably, as the simulated infiltration pond was designed to go dry at the end of April when potential evapotranspiration has not yet reached its annual maximum.

The MODFLOW simulations indicate that increased infiltration from a pond increases the overall volume of groundwater in the short term, but the lasting effects of additional water diminish within about two months following the drying up of the pond. The total volume increase can be directly attributed to infiltration. However, the cobble-rich alluvial aquifer transmits water out of the

floodplain efficiently, and the higher water elevations from the pond water infiltration are not maintained into the late summer months when stored groundwater is desired.

Chapter 3. Evaluation of Soil Moisture and Evapotranspiration on Taneum Creek.

Evapotranspiration (ET) is the process by which water is transferred from the land surface and vegetation to the atmosphere through the combined processes of evaporation and transpiration. A difficult water budget component to quantify, ET plays a critical role in hydrologic cycling in both agricultural and natural settings. Quantifying evapotranspiration rates is important for managing water resources, especially in regions where water availability is limited. Stream restoration efforts that reconnect a channelized river with its floodplain also increase groundwater recharge into that floodplain. These efforts often increase vegetation cover, which in turn removes water through ET. As a result, it is not certain whether the combined effects of restoration and ET will have a net positive or negative effect on the water budget components, in particular summer streamflow.

We combined several techniques to quantify evapotranspiration rates in the Taneum Creek floodplain. Our objectives were to estimate the magnitude of evapotranspiration in the water budget and assess how ET is impacted by changes from stream restoration. We set up two soil monitoring sites and an evaporation pan on lower Taneum Creek to collect physical measurements of evapotranspiration and compared those measurement-based ET estimates to satellite-based ET estimates (OpenET, 2023). Details of the evapotranspiration estimates are in the M.S. thesis by Edward Vlasenko (2023). We also analyzed stable isotopes of oxygen and hydrogen in water samples from Taneum Creek, a side channel, and beaver ponds. The stable isotope ratios of oxygen and hydrogen in waters change when they undergo evaporation and thus record the extent of evaporation from different free water surfaces in the study area.

The calculated ET based on the field measurements is nearly identical for the two monitoring sites at Taneum Creek, but is significantly higher than the ET estimate produced by OpenET (2023), which calculates daily values based on satellite data. Chapter 3 describes the possible parameters and assumptions that could lead to this difference. However, regardless of which estimate is used, the ET values, between 0.4 and 0.6 meters in uniform thickness, represent a large outflow of water from the Taneum Creek floodplain. Direct evaporation from the soil and open water sources, such as the beaver ponds, is a very small component of this loss. Stable isotope data further indicate that water residence time in the beaver ponds is short, and water passes quickly through the system. The resulting interpretation is that most of the total ET outflow must be plant transpiration of moisture derived from the floodplain aquifer.

Estimated ET over this four-month period removed a volume of water similar to or larger than the estimated volume of storage available in the shallow floodplain aquifer above the elevation of the Taneum Creek channel bed (see Chapter 2). Thus, although river restoration has many ecological benefits, it is likely that any groundwater storage gained may well be lost through increased vegetation and ET.

1. Floodplain Aquifer Storage Capacity in North Fork Teanaway River and Taneum Creek

INTRODUCTION

The Yakima Basin is home to a robust agricultural economy, essential natural resources, the Confederated Tribes of the Yakama Nation, and several municipalities that rely on the consistent quality and supply of water from the Yakima River. Climate change is predicted to bring changing precipitation patterns, which could alter the seasonal distribution of the water supply within the basin. The Yakima Basin Integrated Plan (YBIP) is taking preemptive measures to anticipate these changes and secure water resources through investments in irrigation, conservation, and water storage (YBIP, 2021). Enhancing groundwater storage during the spring high-flow season is one practical strategy to increase late-summer water supplies within the Yakima River watershed. Floodplain aquifers could store infiltrating snowmelt and diverted river water during peak spring flows and naturally release that groundwater as baseflow through the dry summer.

In recent decades, large wood (LW) restoration projects have been implemented in several Yakima River tributaries. Logging and management practices of the early 20th Century stripped Upper Yakima River tributaries of large wood. Returning streams to their natural state through instream LW installations has the potential to increase floodplain groundwater storage by decreasing channel incision, increasing floodplain-channel connectivity, and raising the water table elevation. The Teanaway River and Taneum Creek watersheds contain multiple established LW projects. If these or other restoration projects function to reconnect the channel and floodplain, those sites could be candidates for future floodplain aquifer storage.

This chapter is based on the Master's thesis research at Central Washington University by Emily Polizzi (2023). It summarizes the potential storage capacity of shallow floodplain aquifers within two Upper Yakima River tributaries: The North Fork Teanaway River and Taneum Creek (Figure 1). The project quantifies the effective storage capacity of the floodplain aquifers by considering the depth of channel incision and the stratigraphy of floodplain sediments with different degrees of permeability. These components are key in understanding the water storage potential. The Teanaway and Taneum study sites were selected as representative of the channel geomorphology and stratigraphy of headwater streams in the Yakima Basin. Both tributaries either hosted glaciers or contain sediments that are associated with nearby glacial valleys, which affect the present-day floodplain geometry and stratigraphy. Both have also undergone large wood (LW) restoration projects that could divert additional channel overflow onto the floodplains, potentially increasing infiltration into the shallow aquifers.

The study area for the North Fork Teanaway River extends from the upstream boundary of the Teanaway Community Forest to the confluence with the Middle Fork Teanaway River, including the lower portions of Jack, Indian, Middle and Dickey Creeks. The study area for Taneum Creek extends from the upstream beaver pond meadow to the confluence with the Yakima River (Table 1; Figure 1).

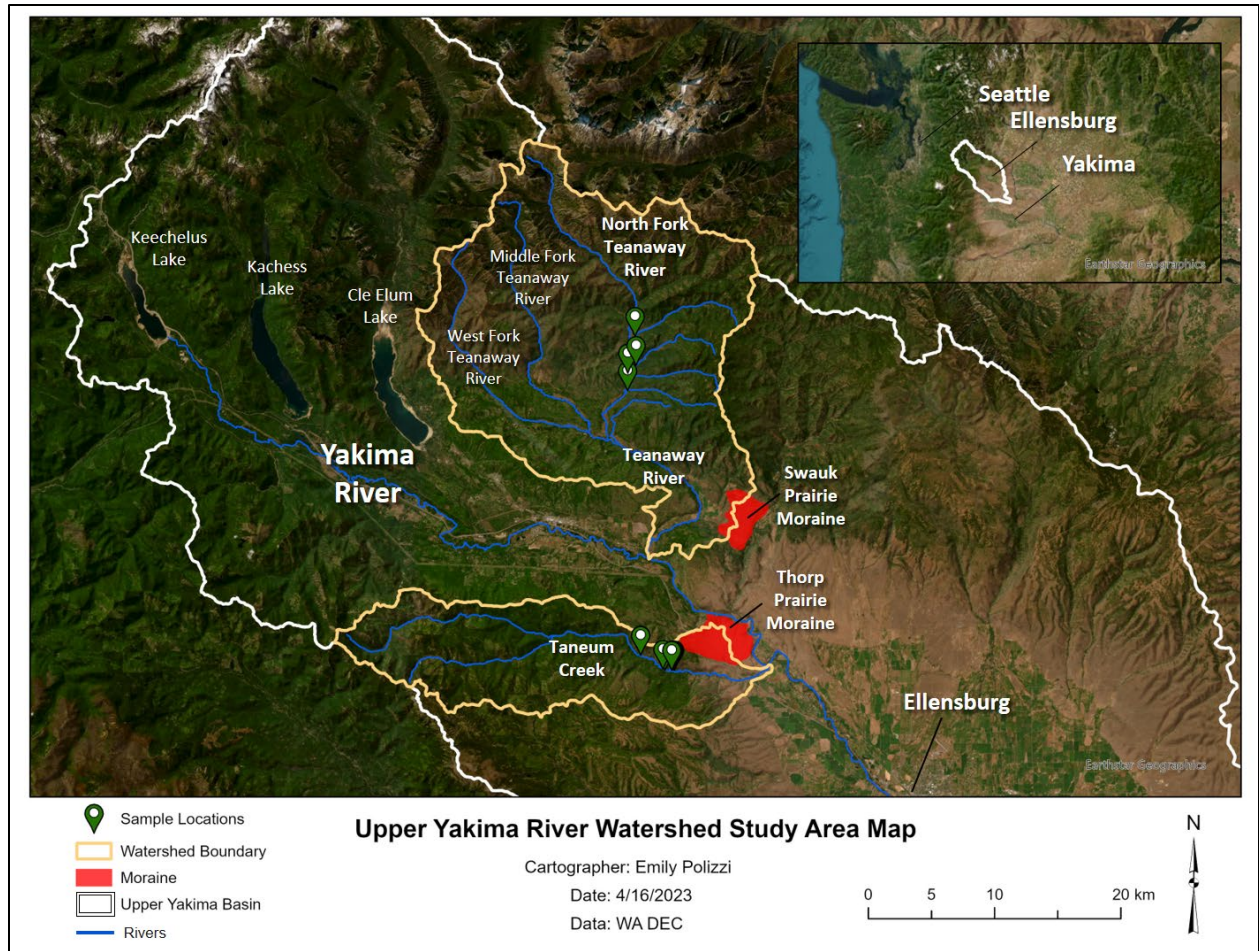


Figure 1. Upper Yakima River study area map. The two watersheds examined in this report are the Teanaway River to the north and Taneum Creek to the south. The moraines were traced using a map from Porter (1965). The proximity of the moraines to both rivers and the presence of the gray silt in both watersheds suggests a lacustrine depositional environment in the glacial past.

Table 1. Study area boundaries.

Watershed	Upstream Boundary of Study Area	Downstream Boundary of Study Area
North Fork Teanaway River	47.346°N, 120.850°W	47.252°N, 120.878°W
Taneum Creek	47.113°N, 120.876°W	47.092°N, 120.709°W

Teanaway River Study Site

The North Fork Teanaway River flows southward through the Teanaway Community Forest: 50,000 acres of land purchased by Washington State in 2013 that hosts several LW channel restoration projects. The northern boundary of the Community Forest is the upstream boundary for the study area in this project (Figure 2). It coincides with the transition from a narrow bedrock canyon confined by Teanaway Basalt into a wider valley with a broad floodplain and alluvial terraces. The valley in the study area is largely bounded by weakly indurated Roslyn Sandstone and Quaternary glacial deposits, alluvial terraces and landslides (Tabor et al., 1982; Figure the 3).

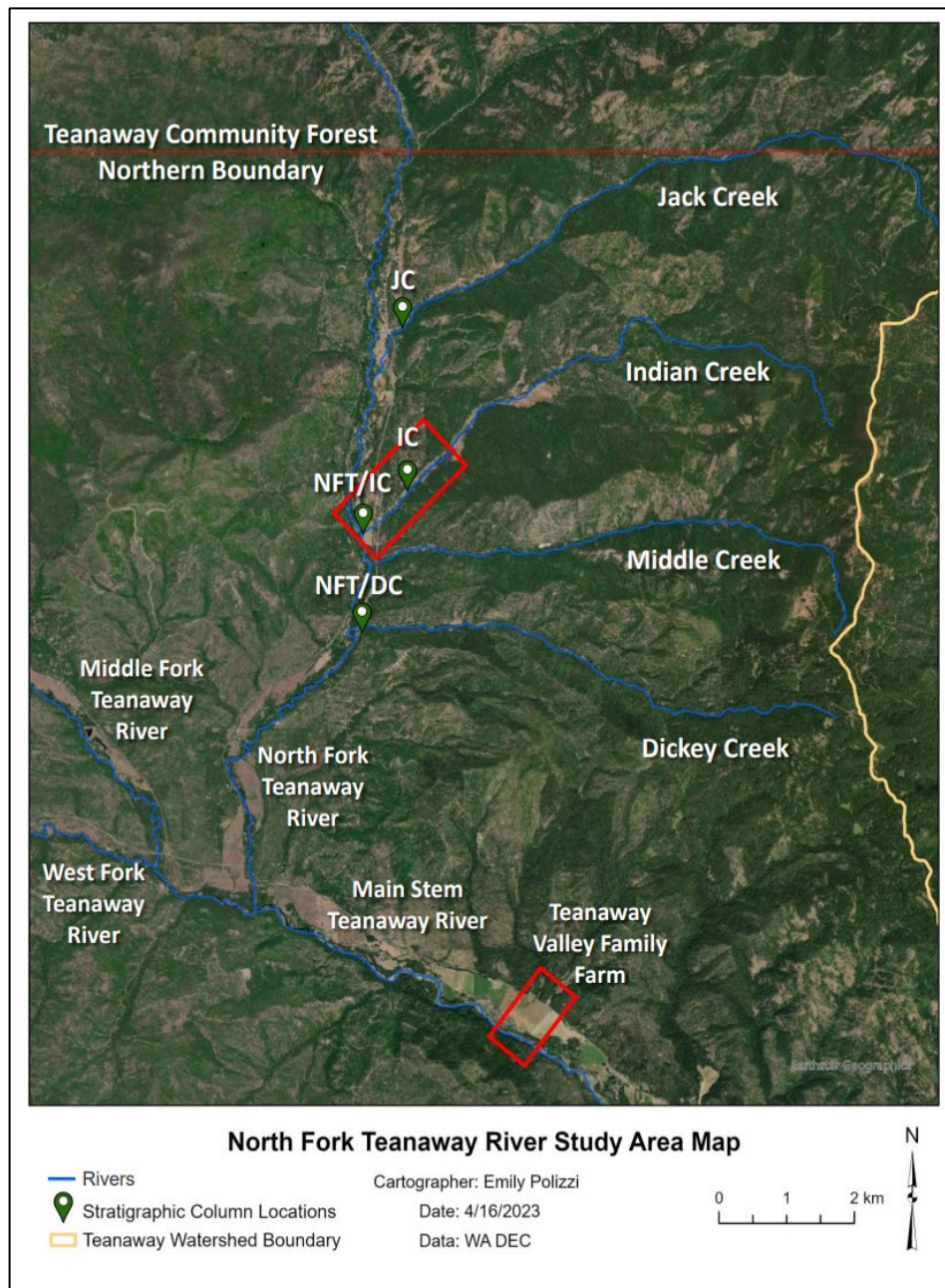


Figure 2. North Fork Teanaway River Watershed study area. Stratigraphic profile sites are denoted by the marked points and abbreviations. Tributaries and the Teanaway Valley Family Farm project site are labeled. The upstream extent of the study area is the boundary of the Teanaway Community Forest at the upper end of this map; the downstream extent is at the confluence of the North Fork and mainstem Teanaway River. JC = Jungle Creek, IC = Indian Creek, NFT = North Fork Teanaway.

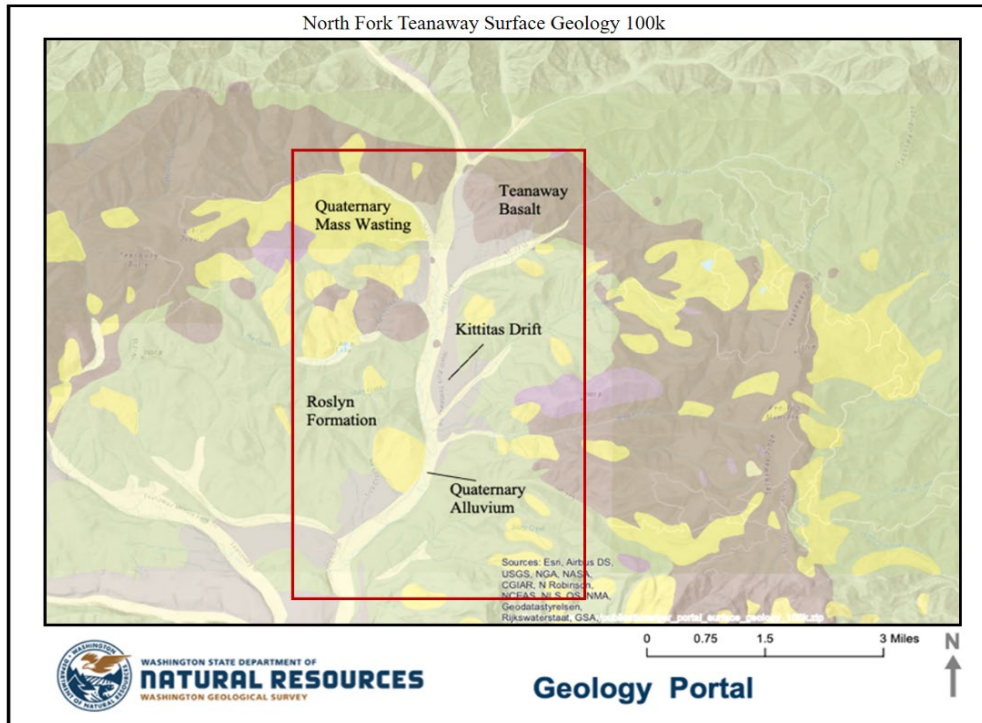


Figure 3. North Fork Teanaway River Watershed 100k surface geology map. Key geological units are annotated on the map in black; the red box denotes the study area. Areas labeled Kittitas Drift include Quaternary till, outwash, and glaciolacustrine sediments. From <https://geologyportal.dnr.wa.gov> (Tabor et al., 1982).

Previous studies in the Teanaway River watershed have addressed various aspects of floodplain storage. The removal of natural large wood, splash damming, and transport of logs down the river channel contributed to alluvial and bedrock channel incision on the Teanaway River since the late 1800s (Collins et al., 2016; Schanz et al., 2019). Dickerson-Lange and Abbe (2019) quantified the potential floodplain storage along the main branches of the Teanaway River. They considered various degrees of future channel aggradation and reconnection of the incised floodplain, which currently lies 1–3 meters above the channel (Figure 4). Their model assumes a uniform, sandy loam floodplain stratigraphy. Here we expand on their results by considering the effects of non-uniform aquifer stratigraphy and floodplain incision on the storage capacity and retention of groundwater into the dry summer months.

Two sites on the North Fork Teanaway River have been the subject of focused research on groundwater dynamics and storage. The Teanaway Valley Family Farm (TVFF) on the main stem of the Teanaway River serves as a project site to inform floodplain restoration based on hydrogeologic data from wells spanning the valley (Henning, 2023; Petralia, 2022; Chapter 2 of this report). Boylan (2019a) modeled the groundwater flow in Indian Creek based on water levels recorded in shallow monitoring wells that were installed in 2014. The model assumes a sandy aquifer of uniform depth and stratigraphy. Bartlett (2022) expanded on that model to consider how the fine and coarse sediment layers within the floodplain stratigraphy constrain and direct the groundwater



Figure 4. Incised floodplain of the Teanaway River at the confluence with Indian Creek. Bank height is ~2 m. The stratigraphy is consistent along the length of the exposed river bank here and at other locations of stratigraphic profile descriptions. The gravel bar in the active floodplain is on the inside of the bend. One of several large wood emplacements for channel restoration is visible against the incised bank. View is looking upstream.

flow in the Indian Creek floodplain. Both investigations in Indian Creek assessed the effect of a large wood (LW) channel restoration project initiated in 2016 on floodplain groundwater levels and storage. Neither detected a change in the elevation or duration of high spring groundwater levels coinciding with or in the five years following the LW installation (Boylan, 2019a; Bartlett, 2022). The projects on Indian Creek were supported by YBIP (Boylan, 2019b; Gazis and Ely, 2023).

Taneum Creek Study Site

Taneum Creek flows eastward into the Kittitas Valley (Figure 5). The valley is bounded by Columbia River Basalt and Quaternary landslide deposits (Tabor et al., 1982. Figure 6).

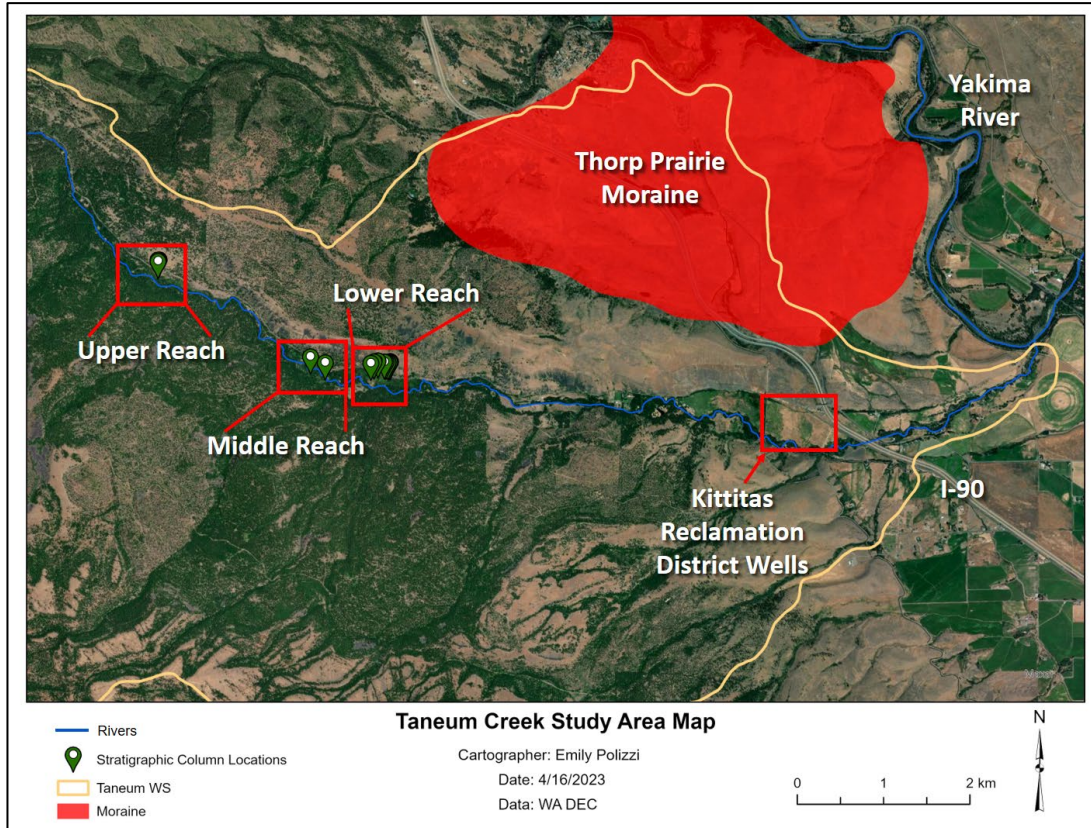


Figure 5. Taneum Creek study area map. Specific areas of interest are denoted with red boxes. Field work was conducted in the upper, middle, and lower reaches to analyze floodplain stratigraphy. The Kittitas Reclamation District is monitoring groundwater levels in response to floodplain inundation.

In 2008-2010, large wood was reintroduced to the channel throughout the study reach. In 2011, a large flood with an estimated discharge of $69 \text{ m}^3/\text{s}$ (24,000-28,000 cfs) mobilized that LW and channel sediment. As a result, Taneum Creek experienced increased channel complexity and development of side channels on the floodplain (Fixler, 2022). The construction of beaver dams on some of the side channels increased the area and duration of floodplain inundation (Figure 7). There are no monitoring wells in the Taneum Creek study site to quantify groundwater levels, but a calculation of the Normalized Difference Vegetation Index (NDVI) from satellite imagery for the years 2006-2020 indicates a significant increase in floodplain vegetation greenness in the summer of 2012, the year following the large flood (Fixler, 2022). This change could be vegetation growth response to the inundation of the floodplain the previous year. The NDVI values remained slightly higher in the years after the large flood relative to those before, which might be a response to increased connections between the Taneum Creek channel and floodplain.

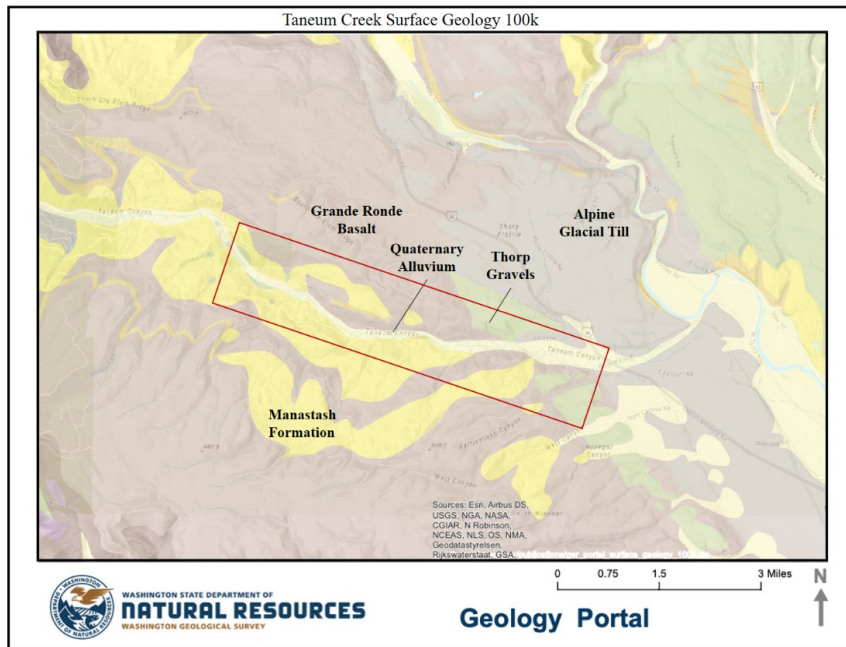


Figure 6. Taneum Creek 100k surface geology map. Key units are annotated on the map in black font, and the red box denotes the study area. From <https://geologyportal.dnr.wa.gov> (Tabor et al., 1982).

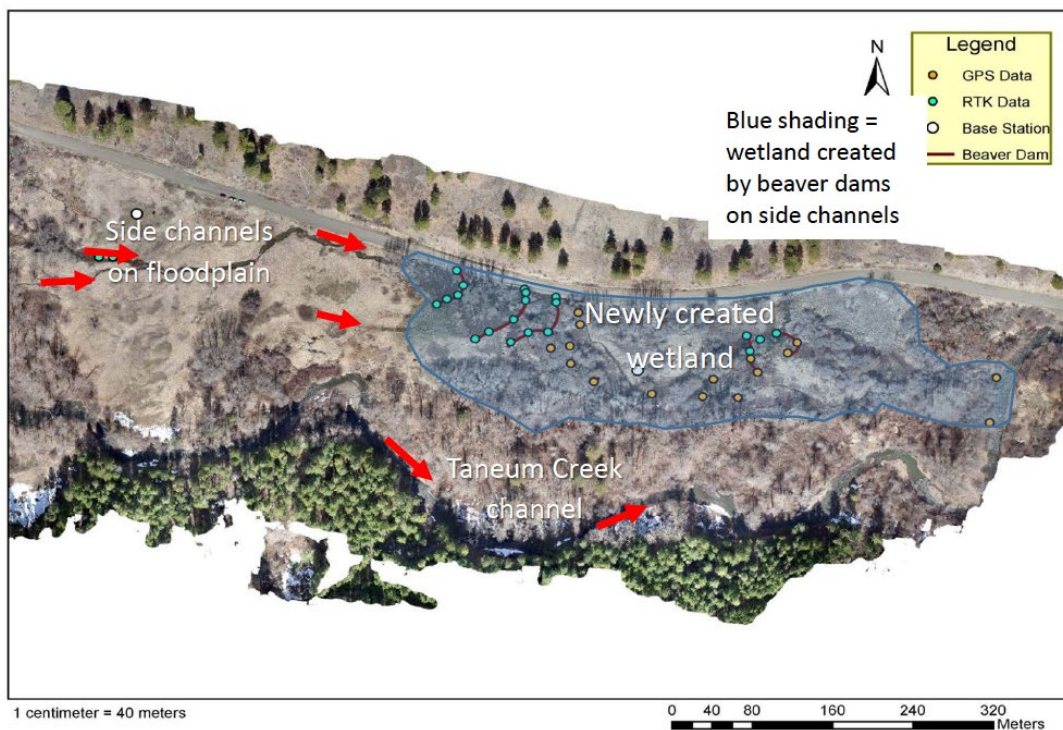


Figure 7. Taneum Creek lower reach map. This area is downstream of an in-stream large wood (LW) installation. Mobilization of the LW by the 2011 flood caused the formation of the side channels on which beavers built several dams, creating a new wetland on the floodplain.

Taneum Creek is also the site of another ongoing YBIP groundwater project, downstream of the study site for this project. The Kittitas Reclamation District (KRD) is using their canal to supply a pilot groundwater recharge/storage project through infiltration on a field at the top of the Taneum Creek fan. They are monitoring the water table response in wells installed in the corners of the field. The stratigraphy for the specific KRD project site is not analyzed here. However, the analyses in this report could be useful in the interpretations of the KRD project results.

Glacial History and Sedimentary Deposits

In addition to channel incision and isolation of the floodplain, another influence on effective groundwater storage within Yakima Basin headwaters is the widespread presence of layers of fine silt and clay within the floodplain stratigraphy (Figure 8). These layers were likely deposited in lakes dammed by glacial ice, moraines and outwash that filled the valleys in the upper Yakima Basin multiple times more than 10,000 years ago (Porter, 1976; Tabor et al., 1982; Figures 3, 5 and 6). The glacial lacustrine layers of silt and clay tend to be sticky, plastic, cohesive and less permeable to groundwater flow than the coarser fluvial deposits that typically comprise floodplains (Bartlett, 2022). A gray clay layer confines the alluvial aquifers in some locations (Petralia, 2022; Gazis and Ely, 2023). Although these distinctive glacial lacustrine deposits behave like clay in the field, the grain-size distribution is often dominated by fine silt rather than clay (Polizzi, 2023). For that reason, these glacial lacustrine deposits will be referred to as the gray silt layers in this report. The glacial gray silt layers occur in both the Teanaway and Taneum floodplains, affecting potential aquifer transmissivity and storage capacity.

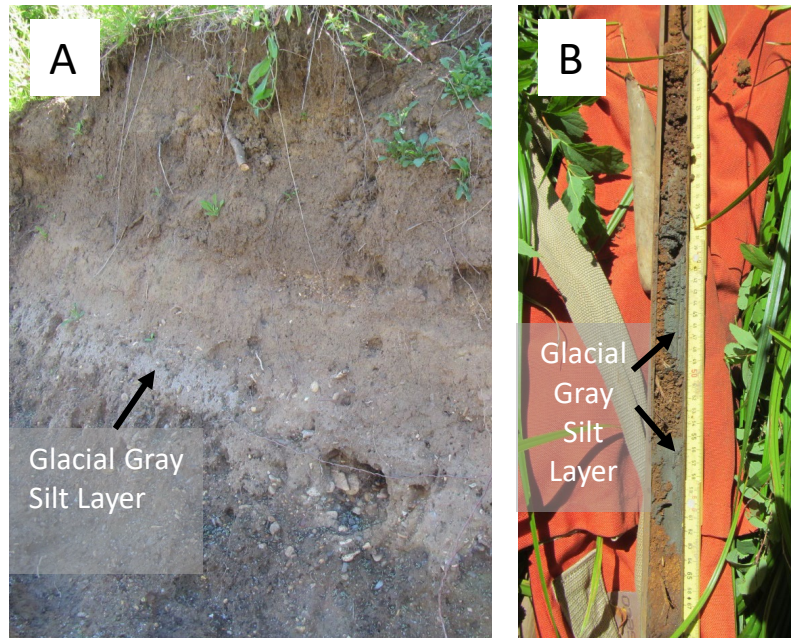


Figure 8. Glacial gray silt layer. A) Stratigraphy of the incised floodplain that forms the bank of the Teanaway River at the confluence with Dickey Creek (Figure 2). Depth of gray silt is ~100-130 cm. B) Sediment core from the floodplain of Indian Creek; depth of gray silt = 35-65 cm.

METHODS

The methods employed to determine the effective groundwater storage capacity of the North Fork Teanaway River and Taneum Creek floodplains include 1) stratigraphic and sediment descriptions, 2) piezometer tests of sediment transmissivity, 3) geomorphic mapping of the floodplain and alluvial terraces in GIS, and 4) calculation of the effective storage volume in the floodplain.

Stratigraphy and Sediment Analysis

Detailed stratigraphic descriptions were conducted in the field at representative sites along the North Fork Teanaway, Indian Creek, Dickey Creek and Taneum Creek (Figures 1, 2 and 5). Coordinates of stratigraphic profile sites were recorded using a handheld GPS unit. The selected sites displayed 2-3m of vertically incised floodplain stratigraphy that extended ~25 m upstream and downstream of the profile location (Figure 4). Additional sites at intermediate locations were examined briefly in the field to verify the lateral extent of similar stratigraphy and note presence/absence of key stratigraphic layers.

The stratigraphic profiles were divided into distinct layers in the field based on a visual and textural examination. The following characteristics of each unit were described in the field: depth, color, sediment sorting, general grain size, organic content, roots and sharpness of upper/lower contacts. Sediment layers of sand size or greater were described in the field. Sediment samples were collected from each stratigraphic unit for analysis of fine sediment grain-size distribution in the laboratory. Multiple samples were collected from units where one sample was not enough to capture the vertical diversity of the entire unit.

We measured the size distribution of sediment grains 1mm or less in diameter using a Malvern Mastersizer 3000 and Hydro LV attachment in the Murdock Research Laboratory in the Geological Sciences Department at Central Washington University. We were particularly interested in the fine silt and clay content of the floodplain sediments, which could indicate a stratigraphic layer that is less effective at transmitting groundwater. Samples were dried in the laboratory oven for 48 hours at 95°F. Once they were thoroughly dried, a mortar and pestle were used to separate the hardened clumps of sediment. The samples were run through a 1mm sieve, and the coarse fraction was weighed and set aside. A portion of the remaining fraction of the sample < 1mm in diameter was mixed in a 30ml solution of sodium hexametaphosphate (5.5g/L) to deflocculate the clay mineral grains. Each sample was shaken with a vortex mixer for 60 seconds and allowed to rest for 24 hours before a final round of shaking immediately before the Mastersizer analysis.

The resulting grain-size percentage distributions were normalized by dividing the volume percent of each grain-size class by the maximum percentage. The normalized volume percent data were then plotted against grain-size (μm) categories to display the grain-size distribution from 0.06 μm to 1 mm (clay to sand size range).

Piezometer Pump Tests

Pump tests in temporary piezometers were conducted to evaluate the transmissivity of the gray silt layer by measuring the rate at which water moved into the gray silt unit and the gravel unit

below. The pump tests were conducted in the Taneum Creek channel only, due to the absence of suitable exposures of the gray silt on the channel bottom of the Teanaway River. The piezometer was 2.5 cm in diameter and approximately 1.5 m long with a closed tip and several open holes along the sides of the lower portion. Pump tests were performed where the gray silt was the surficial unit across the channel bottom and was inundated by the water in the channel. First, a soil probe was used nearby to gage the depth of the gray silt unit in relation to the gravel. The piezometer was then pounded into the unit to an appropriate depth using a rubber mallet. To measure the transmissivity of the gray silt unit, the open holes in the sides of the piezometer were placed approximately at the middle depth of the gray silt. For the gravel below, the piezometer was pounded as deep as possible below the gray silt unit, so that the open holes were completely submerged in the gravel.

After the piezometer was inserted into the stratigraphic unit with no gaps to let in surface water, an initial water-level measurement was taken inside and outside the piezometer. A bailer was used to purge the water from inside the piezometer. As soon as the bailer was pulling clear water or no water, water-level measurements on the inside and outside of the piezometer were recorded at 0, 2, 4, 6, 10, 30, and 60 minutes.

Floodplain Mapping

ArcGIS Pro 3.0 software was used to evaluate the dimensional parameters of the floodplain and calculate potential aquifer capacities. Relative Elevation Model (REM) generation and geomorphic mapping of the active floodplain, incised floodplain, and terrace were conducted using LiDAR (Light Detection and Ranging) data from the Washington State Department of Natural Resources LiDAR portal (Table 2). Digital Terrain Models (DTMs), alternatively known as Digital Elevation Models (DEMs), were used as inputs for the analysis portion while DTM hillshades were used for visualizing purposes only.

For the geomorphic mapping, aerial imagery provided by ESRI was overlaid with the DTM hillshade layer. Maps were created at 1:3,000-foot scale for the Teanaway study area and 1:2,000-foot scale for the Taneum study area. The geomorphic units were initially distinguished based on field observations of their relative elevation above the river channel, position within the valley, stratigraphy and sediment composition, existence of side channels, and surface topography. The contiguous geomorphic units were then located and mapped on the imagery. To prevent gaps and misalignment of features in the geomorphic maps, each polygon was first roughly digitized, leaving a 30-70 foot buffer between the two features. Once finished, the Align Features tool was used to automatically build one polygon onto the border of the other. This step ensured there were no gaps between polygon features and that adjacent polygons shared a border. Once all polygons were digitized, the area of each polygon was calculated using the Calculate Geometry tool in the attribute table and manually summed to calculate the total area of each geomorphic map unit.

Table 2. LiDAR metadata. The metadata for LiDAR files used in GIS Analysis and Visualization. All files are from the Washington State Department of Natural Resources LiDAR Portal.

WA DNR LiDAR File Names	Resolution	DTM Hillshade	DTM	Geotiff File Numbers	Imagery Location
Teanaway 2015	1.5 feet	X	X	7, 8	North Fork Teanaway Watershed
Teanaway Bathy 2015	1.5 feet	X		7, 8	North Fork Teanaway Watershed
Kittitas FEMA 2011	1.5 feet	X	X	11	Lower Taneum Creek
Yakima Basin 2018	1.5 feet	X	X	85, 86, 87	Taneum Creek Canyon

The valley bottom of the North Fork Teanaway River and its tributaries were divided into three geomorphic map units: Alluvial river terraces, incised floodplain, and active floodplain. The alluvial river terraces represent former Teanaway River deposits that are no longer inundated by the river, and they served as an outer boundary for the digitization of the floodplain. The incised floodplain is of intermediate elevation, 1-3 meters above the modern Teanaway River channel (Bartlett, 2022; Collins et al., 2016; Dickerson-Lange and Abbe, 2019; Schanz et al., 2019). The incised floodplain consists largely of overbank silt and fine sand; the glacial gray silt is exposed in the lower portion of the stratigraphy in many places (Figure 8). As mentioned in the introduction to this chapter, much of the incision into this geomorphic unit occurred in historic times (Collins et al., 2016; Schanz et al., 2019). The active floodplain is the lowest in elevation immediately adjacent to the channel and is largely composed of river gravel.

Taneum Creek is not as deeply incised as the North Fork Teanaway River, and therefore was divided into only two geomorphic units: alluvial river terraces and floodplain. The lower reach of Taneum Creek contains infrastructure such as roads and buildings. The interstate highway was not included in the calculated floodplain area because it is a large impervious surface that would not allow water infiltration and storage. Farther upstream, the floodplain is dissected with side channels, which required digitization of more separate polygons than in the Teanaway study area.

As an alternative to the geomorphic mapping method, a relative elevation model (REM) of valley surfaces above the adjacent channel was also created. The REM allowed a comparison of the final results with those of Dickerson-Lange and Abbe (2019) for the Teanaway study area. This method allowed for a finer resolution of the area designated as floodplain but lost the context gained with the geomorphic mapping method. REM generation methods from Olson et al. (2014) and Dilts et al. (2010) were adopted to create REMs for the North Fork Teanaway River, Dickey, Middle, Indian, Jack, and Taneum Creeks.

The first step in creating a REM required digitizing the channel thalweg. The North Fork Teanaway, Jack Creek, and Indian Creek bathymetric data collected in 2015 was used as a hillshade layer to more accurately digitize the channel bed. Instructions for creating the REM are in an

appendix to Polizzi (2023). To extract an area value from the REM, the layer was transformed from raster to vector. This involved making the numeric values integers, using the raster to polygon tool, turning the integer values back to decimals, then selecting elevation data that represented floodplain elevations likely to be inundated based on the height above the digitized channel.

REMs are inherently skewed at the upstream and downstream ends, which introduced a source of error to consider in the accuracy of the final area value. The final polygon product of the REM method was more like a fishnet than a traditional vector polygon. The data could not be manipulated or manually edited to exclude artifacts like the skewed floodplain where the tributaries meet the North Fork Teanaway valley. Similarly, because the study area of Taneum Creek is composed of several different DEM files, some of the floodplain was cut off in the REM. Joining these DEMs caused an offset of the relative elevation values at the upstream and downstream ends where two REMs meet.

Aquifer Storage Volume Calculations

The mapped areas, depths from stratigraphic profiles, and grain size interpretations were used to calculate the aquifer storage capacities based on the various scenarios of the ability of the stratigraphic layers within each geomorphic unit on the floodplain to store and transmit water. The formula used to calculate the volume was $\text{Volume} = \text{Area} * \text{Height} * \text{Porosity}$. The area was calculated based on the geomorphic mapping and the REM. Height represents the height of the geomorphic unit above the channel bottom, or if it is subdivided into multiple stratigraphic layers, the thickness of the relevant stratigraphic layers under consideration. A rectangular volume calculation was used to represent the assumed flat floor of a u-shaped glacial valley, rather than a V-shaped valley floor. The depths for this calculation were specifically chosen for each individual tributary based on the incision observed in the field and the elevation range chosen during the REM-derived floodplain process. The porosity values were derived from Bartlett (2022) and Dickerson-Lange and Abbe (2019).

Three depths were chosen to simulate different inundation possibilities. The active floodplain volume only accounts for the area of the lowest-elevation, active floodplain on the North Fork Teanaway River. The height chosen for this calculation was 3 feet, as this is well below the incised floodplain but high enough to inundate the boulder bars. This is the same value used by Dickerson-Lange and Abbe (2019) in their minimum volume calculation. The minimum and maximum aquifer volume calculations for the incised floodplain geomorphic unit were based on the stratigraphy at each tributary considering the silt-dominated layers. The minimum volume excluded the less permeable, silt-dominated layers that were interpreted as less likely to readily store and transmit groundwater, while the maximum volume includes the entire stratigraphic profile from the incised floodplain surface to the channel bed. All data collected in the field and lab were recorded using the metric system. For consistency with GIS and the use of results by watershed management in the United States, the remainder of the project was completed using the imperial system.

FLOODPLAIN STRATIGRAPHY AND SEDIMENT CHARACTERISTICS

The floodplain sediment composition plays a key role in how water will be transmitted and stored in the floodplain aquifer (Figure 9). Here we consider the potential role of the floodplain stratigraphy for the recharge, transmission and retention of groundwater in the shallow floodplain aquifers in the two Yakima headwater tributary study areas. A range of possible storage capacity estimates were



Figure 9. North Fork Teanaway River and Dickey Creek confluence. This site has a well-exposed riverbank where the floodplain is incised, revealing the stratigraphy. The gray silt unit forms an erosion-resistant layer on the edge of the channel at the base of the bank. The inset shows a close-up photograph of the mixed-sediment layer containing nodules of gray silt that overlies the massive gray silt layer. The lower photographs are views of the incised floodplain upstream and downstream from the profile in the upper photograph. The red lines bound the laterally continuous stratigraphy of the incised floodplain.

calculated based on the stratigraphy at individual locations in the watershed and the interpretation of the permeability, thickness and lateral extent of the different stratigraphic units. A particularly important factor in the hydrogeology of the formerly glaciated headwater tributaries of the Yakima Basin is the presence of the relatively low-permeability, gray silt layer deposited in lakes that were dammed by glacial ice or moraines during past glacial periods (Porter, 1976; Tabor et al., 1982). This massive gray silt layer and the layers where it has mixed with overlying sediment (Figure 9) could limit the available volume of the floodplain as an effective aquifer.

Teanaway River Stratigraphy

The general stratigraphy is consistent across the incised floodplain of the North Fork Teanaway River and its tributaries (Figure 10). Sites along the North Fork Teanaway River at Dickey Creek (Figure 9) and Indian Creek (Figure 11) provide examples of the major stratigraphic zones found within the study area. Generally, with depth in the profile, the upper units (Zones 1 and 2) became sandier with less clay.

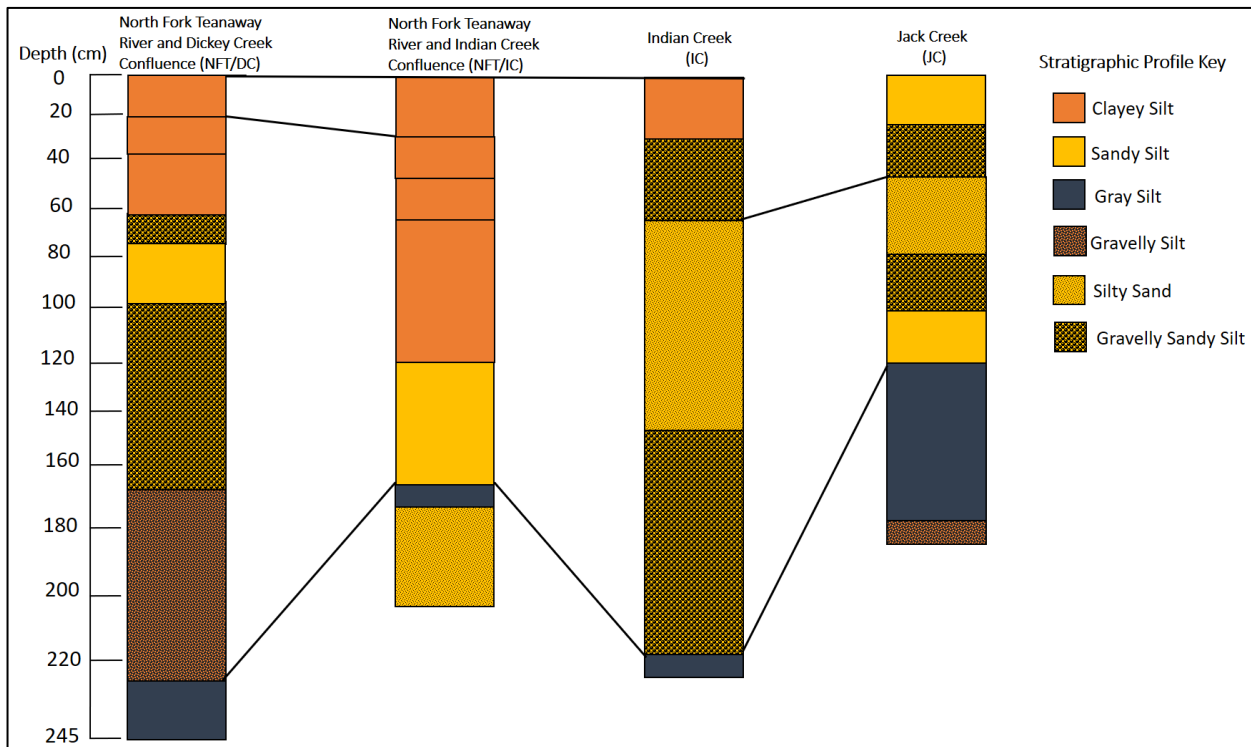


Figure 10. Correlation of stratigraphic profiles in the North Fork Teanaway watershed. The profiles display the similar stratigraphy observed throughout the incised floodplain, including the distinctive gray silt layer. See Figure 2 for profile locations.

Stratigraphic zones of Teanaway River and tributary floodplains:

Zone 1: Silt with high clay content and low sand content. In some locations, nodules of the massive gray silt (Zone 3) are mixed with the coarser, reddish silt and sand in the lower portion of this zone (Figure 9). These nodules appear to be ripped up from the underlying gray silt layer. The mixed silty sediment probably has a lower transmissivity than sandier layers in the stratigraphy and might not be as effective for groundwater storage and flow.

Zone 2: Silty sand. This zone represents layers of coarser sediment, ranging up to sand and gravel. In some locations, these sandy layers directly overlie the gray silt in Zone 3, and in locations they are interbedded with the overlying silt layers. The coarser-grained layers probably have a relatively high transmissivity and represent an effective portion of the floodplain aquifer for groundwater storage and flow.

Zone 3: Massive, fine-grained gray silt. The gray silt layer occurs at depths of 1.2-2.2 m below the surface and ranges from 10-60 cm thick along the channel banks. This layer is sticky, plastic and cohesive in hand samples. Field tests and observations indicate that it is largely impermeable to groundwater flow. A correlative glacial clay deposit ranges up to 4 m thick in the well logs at the Teanaway Valley Family Farm and forms a confining layer for the underlying aquifer (Gazis and Ely, 2023; Petralia, 2022.)

Zone 4: Silty sand and gravel; fluvial deposits. This zone probably has a high transmissivity. However, aggrading the channel to reduce incision would not have a significant effect on the groundwater storage in this zone, because it is generally at or just below the current elevation of the Teanaway River and tributary channels.

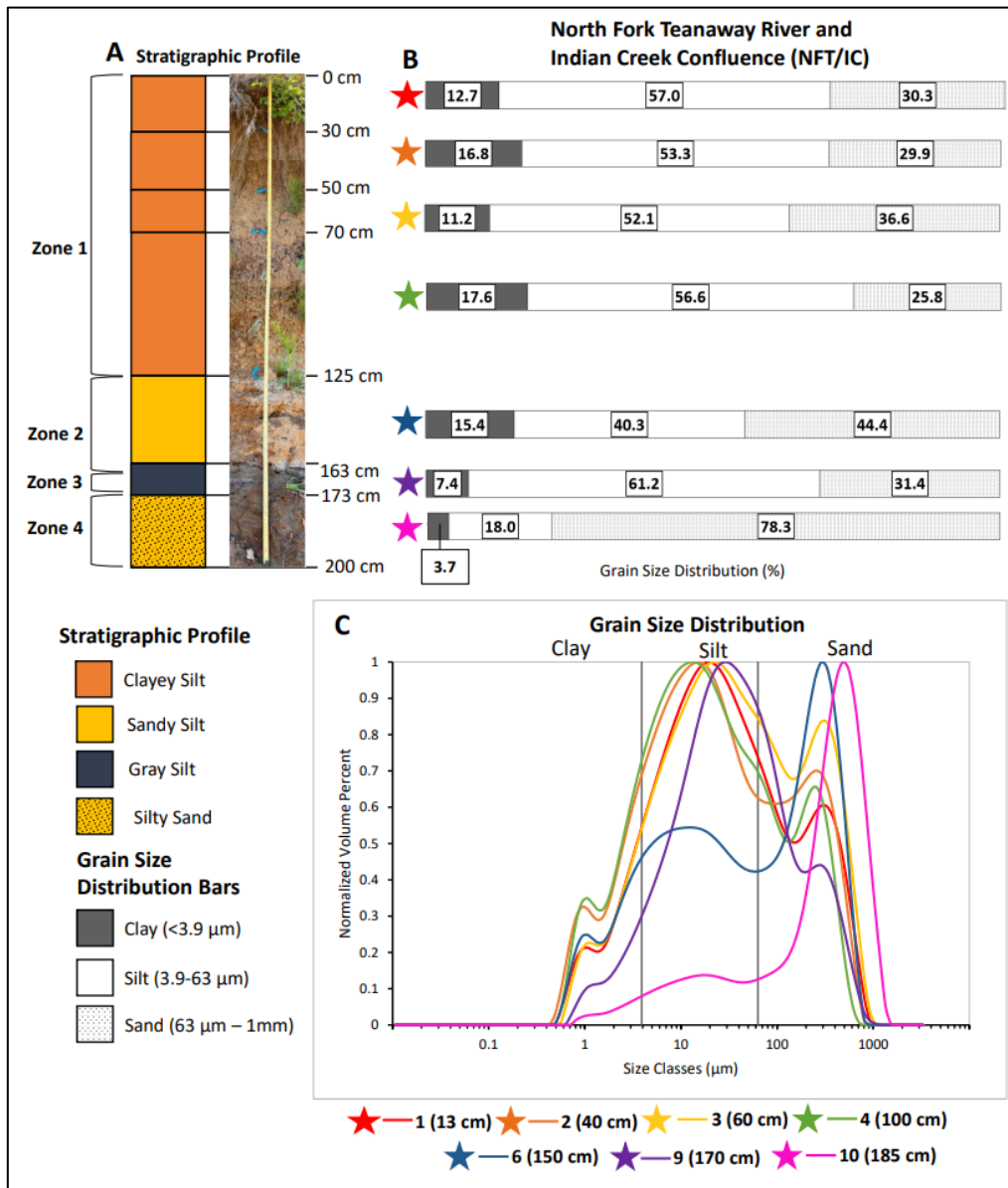


Figure 11. Stratigraphy and grain-size distribution of the incised floodplain of the North Fork Teanaway at Indian Creek. A) Stratigraphic profile displaying the stratigraphic units observed in the field, grouped into laterally consistent zones with similar properties. B) Grain-size distribution graphs with colored stars indicating the corresponding grain-size distribution curve shown in (C). C) Grain-size distribution curve with samples plotted in corresponding colors. The first number is the sample number and the second is the depth where the sample was collected. The peak in the volume percent from 0.5-1.5 μm is an artificial artifact of the Mastersizer instrument and not a characteristic of the sediment samples.

Taneum Creek Stratigraphy

The stratigraphy and grain-size distributions at Taneum Creek are remarkably similar to those in the Teanaway River study area (Figures 12 and 13). The Taneum Creek floodplain contains a sandy layer on much of the surface that is absent from the Teanaway profiles (Zone 1), resulting in a maximum of five general stratigraphic zones compared to four in the Teanaway. The gray silt layer is identified as Zone 4 in Taneum Creek (Figure 12). The stratigraphic zones are generally consistent throughout the study area, although not all five are present at every site. A transect across the lower reach showed that the floodplain sediment closest to the beaver pond were dominated by silt, while those farther upstream were predominantly sand (Figure 14).

Stratigraphic zones of Taneum Creek:

Zone 1: Sand with low silt and clay content. This zone is most likely fluvial overbank sediment, some of which is possibly from the large flood in 2011. This coarse sandy zone at the surface is absent from the Teanaway sites.

Zone 2: Silt with moderate clay and sand content. This zone is similar to Zone 1 in the Teanaway sites but with lower amounts of sand and clay. It does not contain nodules of massive gray silt.

Zone 3: Silty sand. This zone represents layers of coarser sediment, ranging up to sand and gravel. In some locations, these sandy layers directly overlie the gray silt in Zone 3, and in locations they are interbedded with silt layers. The coarser-grained layers probably have a relatively high transmissivity and represent an effective portion of the floodplain aquifer for groundwater storage and flow.

Zone 4: Massive, fine-grained gray silt. This glacial, gray silt deposit is very similar to the correlative unit in the Teanaway sites (Zone 3). It is sticky, plastic and cohesive in hand samples. In general, the gray silt layer in Taneum Creek contains higher clay and silt and lower sand content than the correlative unit in the Teanaway.

Zone 5: Gravelly silt and sand; fluvial deposits. This zone probably has a high transmissivity.

Overall, the floodplain stratigraphic profiles at Taneum Creek were more variable in composition, less incised, and more heavily vegetated than in the NFT watershed. This could possibly be due to more connectivity between the channel and floodplain than in the NFT watershed. The samples with the highest percentage of sand were in seasonally dry side channels.

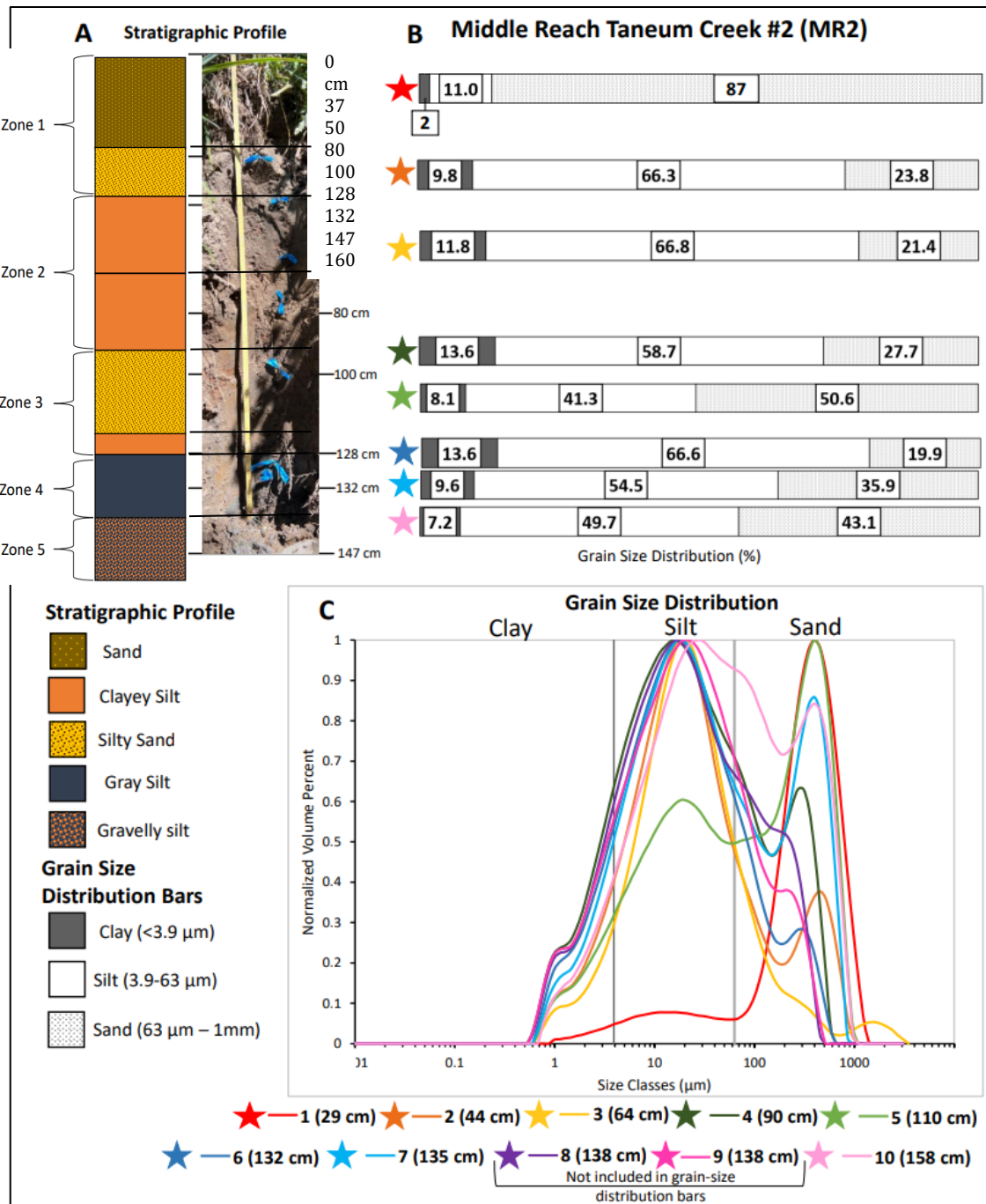


Figure 12. Stratigraphy and grain-size distribution from Middle Reach Taneum Creek, Site 2. A) Stratigraphic profile displaying the stratigraphic units observed in the field, grouped into laterally consistent zones with similar properties. B) Grain-size distribution graphs with colored stars indicating the corresponding grain-size distribution curve shown in (C). C) Grain-size distribution curve with samples plotted in corresponding colors. The peak in the volume percent from 0.5-1.5 μm is an artificial artifact of the Mastersizer instrument and not a characteristic of the sediment samples.

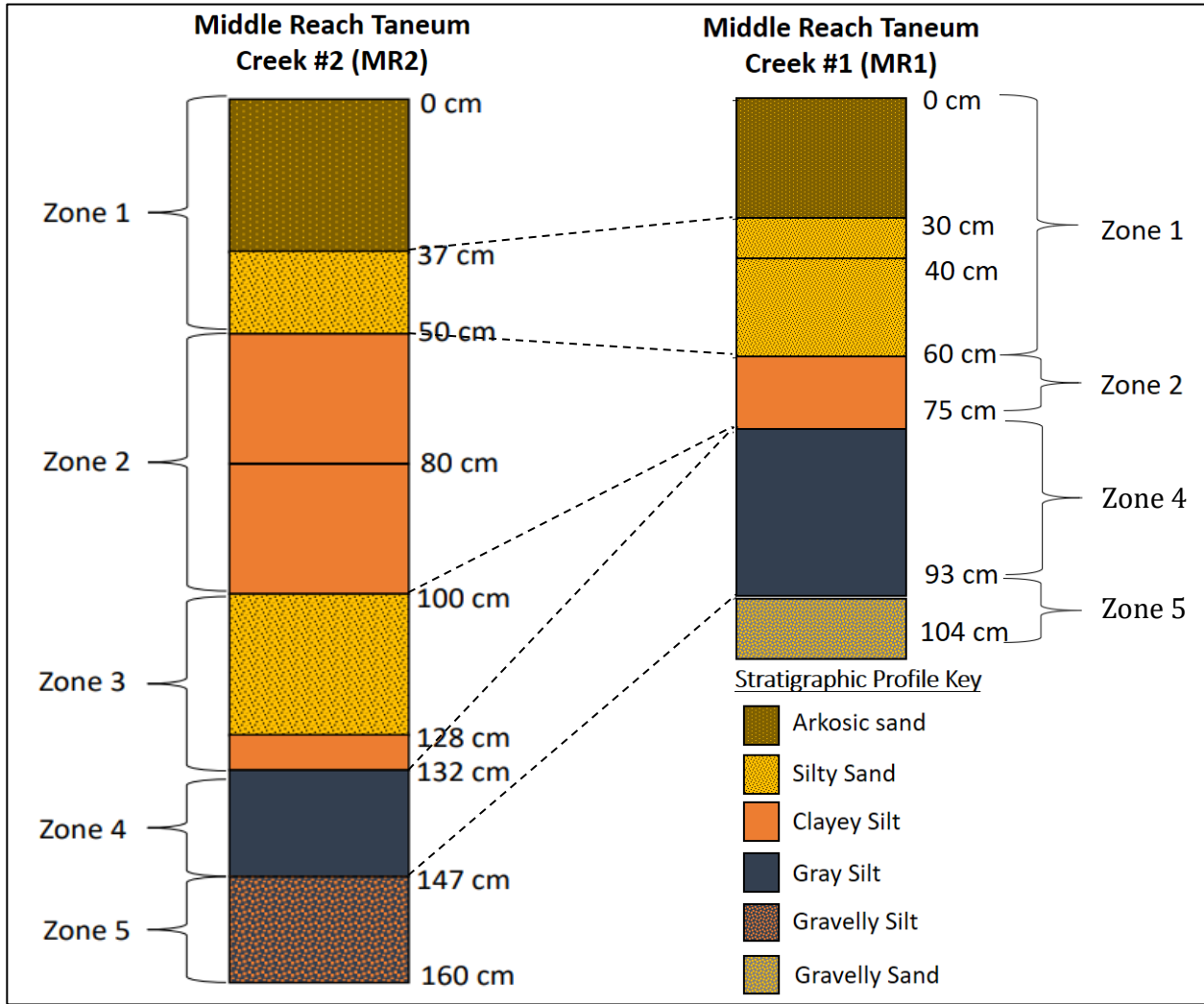


Figure 13. Correlation of stratigraphic profiles in the Middle Reach of Taneum Creek. See Figure 5 for profile locations.

The lower reach of Taneum Creek provided an opportunity to evaluate the grain-size distribution variability across the floodplain by comparing sediment in the beaver pond and dry meadow (Figure 14). The silt sediment samples from the beaver pond are finer grained than those farther into the dry meadow. The fine silt layer promotes the retention of the surface water in the pond. While the pond shrinks in the later summer, it does not go completely dry.

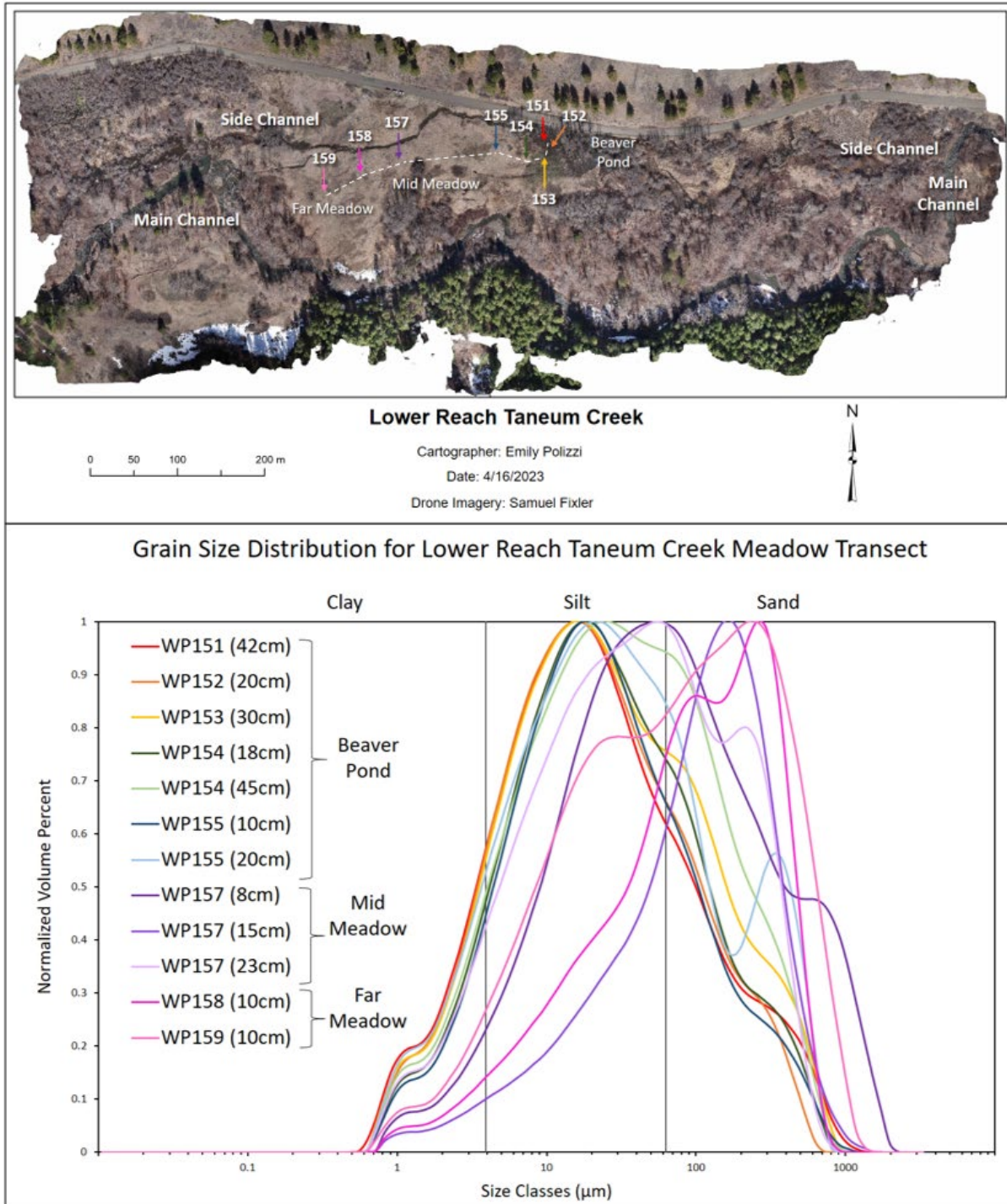


Figure 14. Taneum Creek lower reach meadow transect. The aerial imagery shows sample locations marked with a waypoint number and colored arrow along a floodplain transect (white dashed line). The graph below depicts the grain-size distribution of samples taken at each location, using colors consistent with those marking the sites on the map. Samples closest to the beaver pond (151-155) contain more silt, while samples farther from the pond (157-159) contain more sand.

Relative Permeability of Stratigraphic Layers

Contrary to the field observations, the laboratory grain-size distributions indicated a relatively low percentage of clay in the gray silt layer in both the Teanaway and Taneum Creek study areas (Zone 3, Figure 11; Zone 4 Figure 12). However, the gray silt layer behaved like clay in the field (Figures 8 and 9). It was sticky and cohesive in hand sample (Figure 15) and formed erosion-resistant benches in the channel bottom and banks (Figure 9). At Indian and Dickey Creeks, surface water flows on top of the less permeable, more resistant gray silt layer and forms small waterfalls where it spills over the edge at eroded nickpoints (Figure 16). The glacial gray silt layer creates an impermeable boundary that confines the lower aquifer at the Teanaway Valley Family Farm site, demonstrated by the elevated piezometric surface in the wells that penetrate below it (Gazis and Ely, 2023; Petralia, 2022). The inconsistency between the field observations and the sediment grain sizes measured in the laboratory could be due to the high percentage of very fine silt in this layer (Figure 17), which might cause it to behave like a sticky, cohesive clay. Another possibility is that the laboratory measurements of grain size with the Mastersizer overestimated the diameter of the clay particles if the clay was not completely deflocculated in pre-treatment, or the platy shape of the clay minerals caused the laser to overestimate the diameter as a uniform silt size. Regardless of the laboratory measurements of grain size, our interpretation is that the sediment in the gray silt layer is behaving like clay in terms of the influence on the hydrogeology of the floodplain.

The gray silt layer in the Teanaway contained more clay and less sand farther downstream in the watershed (Figure 17). The grain-size distribution within the gray silt from Taneum Creek was similar throughout the watershed. The Taneum samples contained more clay and silt and less sand than the correlative gray silt in the Teanaway watershed (Figure 18). This difference in grain-size distribution between watersheds could cause a difference in the hydrological properties of the unit with implications for groundwater storage and flow.

Pump tests on four temporary piezometers inserted into the gray silt and underlying silty sand or gravel layer in the channel bed of Taneum Creek indicate that the gray silt layer impedes or confines groundwater flow. At three sites, the water level inside piezometers screened in the gray silt layer remained below the water level in the stream 60 minutes after pumping; at the fourth location water levels eventually reached equilibrium in the gray silt after 60 minutes. Piezometers screened in the sand and gravel layer below the gray silt exhibited upwelling. Our interpretation is that the less permeable gray silt is impeding vertical water flow, hence the upwelling from the underlying sand and gravel layer. It is likely to play a similar role in the groundwater flow through the adjacent floodplain stratigraphy.

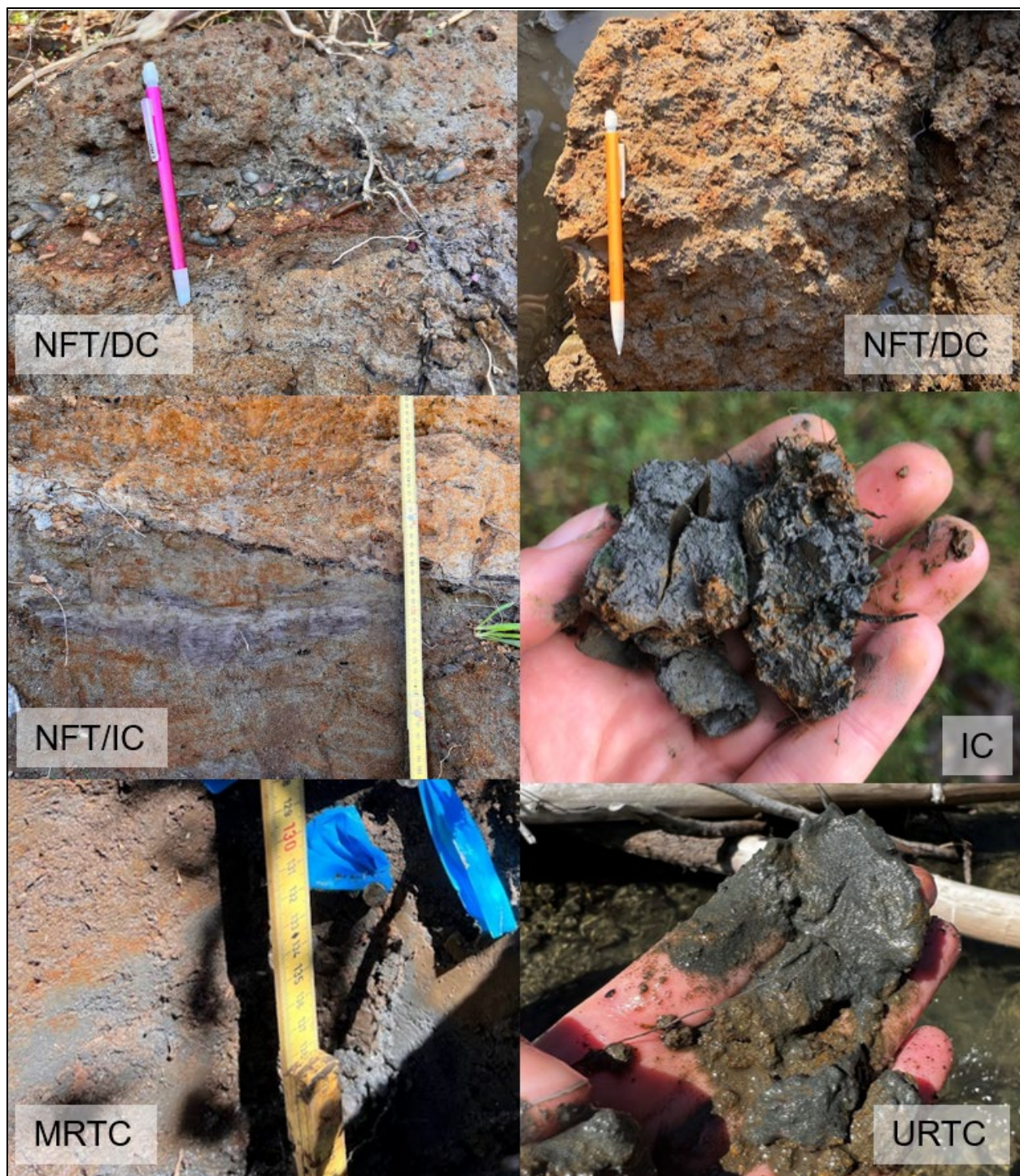


Figure 15. Photographs of the gray silt. Photographs were taken at each stratigraphic profile in the North Fork Teanaway Watershed (NFT) and Taneum Creek (TC). The gray silt is consistently sticky and plastic. It varies spatially in grain-size distribution, mottling, and degree of mixing with surrounding units.

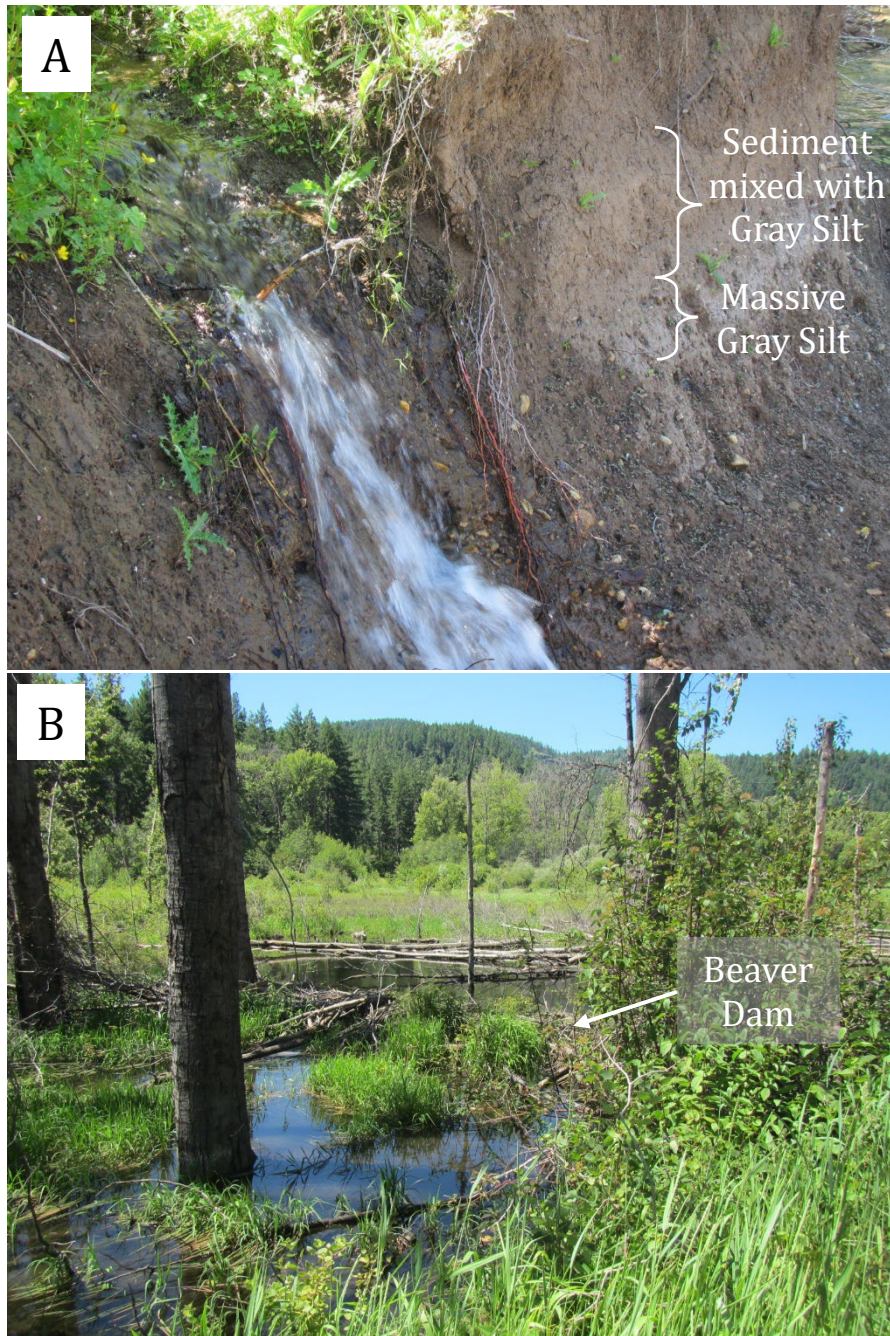


Figure 16. Surface water flow over the gray silt layer at Teanaway River and Taneum Creek. A) Side channel of Dickey Creek flows across the top of the erosion-resistant bench formed by the gray silt layer and overlying cohesive sediment layer containing nodules of gray silt. B) Beaver ponds on Taneum Creek floodplain tend to occur in areas of finer-grained sediment. In both cases, the fine-grained silt and clay layers are slowing or impeding the vertical infiltration of surface water.

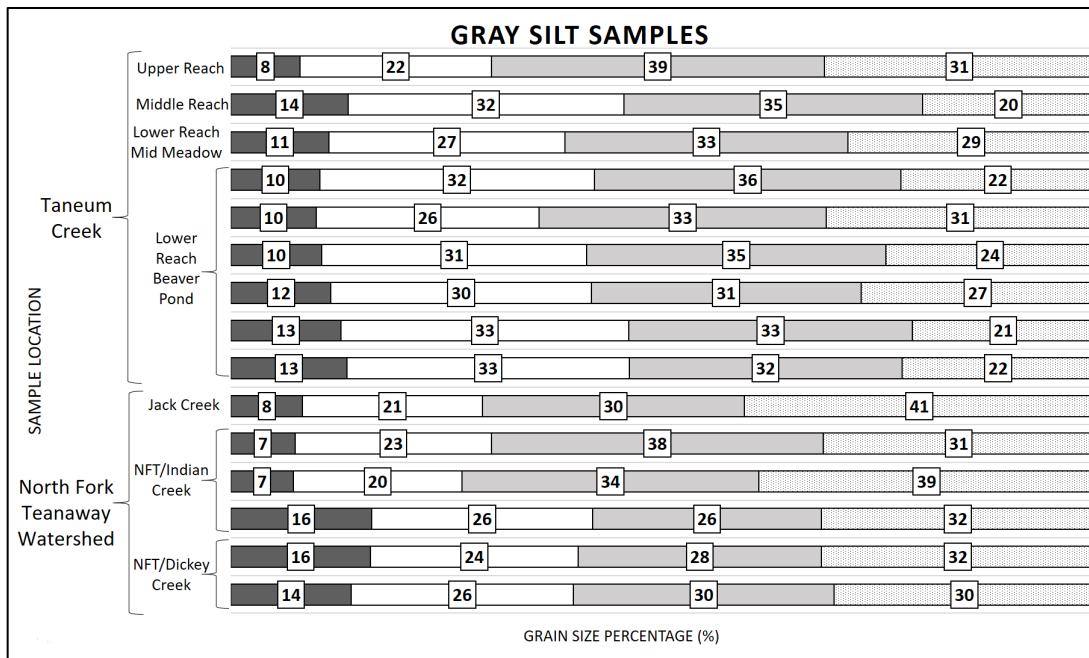


Figure 17. Grain-size distribution within gray silt layers. Grain-size distribution graph for all samples taken from the gray silt units across the Taneum and North Fork Teanaway watersheds. From left to right on the chart, grain sizes are as follows: clay (<3.9 μm), very fine to fine silt (3.9 - 15.6 μm), medium to coarse silt (15.6 - 63 μm), and sand (63 μm – 1 mm). Taneum Creek samples contain more silt and less sand; Teanaway samples contain more sand and variable clay content.

Summary of Floodplain Stratigraphy

In summary, the floodplain stratigraphy of these two headwater tributaries of the Yakima Basin is heterogeneous. The laterally continuous fine-grained silt and clay layers could impede vertical movement of groundwater or even create confined aquifers. The interbedded coarse and fine stratigraphic zones influence the transmission of groundwater through the floodplain, causing preferential horizontal flow through the coarser sand and gravel layers. Due to their lower permeability and transmissivity, the fine-grained silt and clay layers, particularly those containing the glacial gray silt, may not function effectively for seasonal groundwater recharge and storage.

FLOODPLAIN GEOMORPHOLOGY AND MAPPING

North Fork Teanaway Floodplain Mapping

The valley floor of the North Fork Teanaway River and its tributaries were mapped using two methods: mapping geomorphic landforms and creating a relative elevation model (REM). The valley was divided into four major geomorphic units: river channel, active floodplain, incised floodplain, and abandoned river terrace (Figure 18). These units were identified on imagery and in the field to create the geomorphic map (Figure 19).

The relative elevation model (REM) was generated to determine the elevation of different valley floor surfaces above the adjacent sections of the river or tributary channel, independent of their geomorphic origin or stratigraphy (Figure 20). The REM was created to compare with the floodplain area and storage values of the geomorphic map as well as to compare with the storage values calculated by Dickerson-Lange and Abbe (2019), who used a similar method. The area of the incised floodplain was extracted from the REM (Figure 21). Finally, the geomorphic and REM maps were overlain to compare the incised floodplain areas (Figure 22).

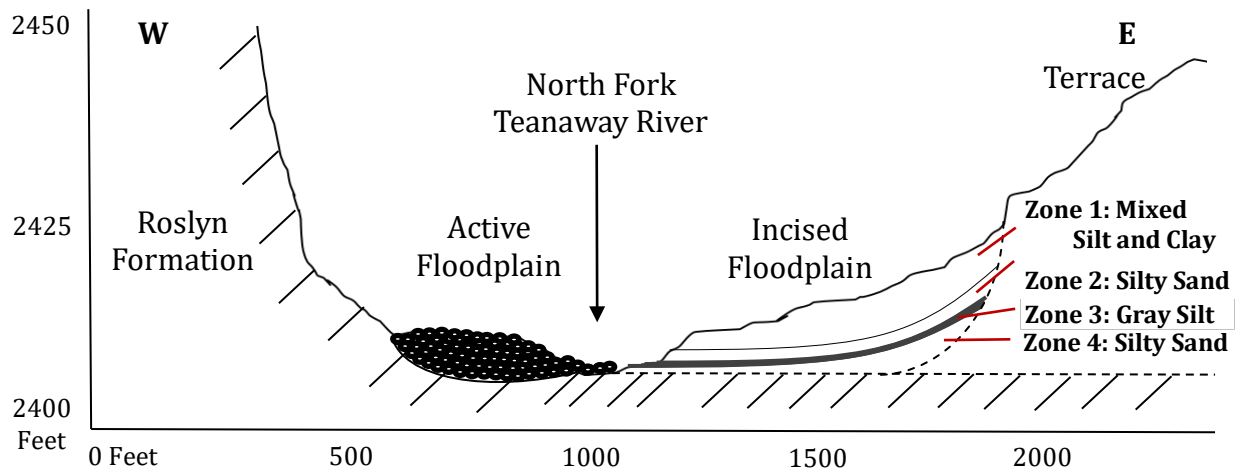


Figure 18. Valley cross section at confluence of North Fork Teanaway River and Indian Creek. The stratigraphic zones represent the generalized stratigraphy of the incised floodplain. The fine-grained gray silt in Zone 3 is a potential confining layer within the floodplain aquifer.

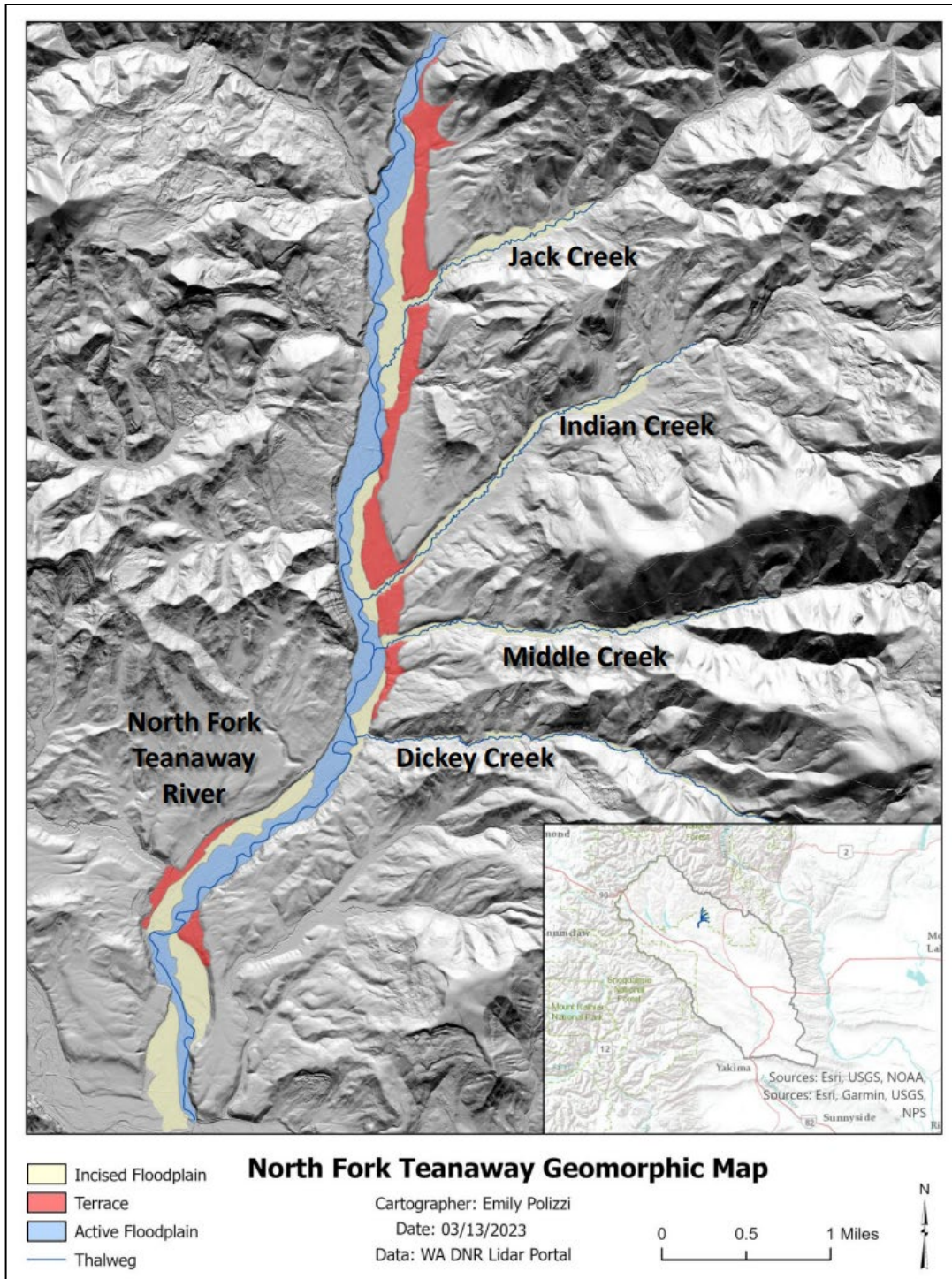


Figure 19. North Fork Teanaway watershed geomorphic map. This map displays the active floodplain, incised floodplain, and abandoned alluvial terrace across the NFT watershed. The terrace lies outside of the current floodplain and was not used in the aquifer capacity calculations.

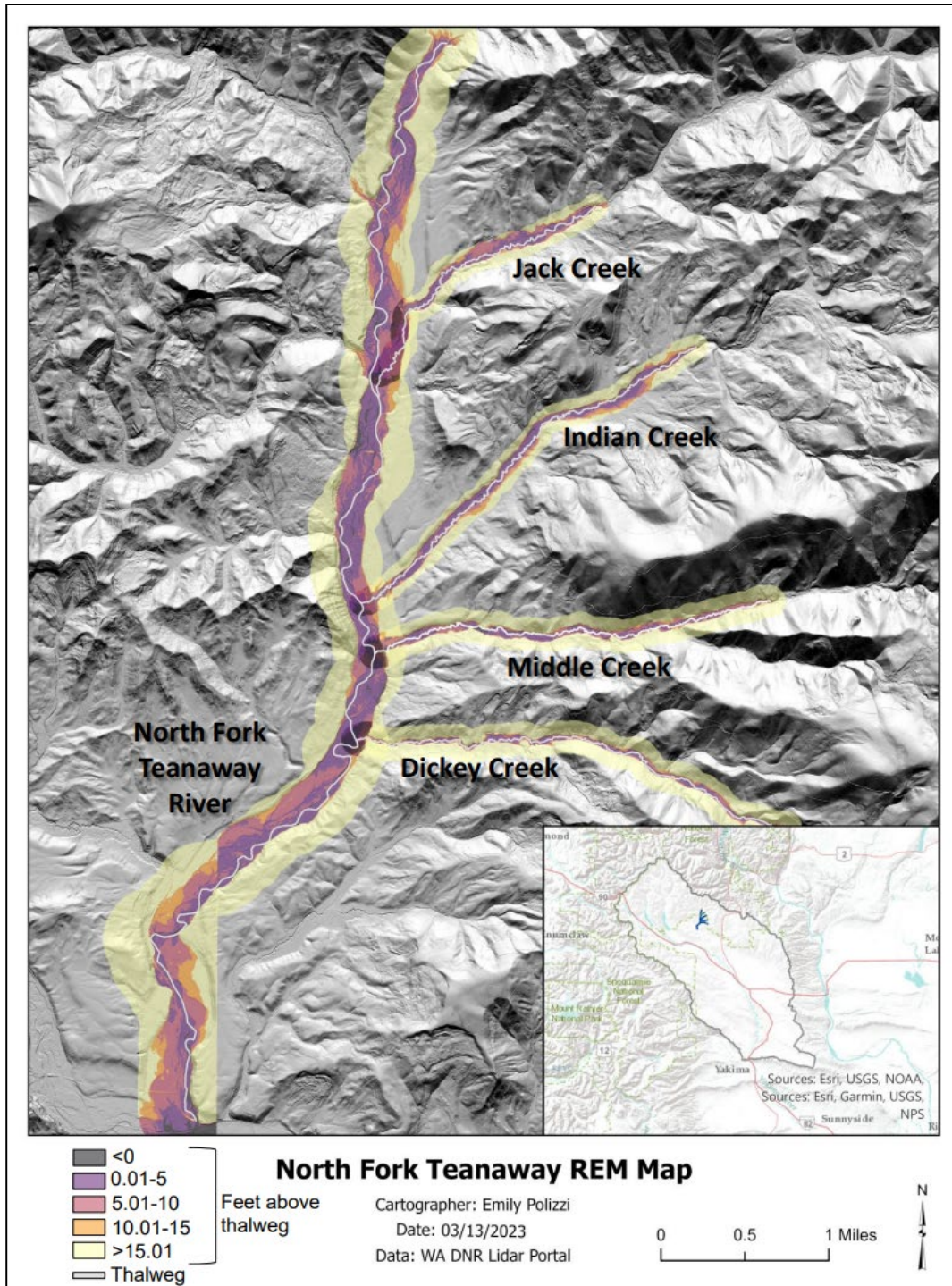


Figure 20. North Fork Teanaway watershed relative elevation model map., The colors indicate the different elevations given to each pixel based on their elevation in feet above or below the water surface in the river. There is a seam between DEM files downstream of Dickey Creek.

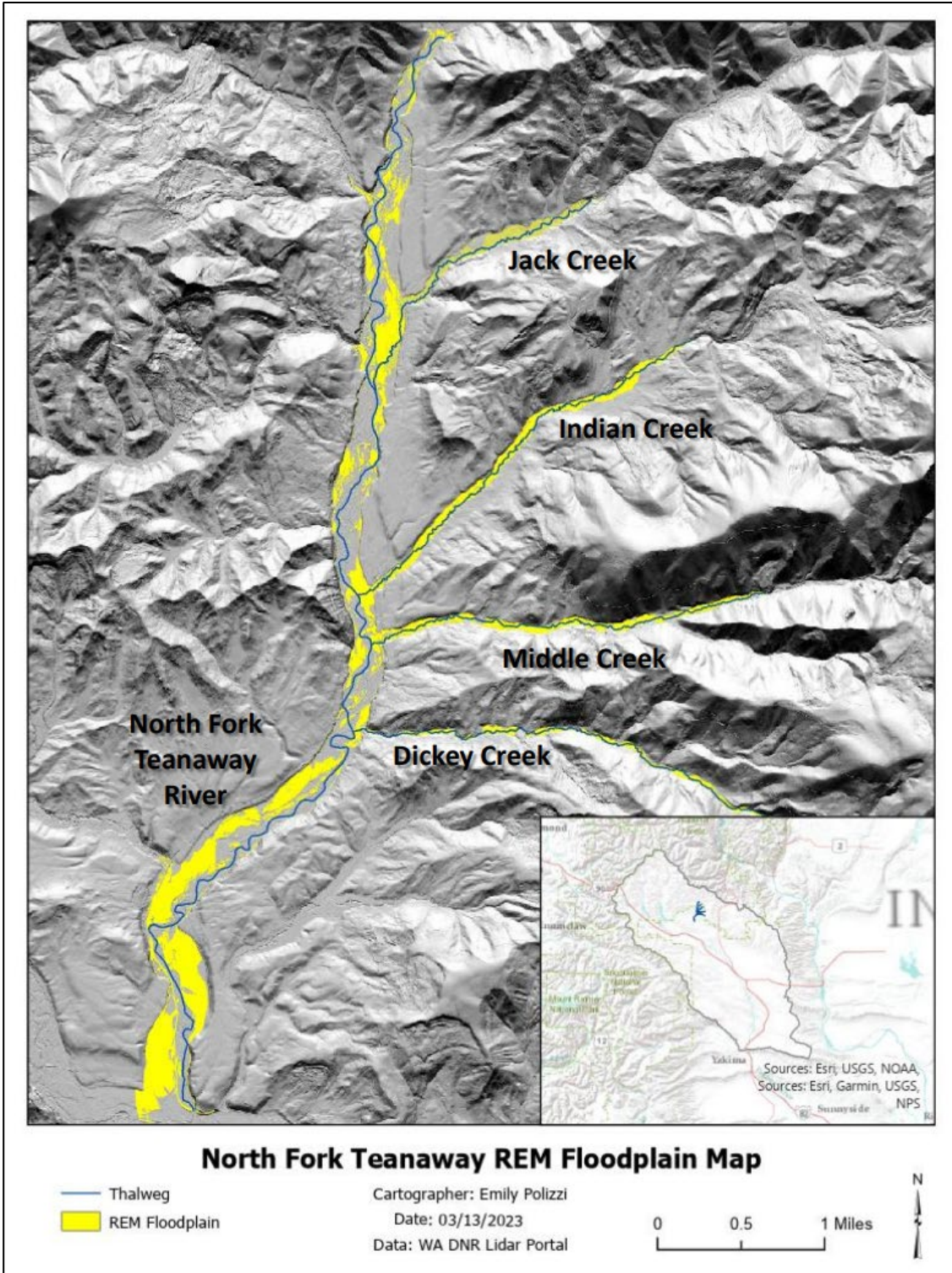


Figure 21. North Fork Teanaway watershed incised floodplain map from relative elevation model. Different elevation ranges were chosen for each tributary to account for variations in incision across the watershed.

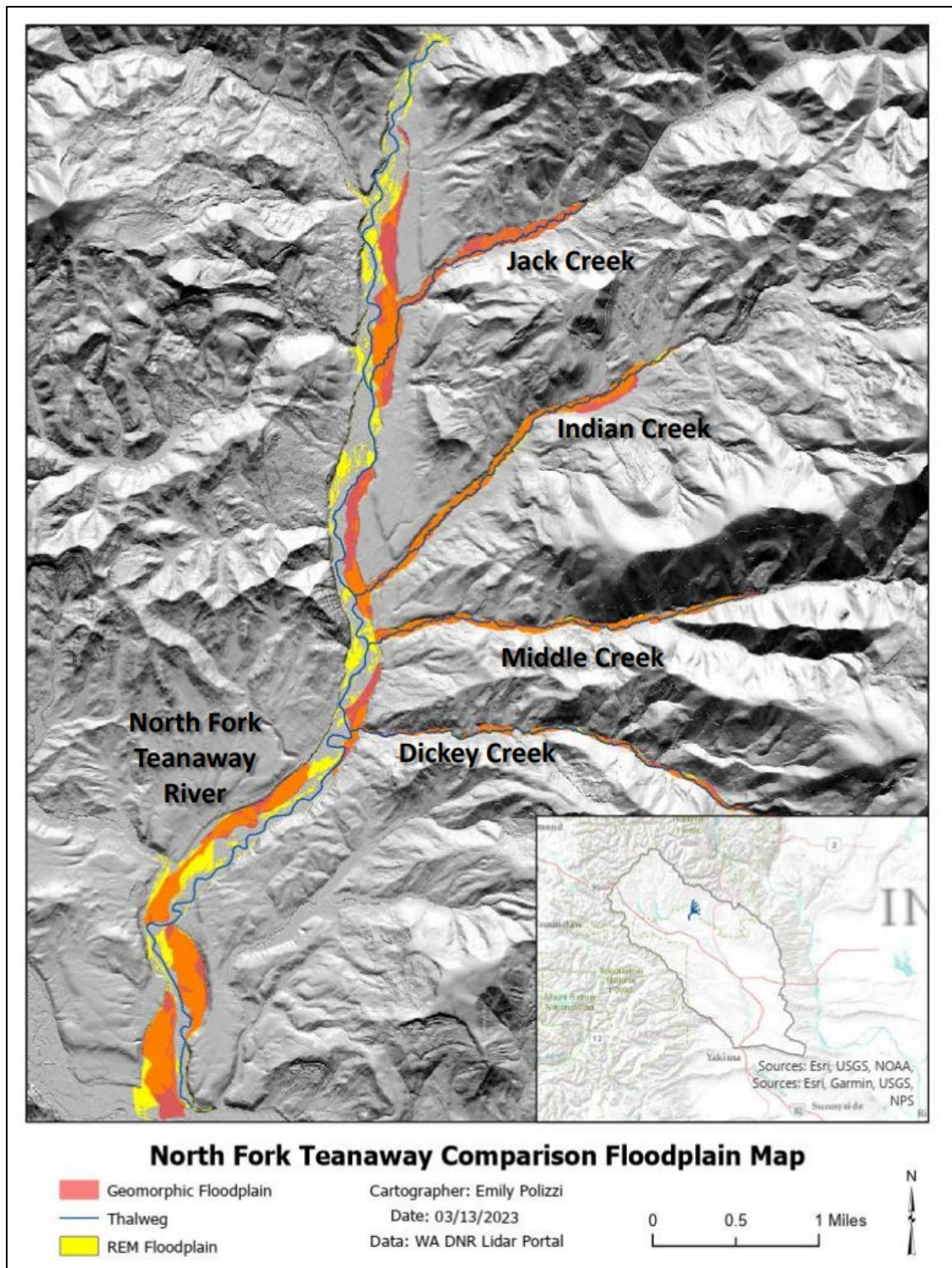


Figure 22. North Fork Teanaway comparison of geomorphic and REM maps. This map compares the geomorphic-map of the incised floodplain (red) and the REM-extracted incised floodplain (yellow). The orange depicts where the two floodplain mapping methods overlap.

Taneum Creek Floodplain Mapping

The valley floor of Taneum Creek was mapped using the same two methods as in the Teanaway watershed. Different geomorphic landform designations were used on Taneum Creek because the floodplain was not incised to the degree of the North Fork Teanaway watershed. These units are: river channel, multi-threaded channel bed, floodplain, and lowest abandoned river terrace (Figure 23). The relative elevation modeling process yielded the REM maps in Figures 24 and 25). An overlay was created to compare the geomorphic and REM maps (Figure 26).

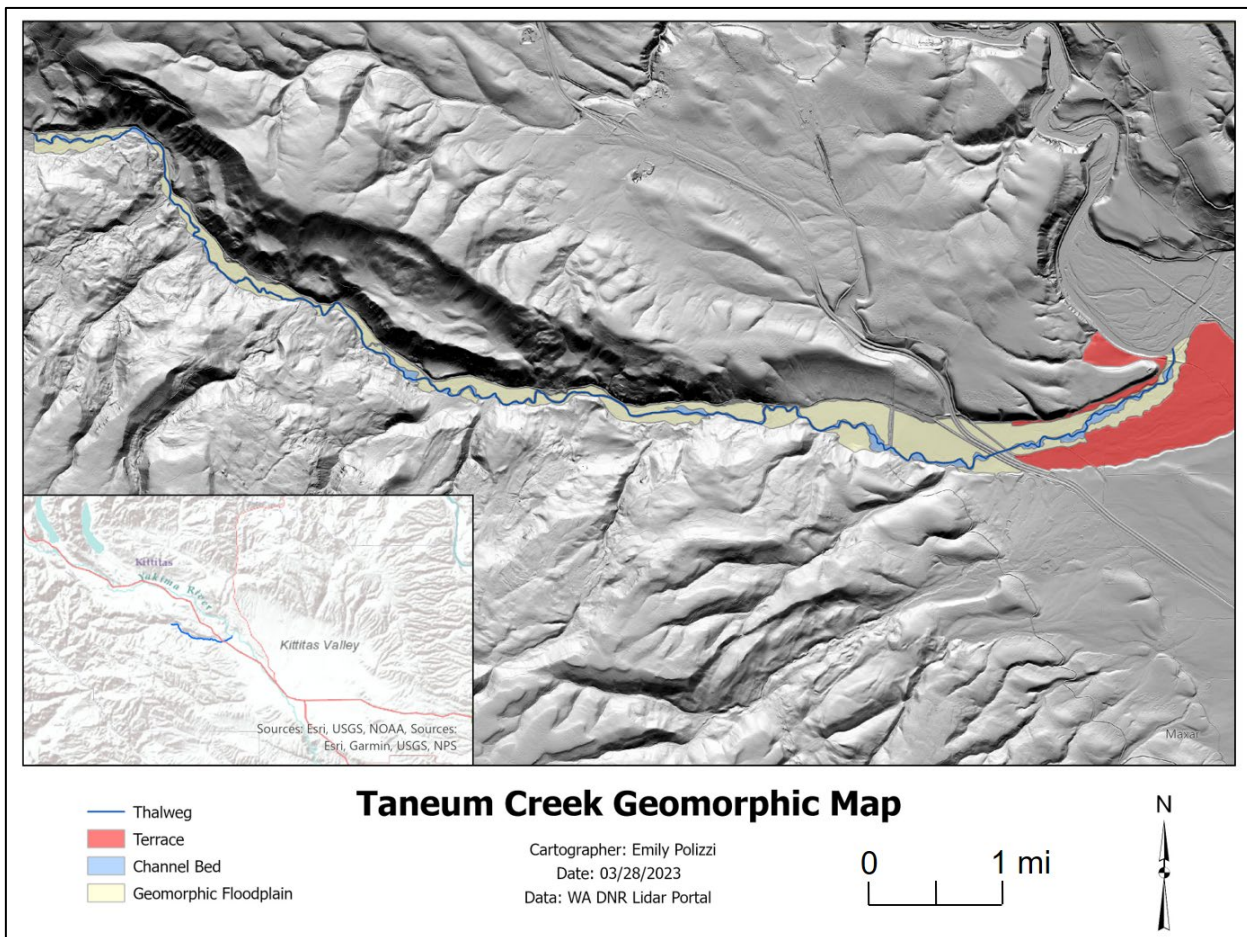


Figure 23. Taneum Creek geomorphic map. Map displaying the different geomorphic units: River channel, multi-threaded channel bed, floodplain, and lowest river terrace.

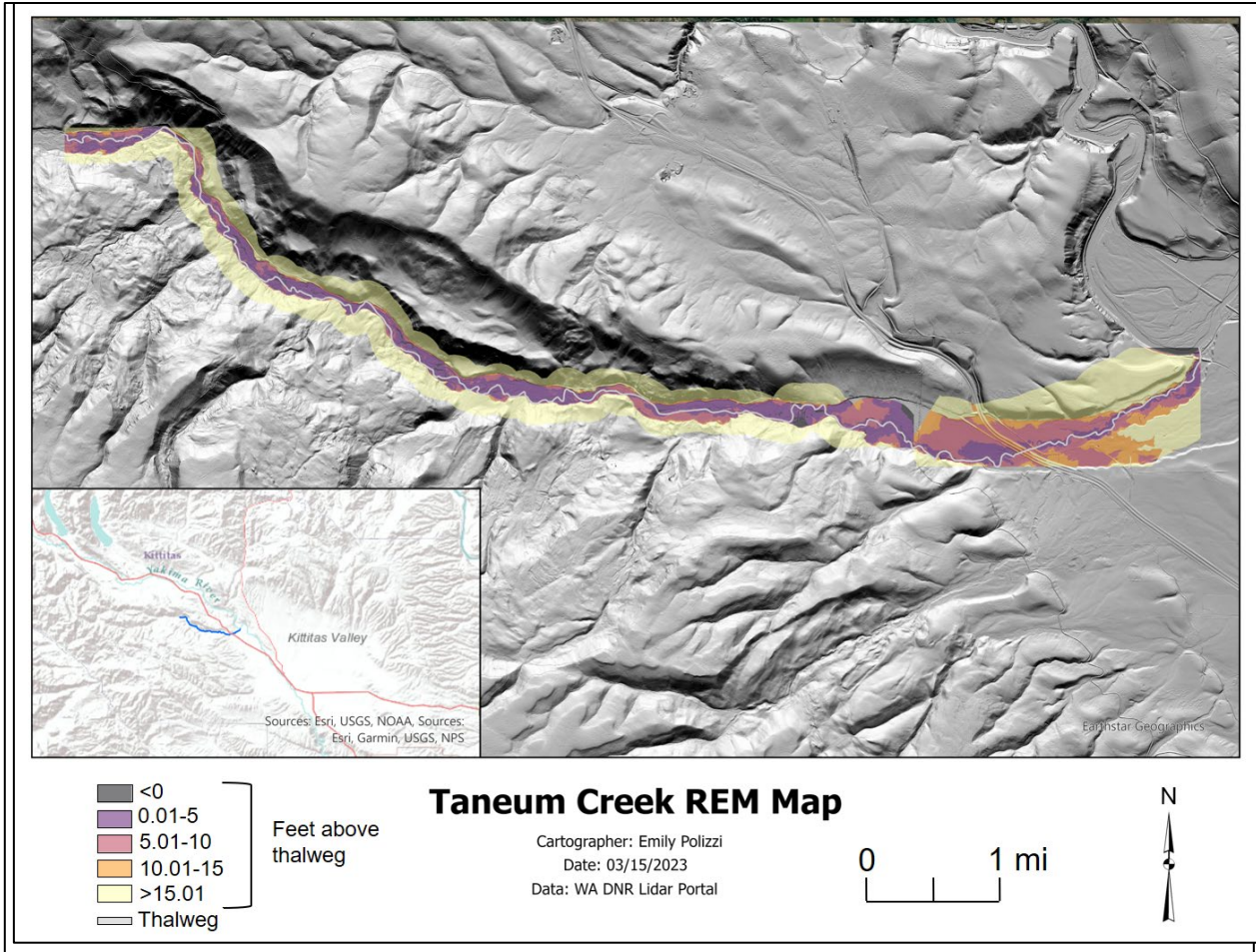


Figure 24. Taneum Creek relative elevation map. The colors indicate the different elevations given to each pixel based on their elevation in feet above or below the water surface in the river. The two DEM files used to generate the REM meet at the KRD well site, just upstream of 1-90. It should be noted that the REM was unable to account for a small portion of the floodplain due to gaps in the DEM overlap.

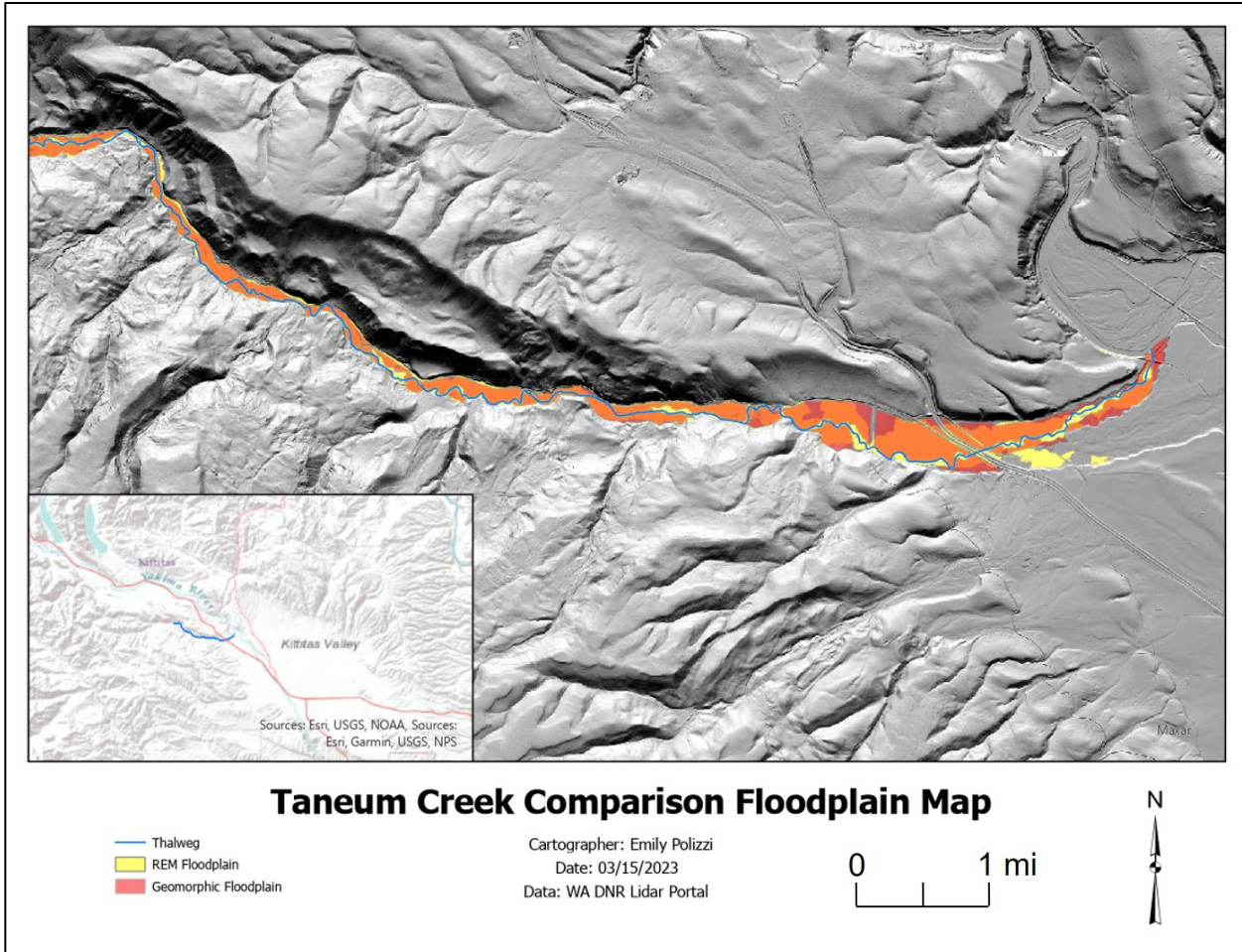


Figure 26. Taneum Creek comparison of geomorphic and REM maps. Comparison of the geomorphic map of the floodplain (red) and the REM-extracted floodplain (yellow). The orange depicts where the two floodplain methods overlap.

CALCULATION OF FLOODPLAIN AREA

The geometry calculation tool in ArcGIS Pro was used to quantify the area covered by the incised floodplain derived from both mapping methods.

Table 3. North Fork Teanaway Watershed incised floodplain area. A comparison between the REM and geomorphic map areas in the North Fork Teanaway Watershed (Figure 22).

Tributary	REM Area (Acres)	Geomorphic Area (Acres)	% Difference
North Fork Teanaway River	363	298	19.6
Dickey Creek	51.0	36.3	33.6
Middle Creek	58.6	55.8	5.0
Indian Creek	77.4	81.9	5.6
Jack Creek	71.3	75.0	5.0
Totals	622	548	12.7

Table 4. Taneum Creek floodplain area. A comparison between the REM and geomorphic map areas at Taneum Creek (Figure 26).

Tributary	REM Area (Acres)	Geomorphic Area (Acres)	% Difference
Taneum Creek	693	616	11.8

The geomorphic mapping and relative elevation modeling methods were both successful in isolating the floodplain area in the watersheds. The REM-derived area of the floodplain was slightly larger than the geomorphic map of the floodplain area in both watersheds due to the nature of the tools used to construct the model and the contextual limitations of the process. The geomorphic mapping allowed more control over the delineation of active vs. incised floodplain based on the geomorphic context of the area. For example, in the NFT watershed, we were able to manually make the distinction between the active floodplain consisting of gravel bars and the incised floodplain. With the REM, the only factor considered by the software is the elevation of a specific pixel, not what geomorphic feature that pixel represents. Selecting the elevation range to depict the REM-incised floodplain was an iterative process based on the geomorphic mapping. The REM method was most consistent with the geomorphic map in Taneum Creek and the tributaries of the North Fork Teanaway where the floodplain topography and geometry was simplest. See Polizzi (2023) for a detailed comparison of the two methods.

Effective Storage Volume of Floodplain Aquifers

A minimum and maximum storage volume was calculated for the active and incised floodplains in the North Fork Teanaway watershed and the total floodplain in Taneum Creek (Tables 5 and 7). These calculations represent the estimated storage capacity of the floodplain aquifers if they were completely void of groundwater. There was no incised floodplain delineated at Taneum Creek, so the entire floodplain is considered to be actively connected to the channel.

The minimum and maximum range of depths for the volume calculations are based on the stratigraphic profiles in the main channel and each tributary. The calculated volume of the active floodplain uses the geomorphic map of the active floodplain area multiplied by a depth of 3 feet.

The maximum volume for the incised floodplain on the NFT and its tributaries uses the incised floodplain area multiplied by the entire stratigraphic profile depth from the channel bed to the surface. The minimum volume for the incised floodplain uses the incised floodplain area, but the depth value excludes the silt units inferred to be less permeable (Zones 1 and 3; Figure 11). The volumes were multiplied by a minimum and maximum porosity to better estimate the storage capacity of the incised floodplain considering the sediment composition. The minimum porosity (0.3) was used by Dickerson-Lange and Abbe (2019) in their potential volume calculations of the Teanaway River watershed and represents a sandy loam (Table 6). The maximum porosity (0.38) was used by Bartlett (2022) in the Indian Creek floodplain volume calculation and represents a silt/clay floodplain. A similar process was used to calculate the total floodplain aquifer volume at Taneum Creek, where the minimum volume of 2 feet excludes the fine-grained stratigraphic zones 2 and 4 (Figure 12).

Table 5. Potential aquifer storage capacity in the North Fork Teanaway Watershed. Volume estimates under varying scenarios of aquifer thickness and porosity. All areas in this table are from the geomorphic mapping method (Figure 19).

Tributary	Floodplain Description	Thickness (feet)	Area (acres)	Volume ac-ft (m³) 0.3 Porosity	Volume ac-ft (m³) 0.38 Porosity
North Fork Teanaway River	A	3	506	455 (561,000)	576 (710,000)
	B	2.1	298	188 (232,000)	238 (294,000)
	C	6.6	298	591 (729,000)	749 (924,000)
Dickey Creek	B	5.4	36	59 (73,000)	75 (93,000)
	C	8	36	88 (109,000)	111 (137,000)
Middle Creek	B	5.4	56	91 (112,000)	115 (142,000)
	C	8	56	134 (165,000)	170 (210,000)
Indian Creek	B	6.2	82	153 (189,000)	194 (239,000)
	C	7.5	82	185 (228,000)	235 (290,000)
Jack Creek	B	4.1	75	92 (113,000)	117 (144,000)
	C	5.2	75	118 (146,000)	150 (185,000)
Total (min. thickness)	A + B	-	1053	1040 (1,290,000)	1320 (1,630,000)
Total (max. thickness)	A + C	-	1053	1570 (1,930,000)	1990 (2,450,000)

A = Active floodplain area, B = Incised floodplain area (excluding stratigraphic profile zones 1 & 3), C = Incised floodplain area (entire stratigraphic profile thickness). All values are rounded to three significant figures and represent the maximum amount of storage in the floodplain aquifer if it were completely void of water.

Table 6. Potential aquifer storage capacity comparison of methods. Comparison between methods by Polizzi (2023) and Dickerson-Lange and Abbe (2019) in the calculated estimates of potential storage capacity for the North Fork Teanaway River floodplain aquifer (excluding tributaries).

Study	Floodplain Description	Thickness (feet)	Area (acres)	Volume ac-ft (m³) Minimum Porosity (0.3)	Volume ac-ft (m³) Maximum Porosity (0.38)
This study: Geomorphic Mapping Method	A	3	506	455 (561,000)	576 (710,000)
	B	2.1	298	188 (232,000)	238 (294,000)
	C	6.6	298	591 (729,000)	749 (924,000)
	A + B	3 and 2.1	804	643 (793,000)	814 (1,004,000)
	A + C	3 and 6.6	804	1046 (1,290,000)	1330 (1,634,000)
This study: REM Method	B	2.1	363	229 (282,000)	290 (358,000)
	C	6.6	363	720 (888,000)	911 (1,120,000)
Dickerson-Lange & Abbe, 2019 Model	minimum	3	-	368 (454,000)	-
	median	6	-	919 (1,130,000)	-
	maximum	9	-	1470 (1,810,000)	-

A = Active floodplain area, B = Incised floodplain area (excluding stratigraphic profile zones 1 & 3), C = Incised floodplain area (entire stratigraphic profile thickness). All values are rounded to three significant figures. Total volume is not included in this table. The calculated volumes do not include the tributaries.

The aquifer storage capacity calculated in this study was compared with the values calculated by Dickerson-Lange and Abbe (2019). Although the methods differed in terms of the geometry, means of classifying the different floodplain features, and the stratigraphy (see Polizzi, 2023 for a detailed description of the comparison). The volume calculations for this study using the combined area of the active and incised aquifer (A + C in Table 5) vs. the median 6-foot incision model from Dickerson-Lange and Abbe (2019) are the most similar in terms of the area, depth and uniform stratigraphy used as input for the calculations. The resulting volume calculations are relatively close, within 12% difference: 1046 ac-ft vs. 919 ac-ft (Table 5), indicating that the modeling approaches yield relatively similar results given similar input parameters. The extent to which the heterogeneous stratigraphy of the incised floodplain reduces the effective capacity of the aquifer does increase the difference in the volume calculations. A comparison of the combined area of the active floodplain plus the minimum estimate of the effective aquifer in the incised floodplain (Table 5 A + B from this study) vs. Dickerson-Lange median incision gives an end-member example of this possible difference of 643 vs. 919 ac-ft (Table 5).

The potential floodplain aquifer storage capacity for Taneum Creek is summarized in Table 7. There are similarities and differences in the storage potential for the floodplain aquifers of the North Fork Teanaway and Taneum Creek, beyond just the simple difference in floodplain area (Tables 5 and 7). In both cases, the presence of layers of fine silt and clay in the stratigraphy could limit the effectiveness of these layers to store water in the spring for later discharge or extraction in the drier summer months. The silt layers in the Taneum Creek floodplain contain less sand than in the Teanaway floodplain (Figure 17), and could therefore be even less permeable.

Table 7. Potential aquifer storage capacity in the Taneum Creek Watershed. Volume estimates under varying scenarios of aquifer thickness and porosity. The geomorphic mapping and REM method areas are both shown in the table to compare volumes (Figures 22 and 26).

River	Thickness (feet)	Area (acres)	Volume ac-ft (m³) 0.3 Porosity	Volume ac-ft (m³) 0.38 Porosity
Taneum Creek	2	587	352 (434,000)	446 (550,000)
Geomorphic Mapping	5	587	880 (1,090,000)	1,120 (1,380,000)
Taneum Creek	2	693	416 (513,000)	527 (650,000)
REM method	5	693	1,040 (1,280,000)	1,320 (1,620,000)

2-foot stratigraphic profile thickness excludes stratigraphic profile zones 2 & 4, 5-foot stratigraphic profile thickness includes the entire stratigraphic profile thickness. All values are rounded to three significant figures and represent the maximum amount of storage in the floodplain aquifer if it were completely void of water.

A notable difference between the Teanaway and Taneum watersheds is the greater incision of the North Fork Teanaway channel below the floodplain (Figures 4 and 18). In Taneum Creek, the established 15-year LW restoration and the mobilization of wood and sediment in the 2011 flood have connected large portions of the floodplain with the channel. Even though the North Fork Teanaway watershed has a higher potential aquifer storage capacity due to the depth of sediment in the incised floodplain, it will require channel restoration and an increased sediment supply to aggrade the channel bed 1-3 meters to the point at which it could regularly inundate the incised floodplain to utilize that potential storage. Currently, very little of the incised floodplain area in the NFT is inundated from channel overflow during spring peak flows. Studies on Indian Creek (Bartlett, 2022; Boylan, 2019 a, b; Gazis and Ely, 2023) found no significant difference in seasonal or long-term groundwater levels in floodplain monitoring wells after LW restoration in 2016-2018.

The difference in elevation between the incised floodplain of the Teanaway River and the channel also create steep hydraulic gradients between the floodplain and the channel. This means that any water that inundates the incised floodplain quickly flows into the channel through the sandy aquifer layers instead of being stored seasonally. This process is demonstrated by the rapid drop in groundwater levels in the monitoring wells in Indian Creek in late spring (Figure 27; Bartlett, 2022; Gazis and Ely, 2023). By June, the high spring groundwater levels return to low base levels until the following spring.

The side channels on Taneum Creek already transfer water from the channel across the floodplain. Multiple side channels filled with water cross the floodplain of the lower study reach (Figure 7) in the wet spring months. The construction of beaver dams on some of the side channels increased the area and duration of floodplain inundation (Figure 16). A calculation of the Normalized Difference Vegetation Index (NDVI) from satellite imagery for the years 2006-2020 (Fixler, 2022) indicates that the floodplain vegetation greenness values for the lower study site in July remained slightly higher in the years after the LW restoration and the flood than before. Green meadow vegetation is sustained later into the summer, possibly indicating increased groundwater in the floodplain. The extent to which this stored groundwater augments return flow to the channel depends partly on the amount that is lost to evapotranspiration, as discussed in Chapter 3 of this report.

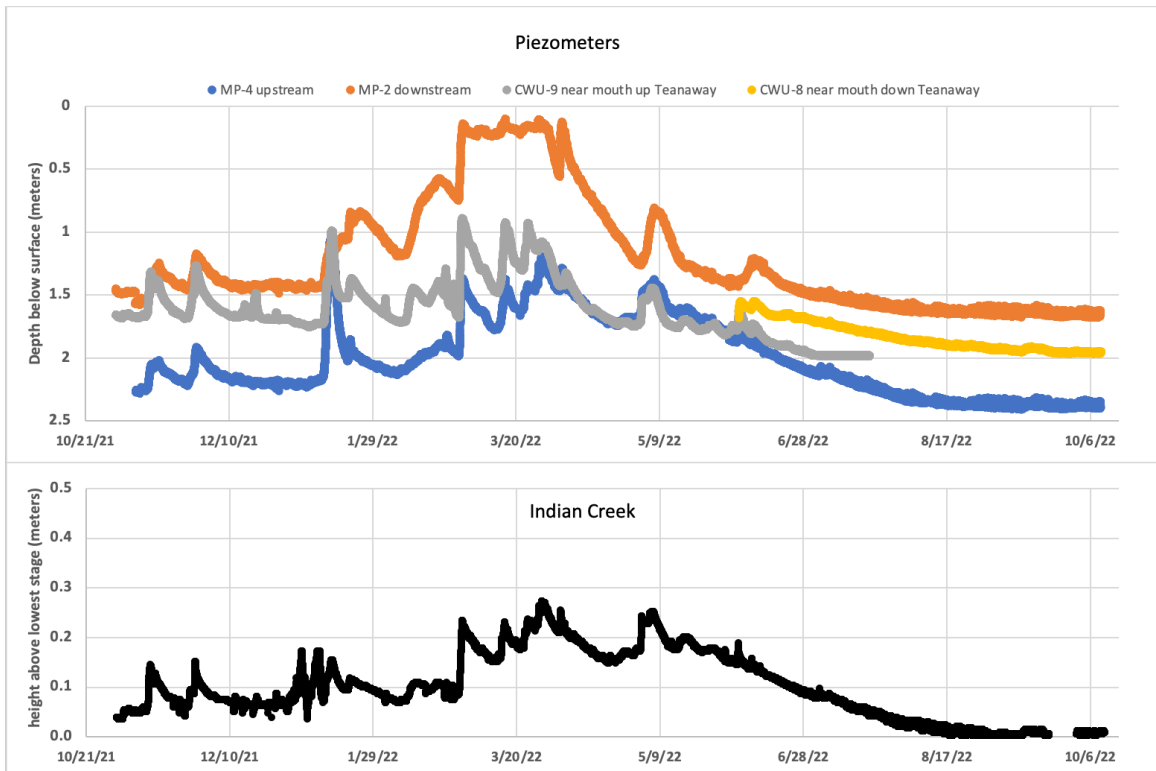


Figure 27. Indian Creek piezometer data. The top graph shows the water levels in wells in the Indian Creek floodplain. CWU-8 and CWU-9 are at the confluence of Indian Creek and the North Fork Teanaway River, and MP-2 and MP-4 are 0.9 and 2.2 km upstream along Indian Creek (Bartlett, 2022). The bottom graph shows Indian Creek water height above the lowest stage. The seasonal and even some shorter-term variations in the groundwater levels are similar across a distance of 2 km. From Gazis and Ely (2023).

The potential additional groundwater storage from increased channel overbank flow must consider the preexisting groundwater levels in the floodplain aquifers during the spring in these watersheds. The potential floodplain storage capacities calculated in this study (Tables 5, 6 and 7) represent the total volume of the floodplain aquifers without any water. Groundwater levels in the floodplain of Indian Creek currently rise in the spring to < 1 m below the ground surface in some locations (Figure 27; Bartlett, 2022; Boylan, 2019; Gazis and Ely, 2023). Water sources include direct precipitation, snowmelt, and groundwater flow from the hillsides and bedrock aquifers. If inundation from channel overflow coincided with already-high groundwater, the additional accommodation space would be limited. The peak in the groundwater levels in the Teanaway generally occurs slightly before the peak stage in the adjacent stream channel (Bartlett, 2022; Gazis and Ely, 2023), which might allow more space for additional storage from channel overflow.

CHAPTER 1 CONCLUSIONS

The floodplain sediment composition plays a key role in how water will be transmitted and stored in the aquifer. Through fieldwork, mapping, and grain-size analysis, the groundwater storage volume was quantified taking into consideration the effects of the stratigraphy on groundwater storage, recharge, and flow. Volume estimates indicate a potential floodplain aquifer capacity of 1,040-1,990 acre-feet in the North Fork Teanaway watershed and 352-1,120 acre-feet in Taneum Creek. In both cases, the minimum value in the range excludes the fine-grained stratigraphic layers that we interpreted as less effective aquifers, and the maximum value assumes a uniform stratigraphy and greater porosity.

The floodplain stratigraphy of these two headwater tributaries of the Yakima Basin is heterogeneous. Widespread fine-grained gray silt and clay layers were likely deposited during past glacial periods. These and other laterally continuous fine-grained sediment layers could impede vertical movement of groundwater or create confined aquifers within the floodplains, as indicated by piezometer pump tests, perched surface water and elevated piezometric surfaces in wells that penetrate the clay. The interbedded coarse and fine stratigraphic zones within the floodplain sediments can influence the transmission of groundwater through the floodplain, probably causing preferential horizontal flow through the coarser sand and gravel layers. Due to their lower permeability and transmissivity, the fine-grained silt and clay layers, particularly those containing the glacial gray silt, may not function effectively for seasonal groundwater recharge and storage.

The effective capacity of the floodplain aquifer in the North Fork Teanaway watershed to store groundwater in the spring for use later in the summer dry season is limited by the presence of these low-permeability stratigraphic layers, the elevation difference between the floodplain and the channel, and the rapid draining of the floodplain aquifer into the incised channel. If the channel aggrades to the point at which overbank flow broadly inundates the floodplain, the preexisting groundwater could further limit the additional accommodation space, depending on the timing. Unless the channels of the North Fork Teanaway River and its tributaries aggrade 1-3 meters, significant overbank inundation of the incised floodplain is unlikely to occur during normal or even high spring stream discharges.

Under current conditions, Taneum Creek is more conducive to additional groundwater storage from channel overbank flow than the North Fork Teanaway River. Taneum Creek is not deeply incised below the elevation of the floodplain in the study reaches. Large wood restoration and mobilization of wood and sediment by the 2011 flood have created multiple side channels that transfer water from the creek across the floodplain. However, the floodplain stratigraphy of Taneum Creek also contains low-permeability glacial gray silt layers that impede vertical groundwater movement and limit aquifer capacity. Calculations of NDVI greenness indicate that the Taneum Creek floodplain might retain groundwater later into the summer following the LW restoration and flood. The extent to which this groundwater augments summer return flow to the channel depends partly on the amount that is lost to evapotranspiration from the increased vegetation growth (see Chapter 3).

REFERENCES

- Bartlett, S.P. 2022, Assessing the Effects of Instream Large Wood on Floodplain Aquifer Recharge and Storage at Indian Creek, Kittitas County, Washington, USA. M.S. Thesis, Central Washington University. <https://digitalcommons.cwu.edu/etd/1735>.
- Boylan, N. 2019a. Assessing the Link Between Large Wood Restoration and Groundwater Storage and Recharge: An Investigation of Indian Creek in Washington State. M.S. Thesis, Oregon State Univ., 78 p. https://ir.library.oregonstate.edu/concern/graduate_thesis_or_dissertations/5425kh699
- Boylan, N. C., 2019b, Assessing the Link Between Large Wood Restoration and Groundwater Recharge and Storage: An Investigation of Indian Creek in Washington State. Report prepared for Washington Department of Ecology and the Groundwater Subcommittee of the Yakima Basin Integrated Plan.
- Collins, B. D., Montgomery, D. R., Schanz, S. A., and Larsen, I. J., 2016, Rates and mechanisms of bedrock incision and Strath Terrace Formation in a forested catchment, Cascade Range, Washington. Geological Society of America Bulletin, v. 128(5-6), p. 926–943.
- Dickerson-Lange, S., and Abbe, T., 2019, Potential for Restoration of Alluvial Water Storage in the Teanaway River Watershed. Report prepared for The Nature Conservancy by Natural Systems Design, p. 1-40.
- Fixler, S. A., 2022, Decadal-scale effects of large wood restoration on channel morphology and groundwater connectivity, Taneum Creek, WA. M.S. Thesis, Central Washington University. <https://digitalcommons.cwu.edu/etd/1783>.
- Gazis, C.G. and Ely, L.L., 2023, Effect of Large Wood Restoration on Alluvial Aquifer Storage in Yakima Basin Headwater Tributaries. Report for Washington State Department of Ecology Project #NTA C210007 and Groundwater Subcommittee of the Yakima Basin Integrated Plan.
- Polizzi, Emily, 2023, Floodplain Aquifer Storage Capacity in Upper Yakima River Tributaries, Kittitas County, WA. M.S. Thesis, Central Washington University. <https://digitalcommons.cwu.edu/etd/1872>
- Porter, S.C., 1976, Pleistocene glaciation in the southern part of the North Cascade Range, Washington: Geological Society of America Bulletin, v. 87, p. 61.
- Schanz, S.A., Montgomery, D.R., and Collins, B.D., 2019, Anthropogenic strath terrace formation caused by reduced sediment retention: Proceedings of the National Academy of Sciences, v. 116, p. 8734–8739, doi: 10.1073/pnas.1814627116.
- Tabor, R. W., Waitt, R. B., Frizzell, V. A., Swanson, D. A., Byerly, G. R., & Bentley, R. D. (1982). Geologic map of the Wenatchee Quadrangle, Central Washington. map, Reston, VA; The United States Geologic Survey, Miscellaneous Investigations Map 1-1311, scale 1:100,000.

2. Using MODFLOW to Assess Groundwater Storage in the Teanaway River Floodplain Aquifer

INTRODUCTION

This chapter presents a summary of the M.S. thesis of Lindsay Henning. For her thesis research, Ms. Henning created a MODFLOW model of the Teanaway Valley Family Farm, a 87-hectare site at river kilometer 13 on the Teanaway River. She used an iterative approach in which a steady-state water balance determination for the site was used to inform the inputs to the model and validate model results. This chapter will present a brief overview of the project and study area; the water balance results; the framework of the MODFLOW model; and results from simulations in which retention ponds of different sizes are installed on the site. Details of the model inputs and the many considerations that went into the model development are provided in the M.S. thesis (Henning, 2023).

Overview and Purpose

The Teanaway River flows from the eastern slopes of the Cascade Range to the Yakima River (Figure 28) in central Washington. Elevated water temperatures (Creech, 2003) and anthropogenic channel alterations (Shanz et al., 2019) are contributing to the decline in numbers of anadromous fish and other aquatic species in the Teanaway River (Snyder and Stanford, 2001). The State of Washington, the Yakama Nation, and several conservation groups are actively seeking ways to restore aquatic habitat in the Teanaway River and its tributaries. Because groundwater seepage into rivers is known to reduce stream temperature, enhanced groundwater storage and increased seepage are promising habitat restoration practices.

A possible method for enhancing groundwater storage is managed aquifer recharge (MAR). MAR is the “purposeful recharge of an aquifer for subsequent recovery or environmental benefits” (Ringleb et al., 2016). Zheng et al. (2020) detail the historical development of MAR from ancient agrarian practices to the coining of the term in the early 21st century. MAR is accomplished in a variety of ways, including injection of water into an aquifer through wells, infiltration via ponds, ditches and surface spreading, in-channel and bank modifications of streams, and rooftop rainwater harvesting.

Within the Teanaway River watershed exists a conservation district known as the Teanaway Community Forest (TCF), which is land co-managed by the Washington State Department of Fish and Wildlife (WDFW) and the Washington State Department of Natural Resources (DNR) and set aside with goals of maintaining 5 key elements: watershed protection, forestry and grazing, recreation, fish and wildlife habitat, and community partnerships. A property called Teanaway Valley Family Farm (TVFF) is a part of the TCF. TVFF has both available land and water, making it a site suitable for potential MAR infiltration techniques.

The purpose of this research was to investigate the potential for MAR at TVFF by modeling the effects of an infiltration pond on groundwater storage in the shallow alluvial aquifer at the site. A groundwater flow model was created using the United States Geological Survey (USGS) numerical modeling code MODFLOW and calibrated with observed physical parameters. A

theoretical pond was then added to the calibrated model to evaluate its influence on the existing groundwater regime.

Site Description

The TVFF research site borders an 1800-m reach of the Teanaway River located 13 river kilometers upstream of the confluence of the Teanaway and Yakima Rivers (Figure 28). Land use at the site was conventional hay farming until 2016. In 2017, the property was acquired by WDFW for floodplain and meadow restoration. As part of this conservation effort, 10 groundwater monitoring wells were installed by Mid-Columbia Fisheries Enhancement Group in 2018. The well locations

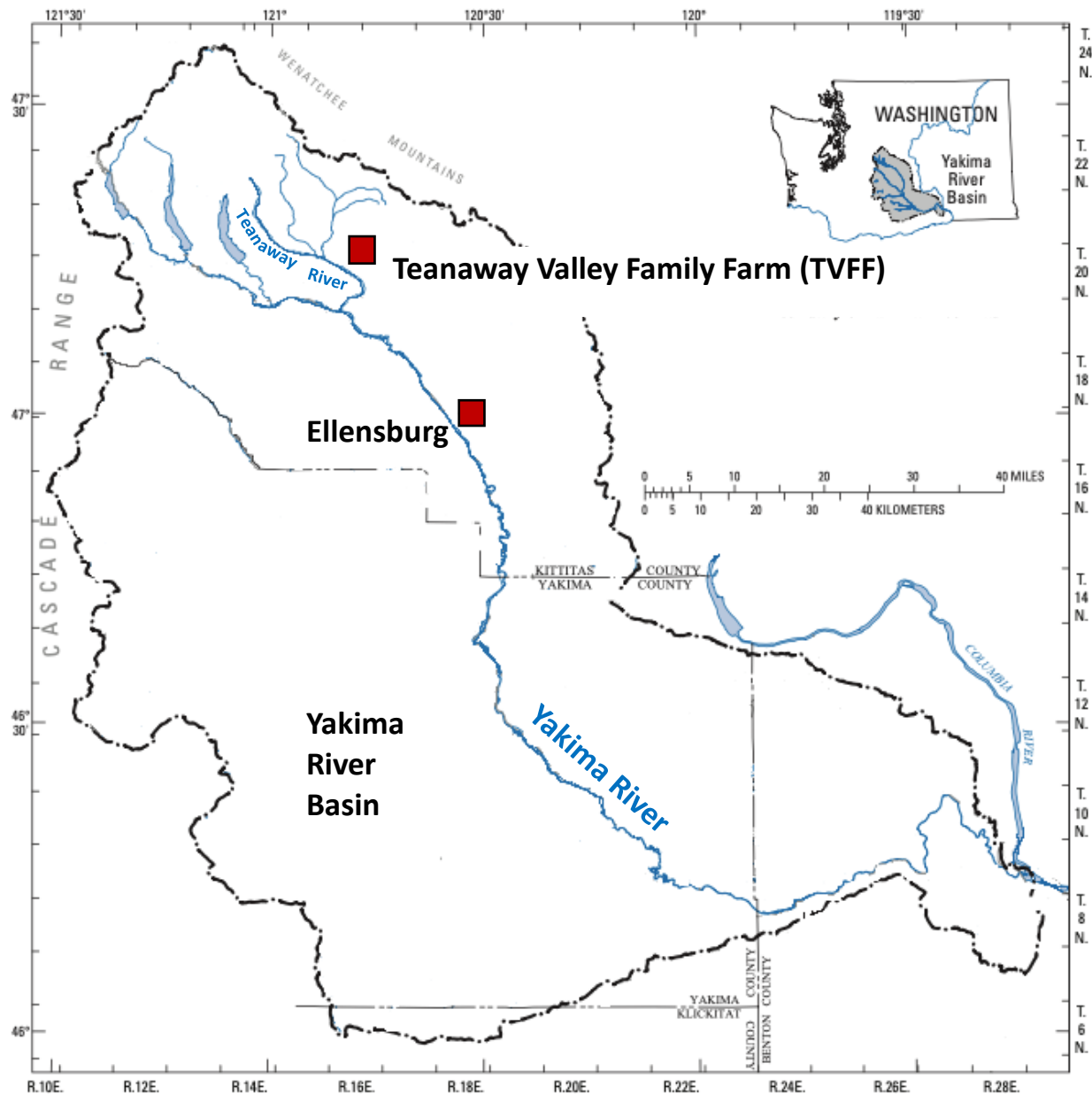


Figure 28. General location of the Teanaway River and the research site, Teanaway Valley Family Farm (TVFF). Adapted from Vaccaro et al., 2009.

are shown in Figure 29. Wells numbered 2 through 10, located in the floodplain, are utilized in this research. Water levels have been monitored at 15-minute intervals in these wells, beginning in August, 2019. Figure 30 presents the two-year interval of water level data that was used for model calibration in this study.

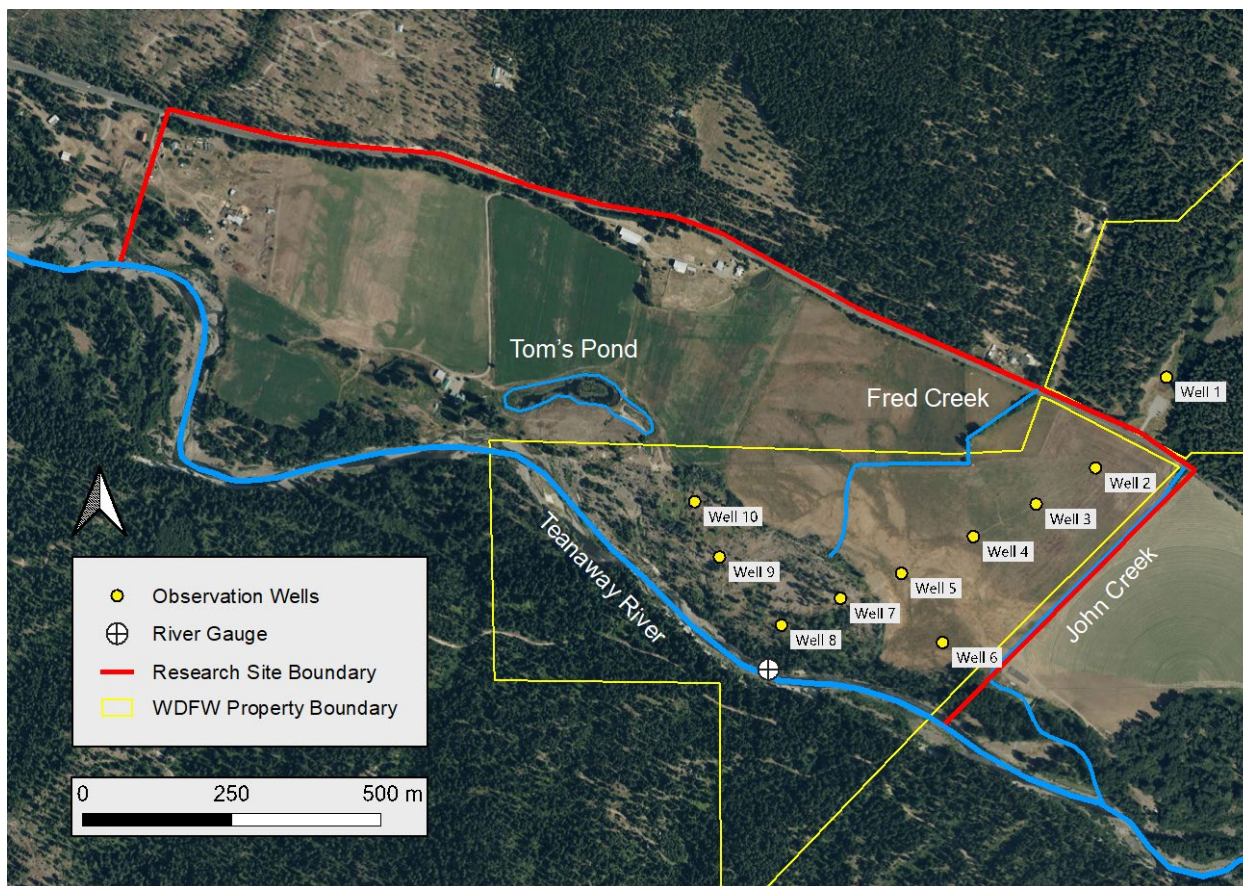


Figure 29. The Teanaway Valley Family Farm (TVFF) site along the Teanaway River. The red perimeter indicates the extent of the groundwater flow model. The yellow boundary delineates property owned by the Washington Department of Fish and Wildlife for floodplain and meadow restoration.

The northern border of the site is the Teanaway Road, which inhibits surface water runoff from the uplands to the north except through limited culverts passing beneath the road, which transmit the flow of ephemeral creeks to the floodplain. An unnamed drainage contributes runoff that is captured by a ditch on private property on the south side of the road at the western end of the site. A creek on the eastern end of the site, named Fred Creek, flows into the TVFF property. Fred Creek was channelized in the past for agricultural practices, but now, as part of the TCF, is a candidate for restoration. Another ephemeral creek, informally called John Creek, flows on private property along the eastern boundary of TVFF.

Interconnected ponds west of the TVFF property are collectively known as Tom’s Pond. Tom’s Pond is an abandoned channel of the Teanaway River that remains full perennially. Water from Tom’s Pond is pumped in the summer to irrigate the nearby alfalfa field.

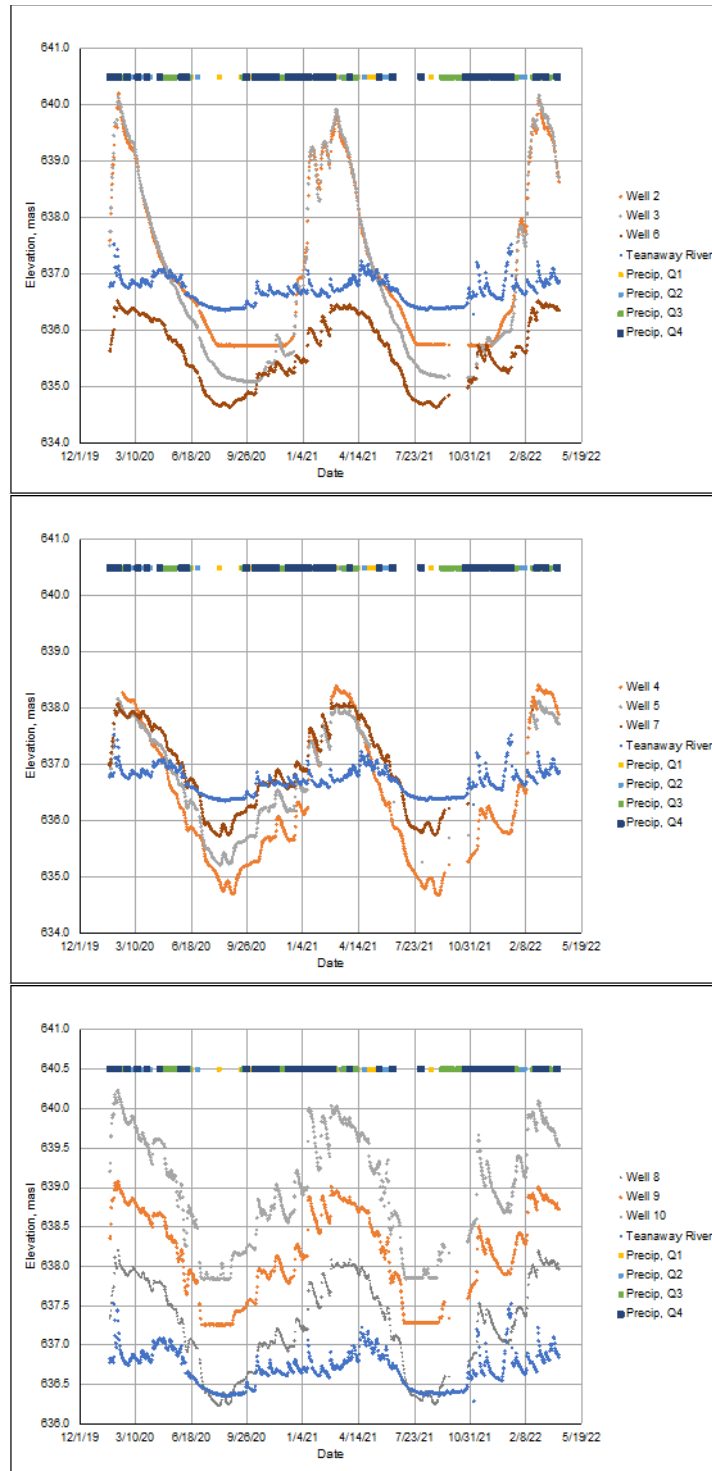


Figure 30. Precipitation, observation-well water levels, and Teanaway River stage. Data are shown for Wells 2, 3, and 6 (top graph); Wells 4, 5, and 7 (middle); and Wells 8, 9, and 10 (bottom) for the period January 24, 2020 to April 7, 2022. Precipitation amounts were grouped by quartile according to increasing magnitude. Water levels in both the river and the wells are responsive to individual precipitation events regardless of magnitude, demonstrating the occurrence of local recharge to the shallow alluvial aquifer.

Discharge in the Teanaway River can be described as “flashy”, with high and variable flows in the winter and spring, particularly after precipitation or melting events. Low flows in the late summer adversely affect aquatic life in the river, and efforts have been made to enhance instream flows, that is, “keep water in the river” through water rights management, improved irrigation efficiency, and restorative plantings.

Another possible way to provide additional instream flows into the Teanaway River may be to enhance groundwater seepage by capturing excess tributary runoff when it is available in the spring and allow it to infiltrate into the shallow alluvial aquifer that underlies the floodplain, thus delaying its discharge into the river until a more critical time. The TVFF site is well suited to provide this type of MAR. Spring runoff in Fred Creek withheld in an infiltration basin could potentially discharge as groundwater into the Teanaway River in the late summer or early fall and supplement low flows.

The hydrogeologic setting for TVFF is influenced by its location in a synclinal basin surrounded by steep uplands, permeable sandstone bedrock on the valley floor, and alluvial deposits of glacial, fluvial, and mass-wasting origins. The unconsolidated alluvial deposits that form the shallow alluvial aquifer are the focus of this study. The deeper sandstone aquifer has been characterized by Gendasak et al. (2014), who determined groundwater movement in the regional bedrock is primarily through fractures and zones of secondary porosity. The site receives recharge from rain in the lowlands and melting snowpack from the surrounding highlands. Irrigation return flows also recharge the shallow aquifer. Water levels in observation wells at the site indicate that groundwater tends to flow toward the Teanaway River in the spring when recharge is abundant, then flows parallel to the river and runs down the valley at other times of the year (Gazis and Ely, 2023).

WATER BALANCE: STEADY-STATE ANALYTICAL MODEL

A steady-state water balance was developed to inform the inputs to the groundwater flow model and validate the model once it produced results. The analytical water balance model is illustrated conceptually by Figure 31. The water balance was calculated for each month by the conservation of mass. For mass to be conserved, the hydrologic fluxes through a volume must balance according to

Equation 1. Change in storage

$$\text{Inflows} - \text{Outflows} = \text{Change in Storage} \quad (1)$$

Here, monthly changes in storage can be positive or negative depending on hydrologic conditions, but the annual change in storage is zero under the steady-state assumption. A control volume approximately the size of the entire site was used with a best-fit plane computed to approximate the water table (Figure 6), which is the top surface of the volume. Inflows into the control volume are the monthly volumes of precipitation, upland runoff, leakage from the Teanaway River into the surficial aquifer, and irrigation return flows. Outflows from the control volume are the monthly volumes of evapotranspiration, baseflow, and the volume of water necessary to refill Tom’s Pond during irrigation season. The east and west boundaries of the site are not natural hydrologic no-flow boundaries, so the exchange with surficial aquifers adjacent to the site is also accounted for.

The right-hand-side of Equation (1), the change in storage ΔS , was taken to be $\Delta S = S_y A \Delta h$, where S_y is the average specific yield of the model domain, A is the area of the plane representing the water table, equivalent to the area of the site, and Δh is the monthly change in the average elevation of the water table. Here, the water table is idealized as the plane of best fit through the average monthly water surface elevations in each of the wells, developed according to Equation (2). Δh is the difference in elevation over consecutive months at the centroid of the plane of best fit. The average specific yield for the site was determined by computing a weighted average by volume using the specific yields of the individual layers of soil, cobbles, clay, and sandstone.

Equation 2. Hydrologic Balance

$$(P + U + L + I) - (ET + B + T) + N = \Delta S, \text{ where } \Delta S = S_y A \Delta h:$$

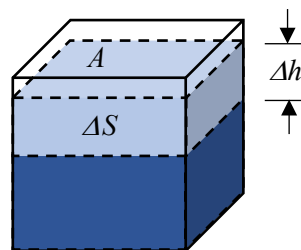


Figure 31. Hydrologic balance equation (2) and schematic of control volume for the analytical water balance model.

The water table was idealized as a least-squares plane of best fit through the average monthly water surface elevation in each well and the centroid of the plane was used to calculate Δh , the average difference in groundwater elevation between two months. More details on the mathematical construct that was used are given in Henning (2023).

The water balance uses the 5-year average monthly precipitation and evapotranspiration amounts over the period from 2017 to 2022. Precipitation and evapotranspiration data are from PRISM (2022) and MODIS (Running et al., 2021), respectively. Runoff from the uplands north of the site was set so that the timing of the runoff mirrors the hydrograph of the Teanaway River and the amount of runoff is determined from catchment precipitation and evapotranspiration and the channel geometry of the ditches that convey the runoff to the site. Inflows from irrigation were assumed to be an average monthly amount of 80 mm applied to the area of the onsite field for the months of May through September. Leakage from the Teanaway River into the surficial alluvial aquifer is determined from streamflow data, as is baseflow.

Water from the on-site pond, “Tom’s Pond,” is pumped to irrigate a nearby field. The pond refills with groundwater seepage from the shallow alluvial aquifer, so the water extracted for irrigation constitutes an outflow from the aquifer. Assuming that 80 mm of irrigation meets the needs of the crop and the irrigated area is 154,000 m², and if the sprinkler irrigation system is 85% efficient, then approximately 14,500 m³ of water is extracted from the aquifer for each of the months of irrigation, May through September.

Baseflow exiting the aquifers of the lower Teanaway River valley into the Teanaway River was computed from baseflow recession curves for hydrographs at two locations: the upstream USDA gauge Teanaway River at Forks near Cle Elum (12480000) and the downstream Ecology gauge Teanaway River at Red Bridge Rd (39D110). Details of the baseflow recession calculation are given in Henning (2023).

Similar to baseflow, river leakage into the aquifer was estimated from the gauged streamflow data, detailed in Equation (3). The Teanaway River was assumed to recharge the shallow alluvial aquifer during the months of October through May when the hydrograph exhibited the variability indicative of non-baseflow conditions. The difference in discharge between the upstream Forks gauge and the downstream Red Bridge was found. This difference was multiplied by the same constant of proportionality used for baseflow: the ratio of the length of the TVFF reach to the distance between the gauges.

Equation 3. Daily river leakage

$$\text{Daily River Leakage, } L = C \frac{1.80 \text{ km}}{9.58 \text{ km}} (Q_{\text{Forks}} - Q_{\text{Rd Bg}}) \times 86400 \text{ s}\cdot\text{d}^{-1} \quad (3)$$

C is an empirical adjustment factor for the percentage of water that actually recharges the shallow alluvial aquifer. For $C = 3.46\%$, the yearly volumes of baseflow and leakage are equivalent. In the water balance, $C = 2.5\%$ was used to replicate conditions where the total volume of baseflow for the year slightly exceeds the total volume of yearly recharge from the river.

The final term of the water balance is the net exchange of water occurring in the shallow alluvial aquifer at the eastern and western extents of the site. These limits are not natural hydrologic boundaries, and it can be assumed that groundwater flows into the site at the upstream (west) end and that flow exits the site at the downstream (east) end. The net exchange was computed monthly by rearranging the equation in Figure 31.

Equation 4. Total annual net exchange

$$N = \Delta S - (P + U + L + I) + (ET + B + T) \quad (4)$$

The total yearly net exchange follows the assumption that for steady-state conditions, the amount of storage in the alluvial aquifer is zero. Thus, net exchange for the site is an outflow in the water balance, meaning that more groundwater exits through the eastern downstream boundary than enters through the upstream western boundary.

Tabulated volumetric amounts for the TVFF annual water balance, in thousands of m^3 , are shown in Table 8. The water balance is presented graphically alongside the mass balance for the groundwater flow model later in Figure 36.

Table 8. Volumetric Amounts for the TVFF Annual Steady-State Water Balance

	Inflows (1000 m^3)				Outflows (1000 m^3)				Avg Water Table Elevation (masl)	Change In Storage (1000 m^3)
	Precip.	Upland Contribution	River Leakage	Irrigation	ET	Baseflow	Pond Refill	Net Exchange		
January	120.6	61.5	58.6		12.9			75	641.3	152
February	91.8	61.5	45.3		18.7			135	641.7	45
March	46.9	61.5	18.5		25.6			127	641.5	-26
April	38.7	120.4	111		27.1			306	640.9	-63

May	29.9		44.9	12.3	57.8		14.5	83	640.2	-68
June	18.1			12.3	71.9	120	14.5	-121	639.7	-55
July	2.30			12.3	68.3	124	14.5	-75	638.6	-117
August	5.39			12.3	52.8	124	14.5	-164.6	638.5	-8.9
September	25.0			12.3	32.8	120	14.5	-189	639.1	59
October	82.9		15.0		15.0			65.5	639.2	17
November	90.8		27.3		12.9			55	639.7	50
December	111.7		32.3		10.1			119.0	639.8	15.0
TOTALS	664	305	353	61.6	406	488	72	417	ΔS =	0

GROUNDWATER FLOW MODEL

This study uses a high-resolution site-scale numerical groundwater flow model to investigate the potential for enhanced groundwater seepage into the Teanaway River by simulating MAR in the form of delayed infiltration of surface water runoff in an ephemeral creek. The work seeks to characterize the exchange of water between the Teanaway River and the shallow alluvial aquifer in the floodplain adjacent to the river. This groundwater flow model uses the program MODFLOW, short for “Modular three-dimensional finite-difference ground-water flow,” a numerical groundwater modeling code from the USGS. The first version was released in 1984 and continues to be the industry standard in groundwater modeling (USGS, 2020). MODFLOW operates with “packages” that handle individual aspects of the numerical simulation. For example, calculations for the hydraulic connection between a river and an aquifer are performed by the “RIV” package. The commercial product Visual MODFLOW Flex 7.0 (Waterloo Hydrogeologic, 2021) was employed here as the graphical user interface for processing the MODFLOW code.

The groundwater flow model was constructed by representing the physical characteristics of the TVFF site mathematically, choosing a temporal scale, and applying boundary conditions to control inputs and outputs of water to the system. The time frame for this model is 5 years and 1 month, commencing on March 1, 2017, and ending on March 31, 2022. Complete records of monthly inputs for precipitation and river stage were available for the entire 5 years, and evaporation records available for years 2017 to 2021. Water level observations in the on-site wells overlap with the last 2 years of this period.

Model Domain and Initial Conditions

The model domain is comprised of the floodplain between the Teanaway Road and the Teanaway River, extending northwest to southeast from a former sawmill to the WDFW property boundary at an ephemeral creek informally known as John Creek (Figures 29 and 32). For the numerical representation of the physical location, the area is discretized horizontally into 10-meter by 10-meter cells, resulting in a 182 × 91 grid. The vertical discretization is 10 total layers of varying depth. Surface topography for the model is constructed from a 1/3 arc-second digital elevation model (DEM) data from the USGS National Map 3D Elevation Program, 3DEP (U.S. Geological Survey, 2017) and provides approximately 10-meter spatial resolution. Subsurface horizons are established by subtracting a prescribed depth from the surface elevation. This depth varies and is informed by

well logs from wells on and adjacent to the site and by the USDA NRCS Web Soil Survey (NRCS, 2022).

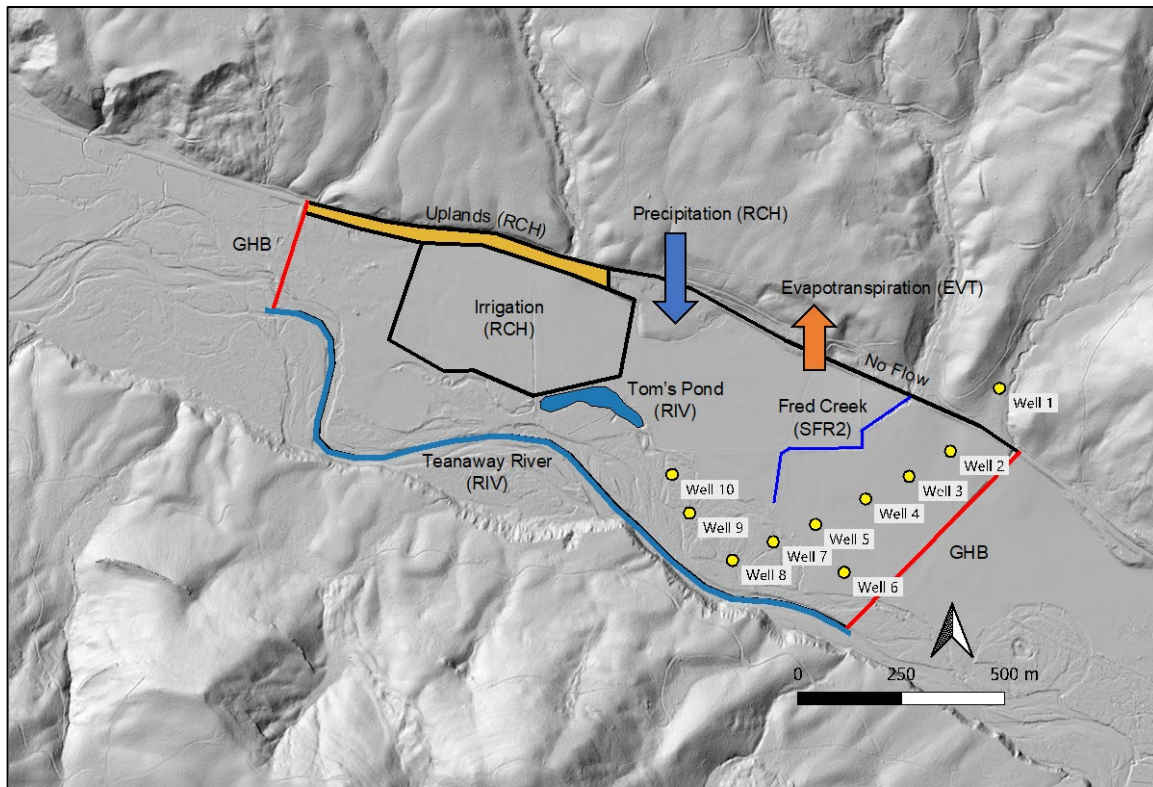


Figure 32. The model domain with its boundary conditions. Teanaway Road on the north side of the model domain is a no-flow boundary. General head (GHB) boundary conditions are on the east and west ends of the model domain, and the Teanaway River is a river (RIV) boundary condition on the south perimeter. Tom’s Pond is also represented by a RIV boundary condition. Recharge (RCH) boundary conditions include the uplands, irrigation, and precipitation, which covers the entire model domain. The evapotranspiration (EVT) boundary condition likewise blankets the model domain. Fred Creek is represented by the streamflow-routing (SFR2) boundary condition.

Three subsurface horizons divide the model domain into four vertical layers according to site stratigraphy based on well logs and site observations. These four hydrostratigraphic units are: an uppermost topsoil unit, a subsurface alluvial unit of silt, sand, and cobbles, a second alluvial unit having lower permeability and composed of silty clay, and the sandstone bedrock of the Roslyn formation. These layers are informally referred to by the names “Soil,” “Cobbles,” “Clay,” and “Sandstone,” respectively. Details of these units, their thicknesses, composition, and relationships are given in Henning (2023). Figure 33 presents a cross section of these four stratigraphic layers in the model. The silty clay layer is similar in composition to the glacial gray silt described in Chapter 2 of this report and in Polizzi (2023).

Within the model, the cobbles and clay layers are each further subdivided into 2 layers, and the sandstone is subdivided into 5 layers. Refinement of the vertical discretization is employed to accommodate the bed elevations of the surface water features more accurately, i.e. the Teanaway River and Tom’s Pond.

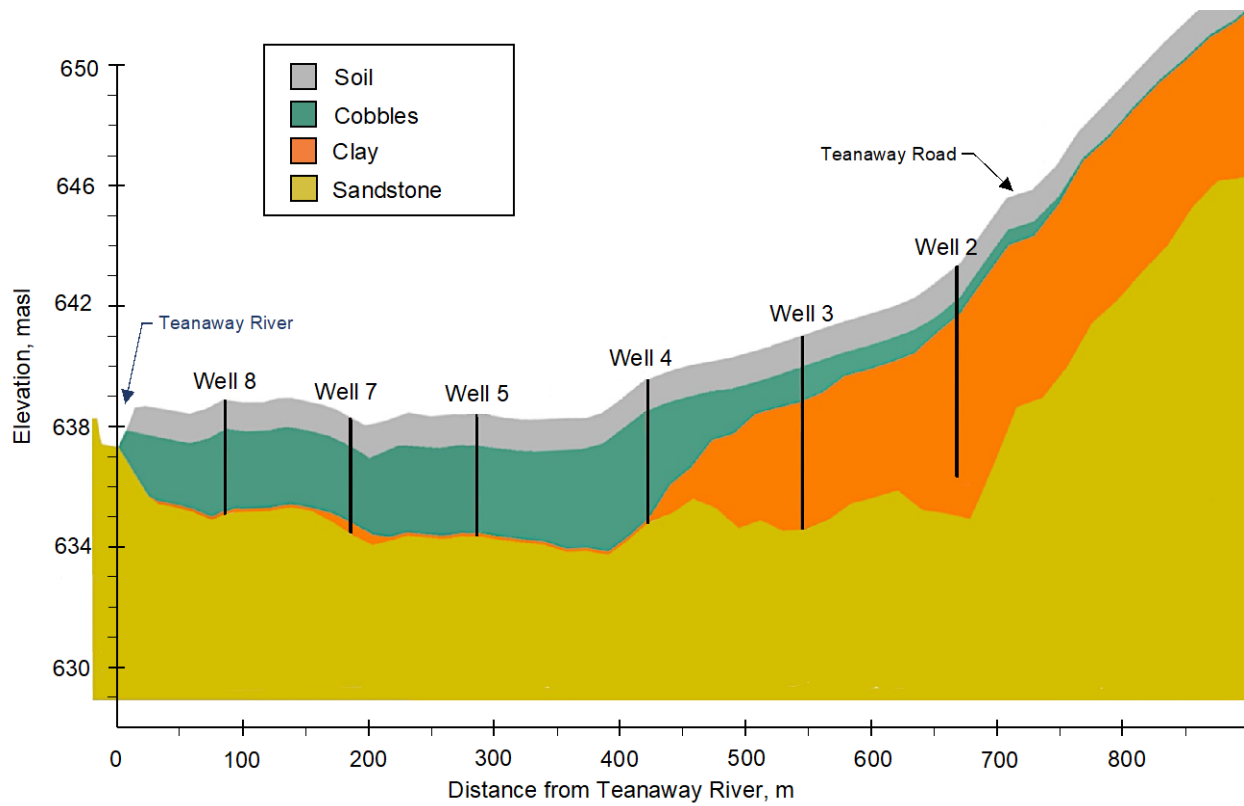


Figure 33. Cross section along the line of Wells 2 through 8 at TVFF. The clay unit terminates between Wells 3 and 4 roughly halfway between Teanaway Road and the Teanaway River. The cross section is generated from DEM surfaces used in the groundwater flow model.

The initial flow parameters for the vertical layers are listed in Table 9. The hydraulic conductivity of the soil layer is approximated from NRCS (2022). The hydraulic conductivity obtained from the Roslyn formation by Gendaszek et al. (2014) is used here as a first approximation for the sandstone layer. Other values of hydraulic conductivity are from the slug tests performed at the site. In the initial model run, horizontal and vertical hydraulic conductivity were taken to be equivalent and no anisotropy is assumed ($K_x = K_y = K_z$). Subsequent model runs adopt a modeling rule of thumb that the vertical hydraulic conductivity is an order of magnitude less than the horizontal hydraulic conductivity: $K_z = 0.1K_x$. Values of specific yield and specific storage used in the model are from literature (Lv et al. 2021, Johnson 1967, Woodward 2002, and Chowdhury et al. 2022). Porosities for sediment samples were measured in the laboratory. The porosity of the sandstone was calculated by the method of Scherer (1987) using properties described in Bressler (1951) and the most recent age information from Eddy et al. (2016).

The start date of the model (March 1) and initial heads for the transient simulation were selected based on the transducer observations of water level data. For the period of observed record, the average maximum water level in the wells occurred around February 24, and the average maximum water surface elevation was approximately 0.74 meters below ground surface if Well 2 is disregarded (0.98 m if Well 2 is included). For the date of March 1, the average water surface elevation was 0.90 m below ground surface without Well 2 and 1.16 m with Well 2 included.

MODFLOW requires that cells do not begin dry, so the initial heads must be within the top model layer. In this case the top layer of the model is the soil layer, which has a 1 m depth, therefore initial heads of 0.75 m below ground surface were used.

Table 9. Initial Flow and Storage Parameters Used in the Model

Model Zone	Well Number	Measured K (m·s ⁻¹)	Initial Model K _x = K _z (m·s ⁻¹)	Specific Yield	Specific Storage	Porosity
1 – Soil		1.4 × 10 ⁻⁵ to 4 × 10 ⁻⁶	1 × 10 ⁻⁵	0.20	1 × 10 ⁻⁴	0.43
2 – Cobbles	4	1.16 × 10 ⁻⁴	3 × 10 ⁻⁴	0.20	1 × 10 ⁻⁴	0.43
	5	1.25 × 10 ⁻⁴				
	6	4.16 × 10 ⁻⁴				
	8	4.59 × 10 ⁻⁴				
3 – Clay	2	7.16 × 10 ⁻⁵	7 × 10 ⁻⁵	0.10	4.3 × 10 ⁻⁵	0.43
4 – Sandstone		5.64 × 10 ⁻⁶	6 × 10 ⁻⁶	0.10	2.6 × 10 ⁻⁶	0.26

Boundary Conditions

Six distinct boundary conditions are assigned in the model (Figure 32). They are the river (RIV), recharge (RCH), streamflow-routing (SFR2), evapotranspiration (EVT), general head (GHB), and no-flow boundary conditions. By default in Visual MODFLOW Flex 7.0, a no-flow boundary condition is assigned to model cells along the perimeter of the model domain when no other boundary condition is assigned at that location. For this model, no-flow boundary conditions are applied at the bottom of the sandstone unit and along a portion of Teanaway Road. The no-flow boundary condition along the road is justified because the road acts as a barrier to surface water flow and precipitation recharge, and the direction of the surficial aquifer groundwater flow in this location generally follows the gradient of the surface topography, which is parallel to the boundary.

River Boundary Condition

The Teanaway River flows from northwest to southeast along the southern perimeter of the model domain. The river is incised through the soil and cobbles layers and has primarily a bedrock channel of the Roslyn sandstone (Schanz, 2019). MODFLOW’s river boundary condition (RIV) is used to model the Teanaway River. In the RIV boundary condition, groundwater flux moves only through the river bottom; no flow takes place through the sides of the channel (Figure 34). This ideally represents the characteristics of water movement in the Teanaway River at TVFF through the incised bedrock channel and not through the banks of the river.

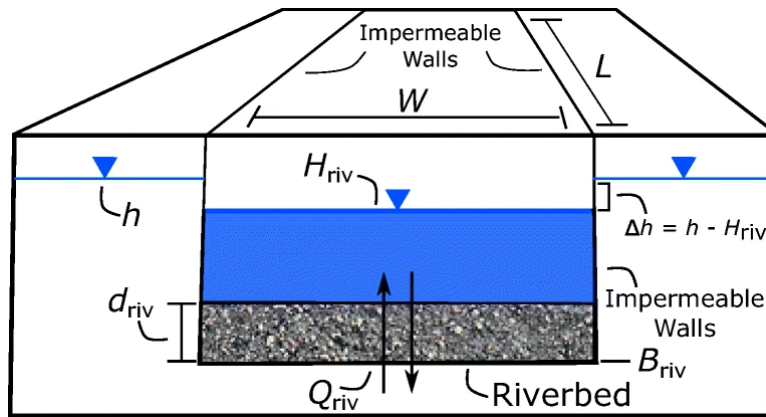


Figure 34. Schematic diagram of the river boundary condition (RIV). The diagram shows that river-aquifer exchange is vertical through the riverbed. Here, Q_{riv} is the flux that is calculated through the bed, B_{riv} is the bed elevation, d_{riv} is the riverbed thickness, also known as the clogging layer, H_{riv} is the stage of the river, W is the width of the river and L is the length (from Ghysels et al. 2019, after McDonald and Harbaugh, 1988). The RIV boundary condition is a head-dependent flux boundary condition.

The required parameters for the RIV boundary condition are the hydraulic conductivity of the clogging layer, K_{riv} ($L \cdot T^{-1}$), the thickness of the clogging layer, d_{riv} (L), the riverbed elevation, B_{riv} (L), the channel width, W (L), and the river stage, H_{riv} (L). Length, L (L), is also an input parameter, and is the calculated length of a reach of river; it is the distance between designated nodes at the start and end points of a reach. For the Teanaway River adjacent to the model domain, the width is fairly uniform and is approximately 30 meters. The thickness of the clogging layer is also estimated to be uniform and is taken to be 0.1 meters. Since the clogging layer is assumed to be the cobble layer immediately above the sandstone of the bedrock channel, the hydraulic conductivity of the cobble layer, $3 \times 10^{-4} \text{ m} \cdot \text{s}^{-1}$, is used as a first approximation for the riverbed conductivity. The riverbed elevation is extracted from the DEM of the top surface of the sandstone layer at 30 nodes along the length of the reach and is linearly interpolated between nodes. Refinement of the vertical discretization of the sandstone layer into 5 model layers and not one single layer contributes to greater accuracy in representing the actual elevation of the river bottom in the model.

The stage of the river was determined from a rating curve based on gage readings from a TVFF Teanaway River site and discharge information from the Teanaway River Forks gage upstream of the site (Station ID 12480000; 47.25 °N, 120.86 °W). The median monthly stage height was calculated and input at each of the 30 nodes of the RIV boundary condition.

The RIV boundary condition was also used for Tom’s Pond. The stage varied seasonally depending on whether irrigation is occurring in the adjacent field or not. During months when no irrigation is being applied (October through April), the stage is “full” at a constant elevation of 641.3 masl. At times when irrigation occurs (May through September), the stage is lowered to 639.7 masl. The lower stage is computed by subtracting the approximate volume of water removed from the pond that is applied as irrigation water to the nearby field and accounting for the efficiency of the irrigation system. Like the Teanaway River, the clogging layer for Tom’s Pond is assumed to be the cobbles model layer, and the same thickness and hydraulic conductivity of 0.1 m and $3 \times 10^{-4} \text{ m} \cdot \text{d}^{-1}$, respectively, are used.

Recharge Boundary Condition

The recharge boundary condition (RCH) was used to apply precipitation and irrigation fluxes to the uppermost active layer of the model domain. Precipitation amounts were obtained from the PRISM Climate Group of Oregon State University (PRISM 2022). Irrigation recharge amounts were informed by the amount of water typically applied to Timothy hay in a semi-arid climate (Efetha, 2009) and the USGS Precipitation-Runoff Modeling System (PRMS) and Deep Percolation Model (DPM) models of Vaccaro and Olsen (2007). Vaccaro and Olsen (2007) estimated 381 mm of annual irrigation recharge in the region containing the TVFF site.

Two catchments in the uplands adjacent to TVFF contribute recharge via runoff to the model domain: the Fred Creek catchment and an unidentified creek catchment (Figure 35). The RCH boundary condition is utilized to simulate recharge from seasonal overland flow from the unidentified creek catchment, and the streamflow-routing package (SFR2) is used to simulate the contribution from the Fred Creek catchment

In the area west of the unidentified creek, overland flow proceeds to the Teanaway River upstream of the model domain, thus recharge from this catchment area is considered with the river. Similarly, overland flow in the catchment east of the Fred Creek catchment is considered elsewhere. This flow is captured by John Creek, the eastern boundary of the model domain. John Creek mainly influences groundwater downstream of the model domain; its influence on the model domain itself is captured by the general head boundary condition (detailed below) imposed on the eastern side of the model.

The recharge contribution from upland catchment areas to the model domain has 2 key components: the volumetric amount of recharge and the timing at which it is delivered. The volume of recharge is net precipitation times the catchment area, where net precipitation is the amount of precipitation that falls in the form of rain or snow less evapotranspiration losses. From the months of October through March, net precipitation is positive, but from April through September, net precipitation, on average, is negative, i.e., evaporative losses exceed amounts of precipitation (PRISM, 2022 and Running et al., 2021). Precipitation generally falls as snow from November to January and is stored as snowpack. In January, snowmelt begins and rain-on-snow events in late January and early February contribute to increases in snowmelt.

Upland recharge is delivered to the model domain via ephemeral creeks that have been observed to flow from January through April. The recharge delivered in January and into February, March, and April includes net precipitation that fell as snow in prior months. To account for this offset in timing, the total volume of net precipitation in the catchment was summed over the months of November through March, and then 20% of this sum was assumed to be delivered to the model domain in each of the months of January through March, and 40% of this sum was assumed to be delivered in April. The percentages are derived from the proportion of the volume of flow in the Teanaway River from January through April, since tributaries in the basin are controlling the runoff in the river during this time. The volume of net precipitation from October is excluded from the total upland recharge calculation because, even though net precipitation is positive for the month of October, no runoff is

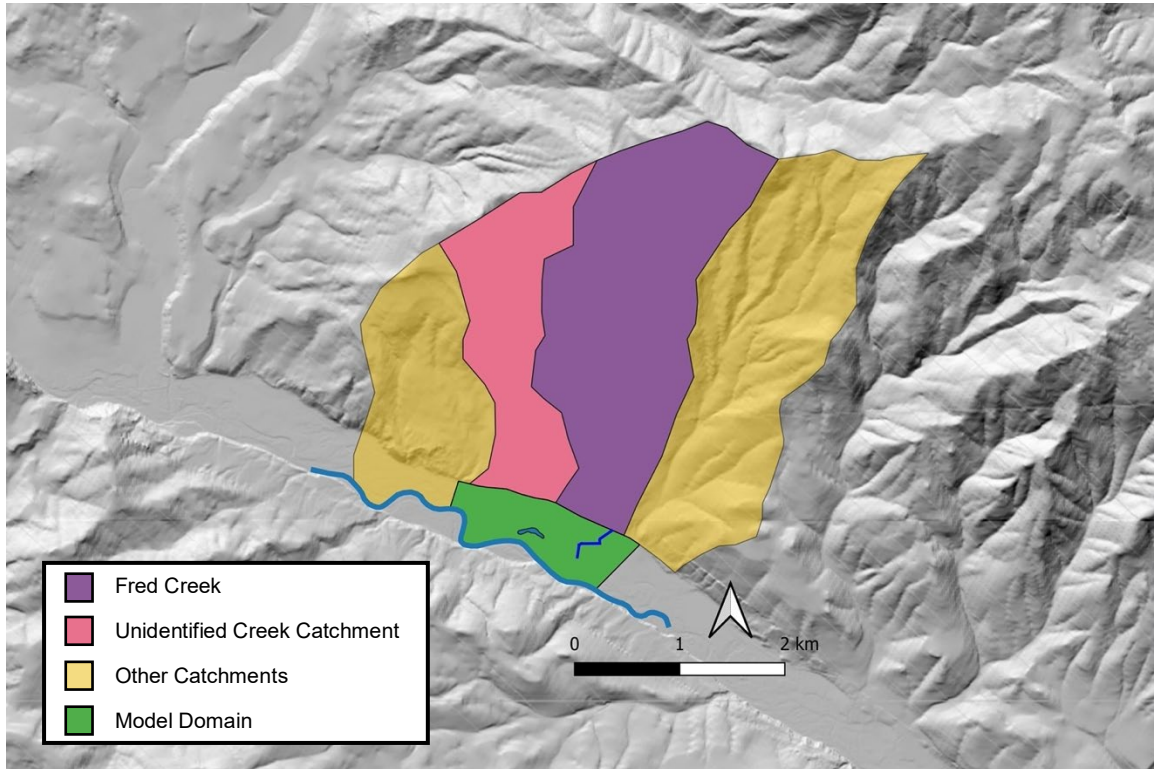


Figure 35. Catchments that contribute runoff to the model domain. The Fred Creek catchment and the Unidentified Creek catchment are shown here. Runoff from the upstream (west) catchment is delivered to the Teanaway River upstream of the model domain. Runoff from the downstream (east) catchment flows into John Creek, which delineates the eastern boundary of the model domain. Flow in Fred Creek, the unidentified creek, and John Creek passes under Teanaway Road via culverts, otherwise it continues downstream in the ditch on the north side of the road.

observed in the on-site creeks at this time. It is assumed that October net precipitation restores soil moisture through infiltration.

After applying the monthly timing percentages to the total volume of upland recharge, an additional volume adjustment based on channel geometry was performed so that the applied amount of recharge is realistic for the size of the channel conveying it. At capacity in April, Fred Creek can convey 2.25% of the 40% of the total volume of net precipitation from its catchment area. The ditch on the northwest border of the site was assumed to be similar, holding 2.25% of the 40% of the total volume of net of precipitation from the unidentified creek catchment. For simplicity, these capacity percentages were assumed to be applicable in January, February, and March also. The computed amount for the unnamed creek catchment was applied to the model as a recharge flux ($\text{mm}\cdot\text{yr}^{-1}$) in the RCH boundary condition, and the computed amount for the Fred Creek catchment was applied as depth of flow (m) in the SFR2 boundary condition, detailed next.

Streamflow-Routing Boundary Condition

Fred Creek is an ephemeral stream that originates in the uplands to the north of the model domain. It reaches the model domain via a culvert under Teanaway Road, and its path across the floodplain is anthropogenically modified into a series of straight segments along property lines to convey water between irrigated (and formerly irrigated) fields. The creek does not have a definitive outlet into the Teanaway River. It terminates with shallow ponding near the river in the cobble-sized alluvium that has never been plowed for farming.

Because of its nature as an ephemeral stream and because different model scenarios required changing this feature, Fred Creek is modeled with the SFR2 boundary condition. For the SFR2 boundary condition, a stream network is discretized in the model domain with the geometry and flow characteristics of the stream channel. Details of this discretization are given in Henning (2023).

It should be noted that the Teanaway River is not modeled as part of the streamflow network. This was for two reasons: Fred Creek does not directly connect to the river at the surface, and the bed of the Teanaway River is the Roslyn sandstone, which is not the uppermost model layer as required by the SFR2 package. Surface flow in Fred Creek terminates with ponding before it reaches the river, which can be represented with the SFR2 boundary condition. The RIV boundary condition is more ideal for modeling groundwater flux through the bedrock channel of the Teanaway River.

Evapotranspiration Boundary Condition

Boundary conditions that removed water from the model domain are evapotranspiration (EVT) and general head (GHB) boundary conditions. The EVT boundary condition was applied as a flux from the uppermost active layer of the model over the entire domain. Evapotranspiration amounts for each monthly stress period from 2017 to 2021 are based on remote-sensing based estimates from the MODIS/Terra Net Evapotranspiration Gap-Filled 8-Day L4 Global 500 m SIN Grid (MOD16A2GF v061) data set, available publicly from the USGS (Running et al., 2021). Data was not available for 2022, so the average of the years 2017 to 2021 was substituted for 2022. The EVT boundary condition is a head dependent flux boundary condition: the rate of water leaving a cell assigned this boundary condition is a maximum when the head is at a high level in the cell but drops to zero via linear interpolation when the head in the boundary cell falls below a specified level, known as the extinction depth. Extinction depth is a function of soil type and land cover. The land cover over the model domain is 82% bare soil and 18% grass in the growing season. A uniform extinction depth of 4 meters is used across the entire model domain, informed by the results of Shah et al. (2007) shown in Table 10.

Table 10. Extinction Depth (cm) for a Given Soil and Land Cover Type.

Soil Type	Land Cover Type (cm)		
	Bare Soil	Grass	Forest
Sand	50	145	250
Loamy sand	70	170	270
Sandy loam	130	230	330
Sandy clay loam	200	300	400
Sandy clay	210	310	410
Loam	265	370	470
Silty clay	335	430	530
Clay loam	405	505	610
Silt loam	420	515	615
Silt	430	530	630
Silty clay loam	450	550	655
Clay	620	715	820

Note: Depths are rounded up to the nearest 5 cm. Maximum rooting depth for grass and forest was assumed to be 100 and 200 cm, respectively. Reproduced from Shah et al. (2007).

General Head Boundary Condition

The model domain is contained within a larger catchment area and does not have natural hydrologic boundaries on either its east or west edges. To account for the exchange of groundwater between the model domain and the areas adjacent to these two ends of the model, general head (GHB) boundary conditions are used at either end. Flow into or out of a GHB cell is calculated in proportion to the head difference between the model domain water table and the specified head in the boundary cell, allowing for water to flow into the model domain if the water table falls below the specified head and out of the model domain if the water table rises above the specified head. The constant of proportionality used in the head calculation is a conductance computed from the average hydraulic conductivity of the material between the edge of the model and the GHB cell and the individual cell geometry. The initial hydraulic conductivity used is that of the cobble layer, $3 \times 10^{-4} \text{ m}\cdot\text{s}^{-1}$. First approximations for the head in the GHB boundary conditions are the linear edges of the best fit plane computed through the average monthly head elevations in the 9 floodplain observation wells. The GHB head elevations and hydraulic conductivity were adjusted during model calibration to improve results.

Unsaturated Zone Flow

Approximation of unsaturated zone flow in the model uses the UZF package. This package simulates vertical flow through the vadose zone, distributing recharge (and evapotranspiration) to the groundwater table from the “top down” rather adding the volume of infiltration to the water table as direct recharge, which would be analogous to addition from the “bottom up.” The rate of recharge is approximated using a kinematic wave equation and requires specification of three additional parameters: the initial water content of the vadose zone, the residual water saturation, and the Brooks-Corey exponent, which is used in the relationship between the saturated hydraulic conductivity and the water content. In this groundwater flow model, a value of 3.0 was used for the

Brooks-Corey exponent, the initial saturation of the vadose zone was taken to be 0.9 (since the model’s starting time is March 1, 2017, and the observed water levels in the monitoring wells at that time are near the ground surface), and the residual saturation was assumed to be 0.2.

Model Calibration

The model was calibrated so that the computed hydraulic heads and the measured hydraulic heads were within a percentage Root Mean Square (RMS) error less than 10%, and the analytical mass balance and model mass balance agreed within 10%. To accomplish the calibration manually, the hydraulic conductivity and specific yield were varied systematically within realistic ranges for alluvium and sandstone, and boundary conditions in the model were adjusted to achieve the appropriate volumetric mass balance output.

Table 11. Flow and Storage Parameters in the Calibrated Model.

Model Zone	Well Numbers	Initial Model $K_x = K_z$ ($m \cdot s^{-1}$)	Calibrated Model K_x ($m \cdot s^{-1}$) $K_z = 0.1K_x$	Initial Model Specific Yield	Calibrated Model Specific Yield
1 – Topsoil		1×10^{-5}	5×10^{-4}	0.20	0.19
2 – Cobbles	4 – 10	3×10^{-4}	1×10^{-3}	0.20	0.23
3 – Clay	2, 3	7×10^{-5}	3×10^{-5}	0.10	0.07
4 – Sandstone		6×10^{-6}	8×10^{-5}	0.10	0.10

Comparison of the analytical mass balance and the MODFLOW model mass balance is shown in Figure 36. It is important to note that the two mass balance results are similar in part because the MODFLOW model parameters were adjusted to bring the MODFLOW model results closer to the analytical model results. All boundary conditions were adjusted in some manner to obtain analytical and model mass balances within 10% of one another. Details of these adjustments are given in Henning (2023).

The two mass balance calculations represent different timeframes and assumptions. The analytical mass balance uses average monthly values of precipitation, evapotranspiration, and river exchange for inputs and is for annual steady-state conditions, that is, there is no net change in storage annually. The MODFLOW model mass balance calculates the average annual values from transient conditions over the 5-year model run. Another key difference to note is that the RIV boundary used in the MODFLOW model to represent Tom’s Pond is absent from the analytical mass balance.

The model was calibrated based on nine monitoring wells located in the floodplain. These floodplain wells tap the shallow alluvial aquifer and have logged pressure and temperature readings at 15-minute intervals from August 2019 to present. The most complete, uninterrupted record of water level data for the nine floodplain wells is from January 24, 2020, to April 8, 2022. End-of-month water elevations during this period were used to calibrate the groundwater flow model, with a total of 217 water-level calibration points from Wells 2 to 9 over this two-year time span.

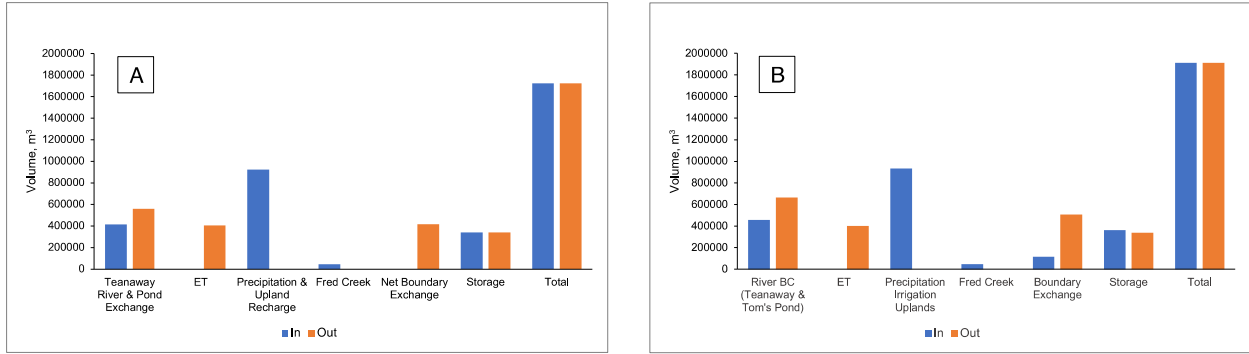


Figure 36. Mass balance. (A) The mass balance obtained using the best-fit plane for water table elevations (the steady-state analytical model), and (B) the mass balance for the transient, 5-year groundwater flow model (the MODFLOW model).

Head values calculated by the model were compared to 217 observed values for goodness of fit. The final model inputs (including parameters in Table 11) achieved an RMS error of 0.45 m, or 8.45%. Calibration results are presented in Figures 37 and 38.

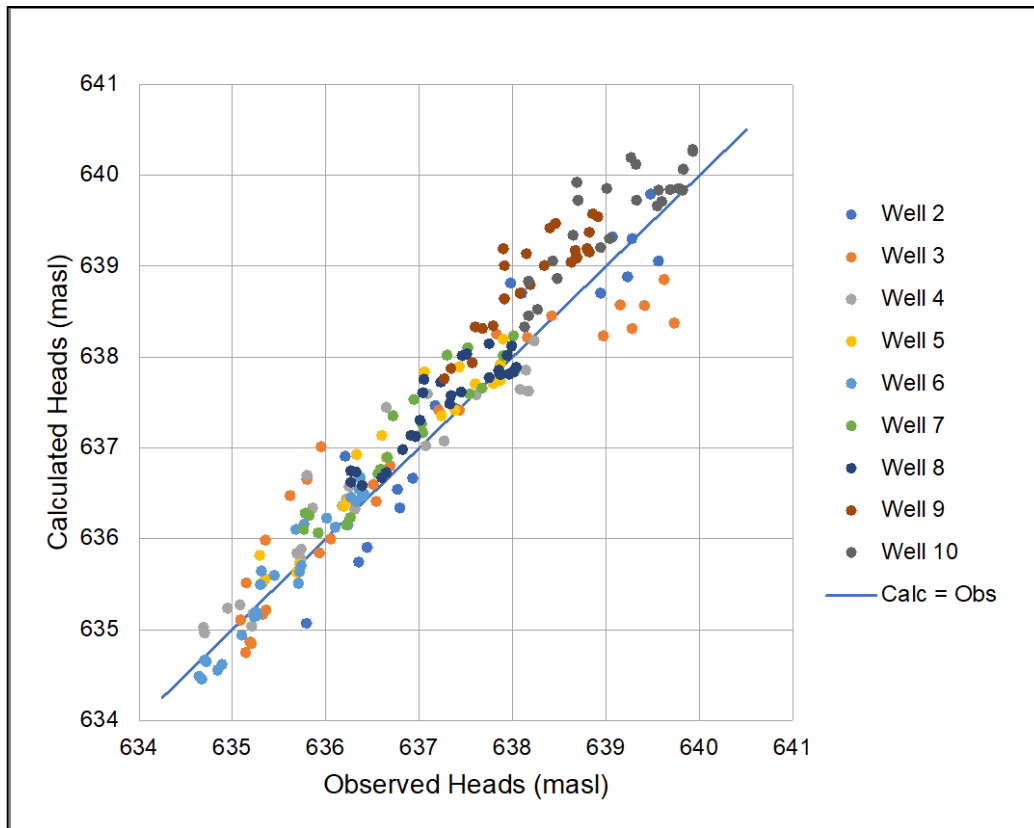


Figure 37. Modeled vs. observed head elevations. Head elevations calculated by the groundwater flow model are plotted against all observed values for times $t = 1067$ days to $t = 1857$ days. The line demonstrates where the calculated head elevation is equivalent to the observed head elevation.

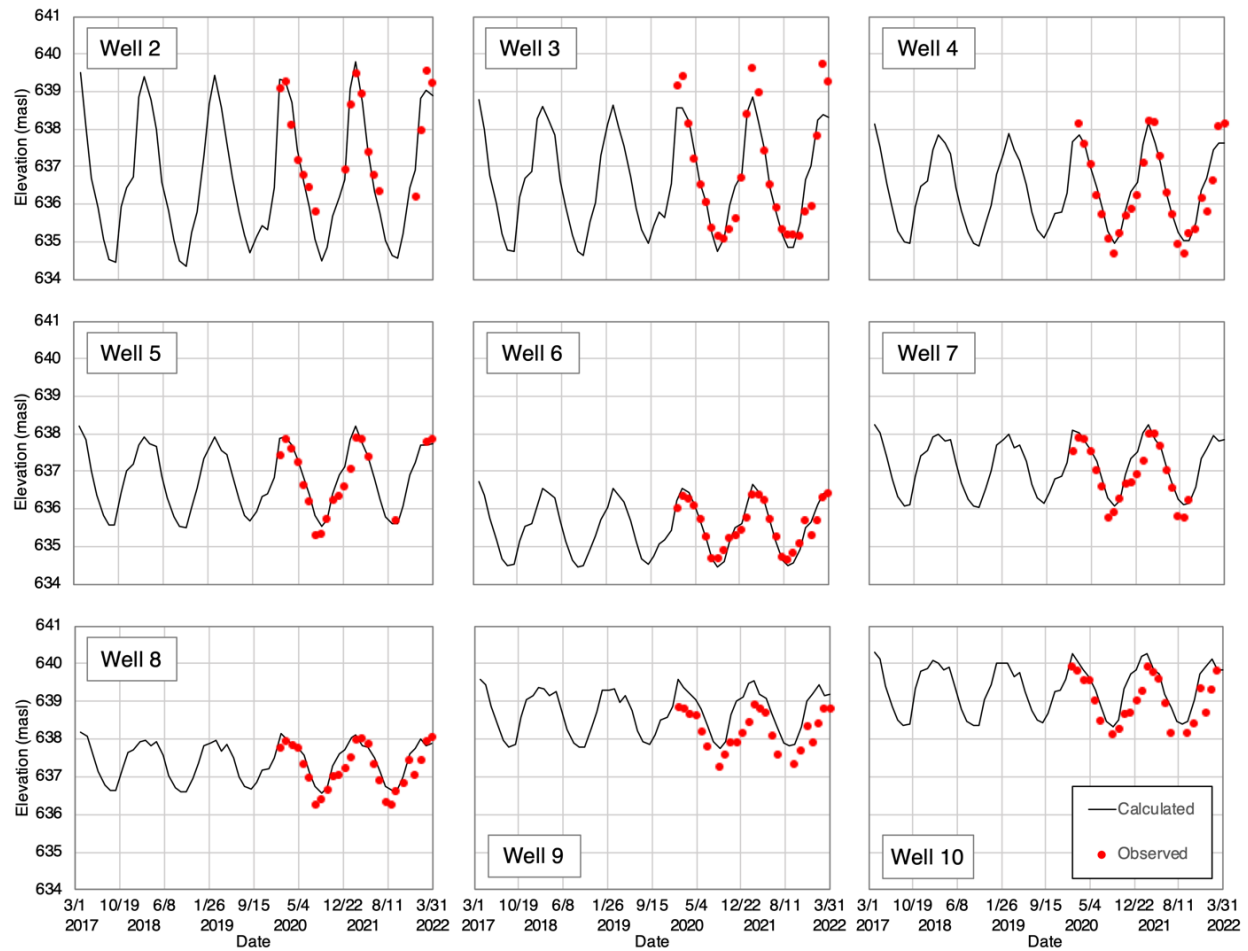


Figure 38. Head elevations calculated by groundwater flow model over the model time frame. Time frame is March 1, 2017 through March 31, 2022 for each of the Wells 2 through 10. Observed values at the end of each month beginning January 31, 2020 through March 31, 2022 are plotted. Data gaps exist for Wells 5 and 7 due to transducer failures, and there are no observations for Well 2 in the months of July through September because the well goes dry.

Model Scenarios

Once the groundwater flow model was calibrated, the SFR2 boundary condition representing Fred Creek was modified to simulate the capture of flow in a shallow pond. The change in heads and mass balances between the calibrated model and the modified model could then be compared to determine any changes in storage realized from an infiltration pond.

In the calibrated model, the existing creek was discretized as 4 segments that followed the anthropogenically channelized course. For the modified creek, the first segment was left unchanged. The remaining segments were modified to follow the theoretical stream course that would have existed had the creek not been channelized. This was the natural low in the surface topography as determined by the Strahler stream-ordering algorithm from the surface DEM in a GIS (van der Kwast and Menke, 2021). No further changes were made to geometry or flow conditions in the third and fourth segments of the creek. The hydraulic conductivity for all segments was fixed at $0.23 \text{ m}\cdot\text{s}^{-1}$.

The second segment of the creek was modified to simulate an infiltration pond. This segment, which is 110 m in length, was widened in successive simulations to 8, 10, 20, 30, and 35 meters, respectively. Numerical instability prevented modeling a pond wider than 35 m. The specified depth condition was used for the channel in the same way that it was used in the calibrated model. In the model scenarios, the depth of the second segment was deepened from 0.24 m in January, February, and March to 0.44 m, and from 0.49 m in April to 0.63 m. The depth of 0.63 m was the maximum depth allowed under the constraints of the SFR2 boundary condition. This depth required reducing the thickness of the soil beneath the channel bottom to 0.1 m to maintain the channel in the topmost layer of the model. At the maximum depth in the month of April, the trial ponds ranged in size from 554 m³ to 2430 m³ (approximately 0.449 to 1.97 acre-feet). The original and modified Fred Creek are shown in Figure 39.

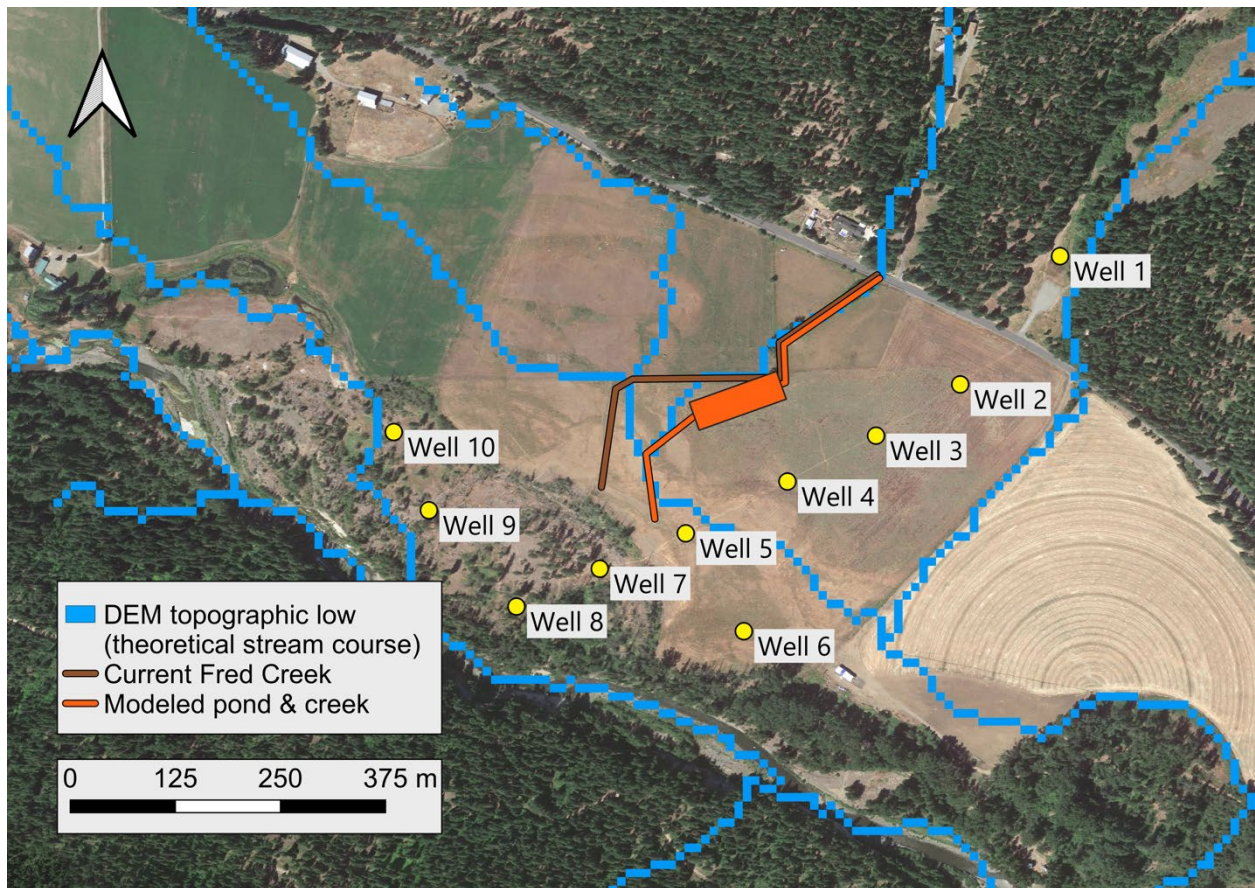


Figure 39. Map of model scenarios. The channelized Fred Creek was modeled as part of the calibrated groundwater flow model. Modeled scenarios modified Fred Creek and created ponds 0.63 m deep of different widths with volumes from 554 m³ to 2430 m³ (0.449 to 1.97 acre-feet), shown as orange. The pond depicted in the figure is the largest modeled, 110 m long and 35 m wide. Blue lines delineate the theoretical stream course calculated from the DEM topography by the Strahler stream-ordering algorithm in GIS.

Scenario Results - Net Storage and Discharge

The addition of an infiltration pond on the TVFF property increases heads in the observation wells and increases the volume of water at the downstream boundary, and it also increases the output of the system to the river and the total volume of the system. Figure 40 demonstrates that the

additional water added by an infiltration pond triggers less additional water input to the system from storage and more water to leave the system via outflow into the river. The greater magnitude of water exiting to the river demonstrates that the additional volume added by a pond does not stay in the system. The timing and volume of discharge into the river is shown in Figure 41, and similar to the behavior of the groundwater heads: discharge is high in the spring when the simulated pond is present and tapers down to baseline levels in the fall.

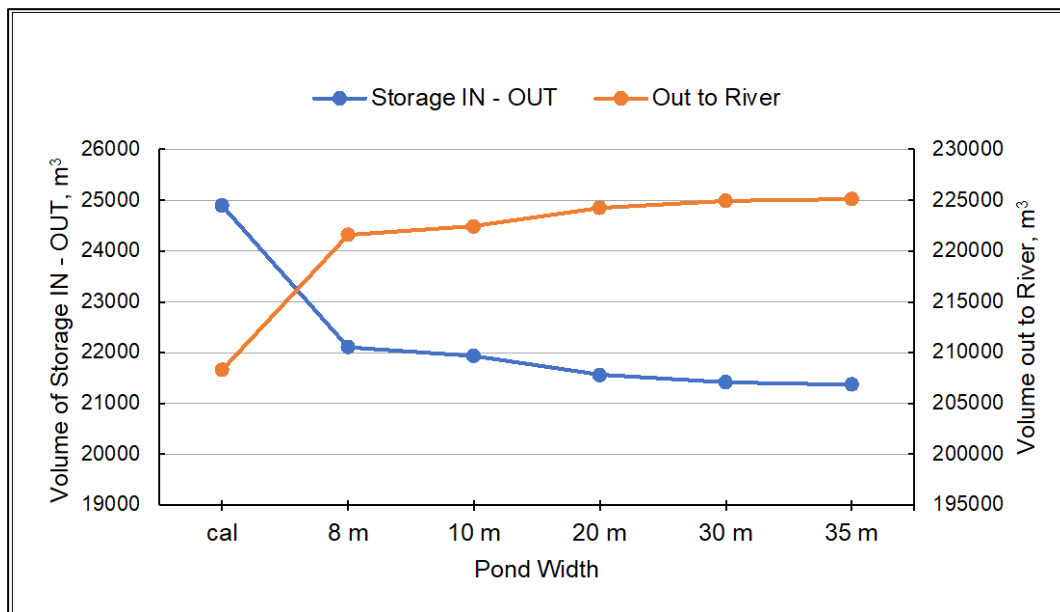


Figure 41. Volume of water input and output for each model scenario. The volume of water added to the system from storage exiting to the river for the calibrated model (cal) and each model scenario.

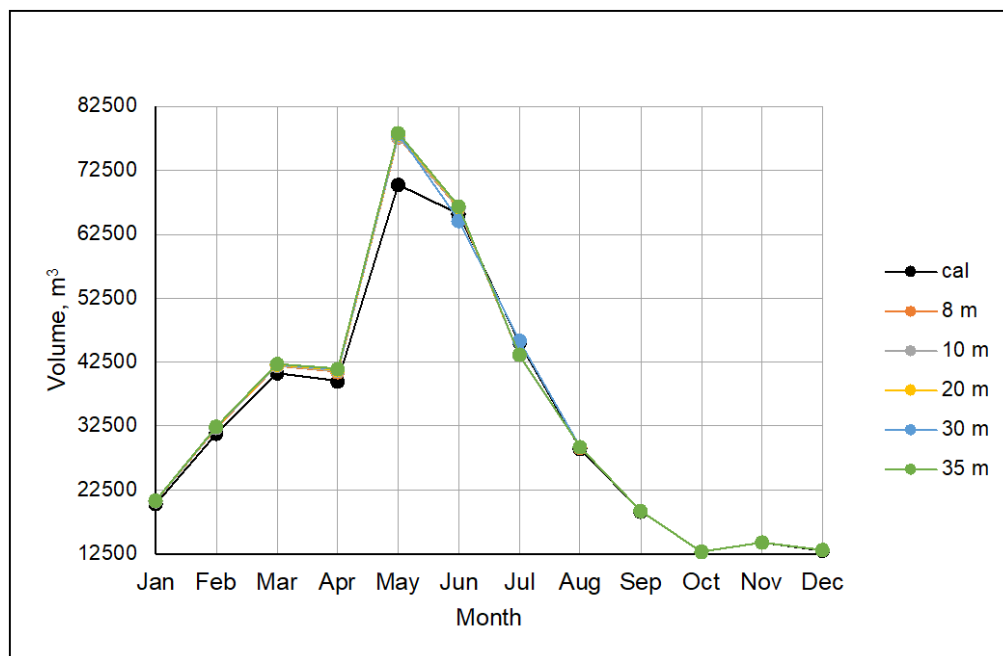


Figure 40. Modeled discharge to the Teanaway River. Average monthly volume of discharge to the Teanaway River for the calibrated model (cal) and the modeled pond scenarios, indicated by pond width.

Scenario Results – Groundwater Levels

The modeled pond scenarios input water to the system in January through April, theoretically capturing additional runoff from the Fred Creek catchment area that would otherwise discharge into the Teanaway River. The infiltrated water from the ponds increases the heads at observation well locations, increases the volume of water output at the downgradient model domain boundary and out to the river, and reduces the input to the system from storage. Overall, the total volume of the system increases. Water levels in each pond scenario increase above the calibrated heads in the months of January through April, but return to baseline levels in the fall months. The greatest increases over the calibrated model occur in April when the simulated pond has the greatest depth. These are summarized in Table 12. Well 4, immediately downstream of the pond location, has the largest increase of all the wells at 0.76 m, which occurs during the simulation with the largest 35-meter wide pond. This simulated maximum water elevation of 638.56 masl is 0.45 m below the true ground surface elevation. The maximum water elevation at Well 5 comes within 0.03 m of the true ground surface, which is the closest of any well. Well 10 experiences the least amount of increase in head from the pond simulations, and Well 9 has the least variance. Both Wells 9 and 10 are upgradient of the pond location.

Table 12. Average Increase in Water Elevation in April.

	Pond Width in Different Model Scenarios					Maximum (m)
	8 m (m)	10 m (m)	20 m (m)	30 m (m)	35 m (m)	
Well 2	0.20	0.21	0.25	0.27	0.27	0.31
Well 3	0.36	0.38	0.45	0.47	0.48	0.54
Well 4	0.54	0.57	0.64	0.67	0.68	0.76
Well 5	0.33	0.35	0.39	0.40	0.41	0.47
Well 6	0.14	0.15	0.17	0.18	0.18	0.21
Well 7	0.18	0.19	0.21	0.22	0.22	0.26
Well 8	0.09	0.09	0.10	0.11	0.11	0.13
Well 9	0.07	0.07	0.08	0.09	0.09	0.11
Well 10	0.06	0.06	0.07	0.08	0.08	0.09

Figure 42 shows the water level contours in the months of April and September for the calibrated model, the 8-meter wide pond scenario, and the 35-meter wide pond scenario. The pond scenarios in April exhibit higher water levels around Fred Creek as expected. The pond scenarios in September show that water levels return to levels similar to the calibrated model without a pond and any lasting effects of water level increases have diminished. The higher water levels result in increased losses from the aquifer to the streamflow routing network (Table 13), but these losses have stopped by June, similar to the calibrated model.

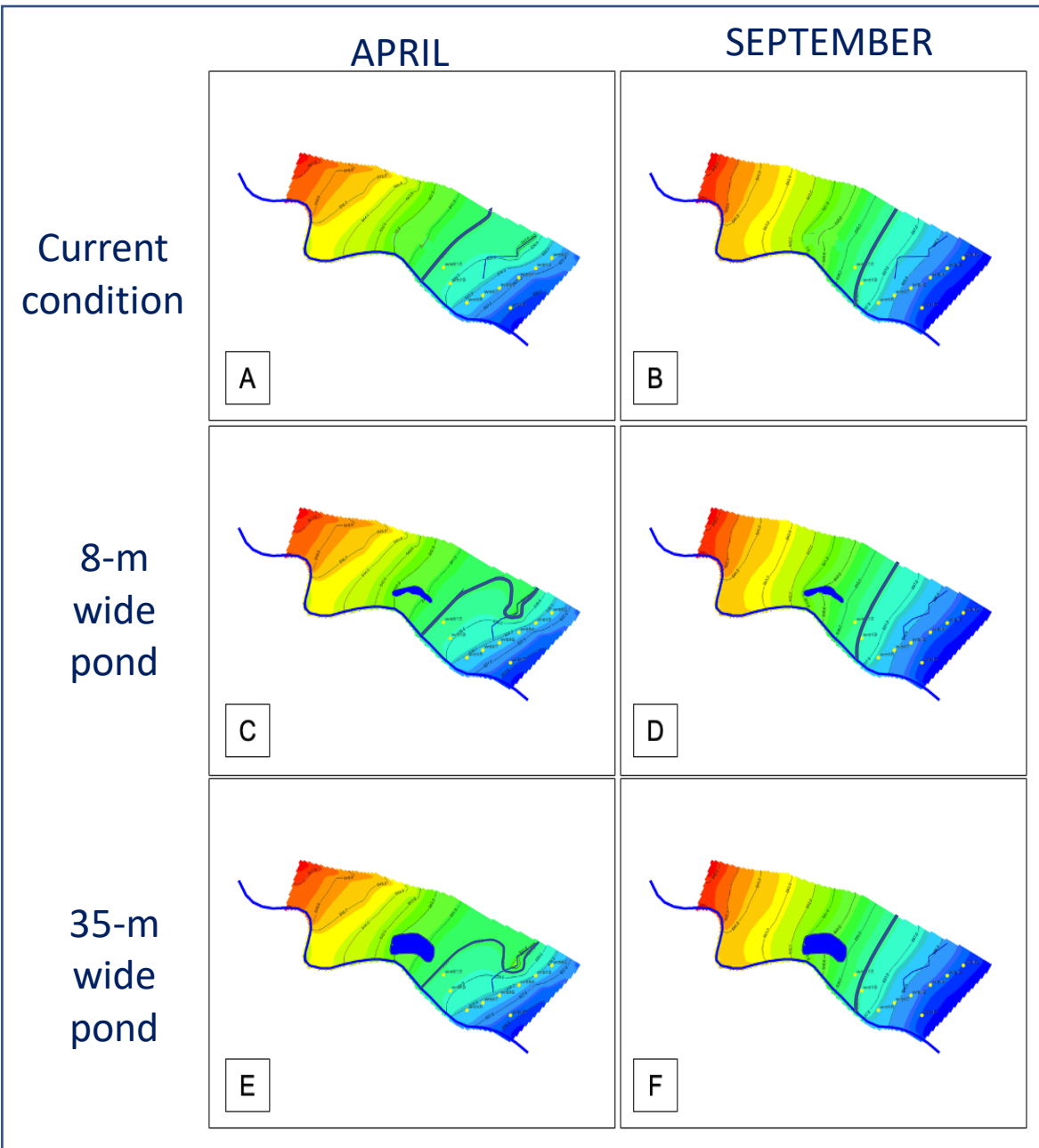


Figure 42. Water elevation contours for different models in April and September of simulation Year 4. (A) and (B): the calibrated model in April and September, respectively, (C) and (D): the model with an 8-meter wide pond in April and September, respectively, and (E) and (F): the model with a 35-meter wide pond, again in April and September, respectively. One contour line is highlighted so that the difference between the different scenario in April and similarities in September can be seen.

Table 13. Average Monthly Leakage from the Aquifer into the Streamflow Routing Network.

	Calibrated	Pond Width in Different Model Scenarios				
	Model (m ³)	8 m (m ³)	10 m (m ³)	20 m (m ³)	30 m (m ³)	35 m (m ³)
January	0	242	282	413	539	566
February	23.2	1057	1187	1600	1833	1918
March	23.3	639	721	1011	1198	1267
April	0	81	95	149	186	201
May	0.6	117	141	227	278	296
June	0	0	0	0	0	0
July	0	0	0	0	0	0
August	0	0	0	0	0	0
September	0	0	0	0	0	0
October	0	0	0	0	0	0
November	0	0	0	0	0	0
December	0	0	0	0	0	0

Scenario Results -- Evapotranspiration

Evapotranspiration is handled in MODFLOW by the EVT boundary condition, which requires an evaporative flux (L^3/T) and a depth below the ground surface where evaporation ceases, known as the extinction depth (Table 10), to be specified. For the calibrated model, the extinction depth was 4 m and the evaporative flux was adjusted from initial values based on MODIS actual evapotranspiration (AET) data (Running et al., 2021) to values which enabled the total evaporative volume to be met.

Figure 43 presents the monthly amounts of AET and potential evapotranspiration (PET) from MODIS data (Running et al., 2021), and the evapotranspiration (ET) computed by the model over the area of the model domain, in mm. Model computed values of ET are nearly identical for all pond sizes. They are greater than AET in the months of November through May, and below AET for June through October. This is not only true of the pond scenarios, but also the calibrated model, and suggests that model calibration should have also considered the temporal nature of the evaporative flux in addition to calibrating for the total annual volume of water removed by evapotranspiration. The slight increase in May of approximately 9 mm for the pond scenarios above the calibrated model denotes the ET contribution from the water surface of the modeled pond.

PET is the upper limit of water loss to evapotranspiration if there were no deficiency in soil moisture for vegetative use. The vertical gap between the AET and PET curves gives insight into the amount of soil-moisture storage, which at the TVFF site is low in the summer months. The modeled pond scenarios do not seem to be improving soil moisture storage, as there is no long-term decrease in the vertical distance between the pond scenario ET curves and the PET curve.

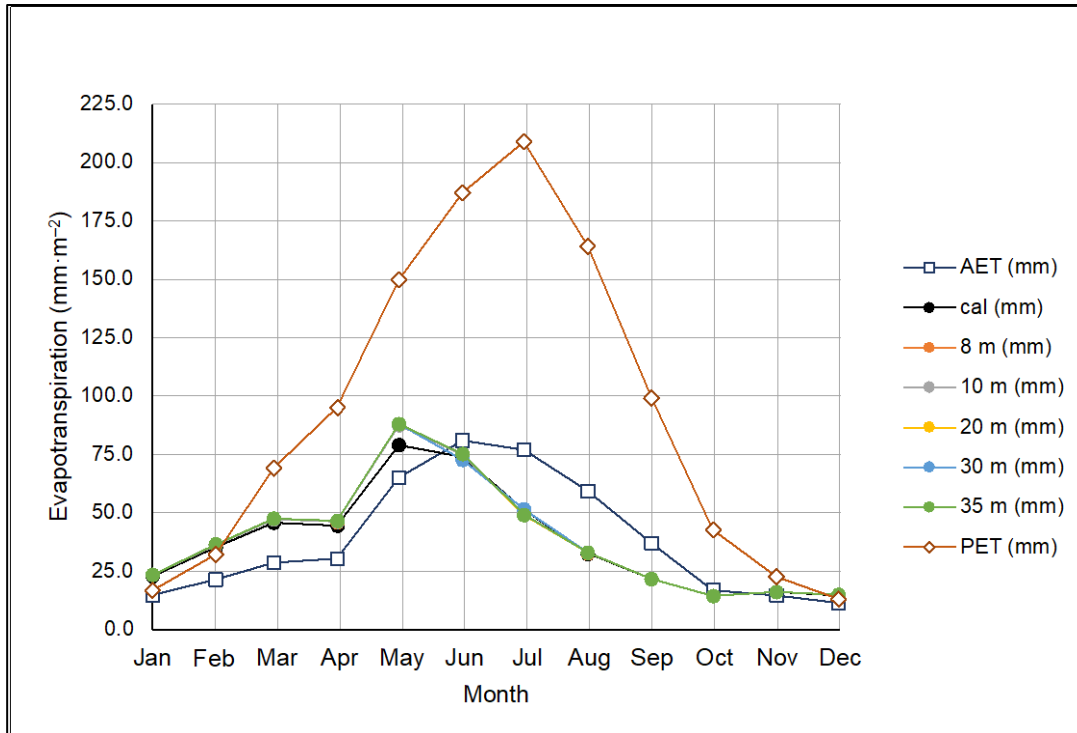


Figure 43. Average monthly actual evapotranspiration (AET), potential evapotranspiration (PET) and evapotranspiration (ET) for the different model scenarios over the model domain (floodplain) at TVFF. AET and PET are from MODIS data (Running et al., 2021) at gap-filled 500-m resolution. ET is calculated by the MODFLOW EVT boundary condition from a monthly specified flux.

Limitations of the Model

The calibrated model is useful but has several limitations. The model has an RMS error of 8.45%. The simulated heads are generally higher than observed values, especially for Wells 9 and 10 (Figure 38). Hydraulic conductivity parameters were based on observed values but were increased during calibration to achieve an RMS error less than 10% for the simulated heads. Furthermore, the calibration was based on comparison of annual mass balances between the analytical best-fit plane water balance and the MODFLOW mass balance, yet temporal discrepancies exist as seen in the evaporation calculations (Figure 43).

Modeling techniques were limited for the pond scenarios. The MODFLOW lake package (LAK) was not used because it renders cells below the lakebed inactive, which was not suitable in this situation. The SFR2 boundary condition was chosen for its ability to model ephemeral streams but required that ponds were confined to Layer 1 of the model and limited in depth. The SFR2 package also has inherent limitations as detailed by Niswonger and Prudic (2005), including numerical stability issues.

One final limitation of the model is the model domain. The domain excluded John Creek, which flows just east of the downgradient model boundary, on the assumption that this creek influences groundwater further downstream. The output of water to the HDB condition demonstrates that considering the effects of and the effect on downgradient features is desirable.

CHAPTER 2 CONCLUSIONS

An analytical water balance model for groundwater the TVFF site was accomplished by estimating the groundwater surface as a best-fit plane and determining the monthly groundwater storage based on this plane and the aquifer geometry. Monthly inflows and outflows were estimated based on available sources (e.g., precipitation from PRISM, 2022). The unknown net outflow of groundwater from the site (Net Boundary Exchange) was calculated based on the other fluxes and the assumption of no annual change in storage. The results of this analytical model (Table 14) serve as a first-order estimate of the magnitude of flows into and out of the groundwater. Precipitation is the largest inflow, roughly equal to the sum of inputs from upland runoff and flow from the Teanaway into the groundwater (River Recharge). The inflow from irrigation on the hay farm upgradient from TVFF is small in comparison. The largest outflow is baseflow to the river. Total annual baseflow is approximately 20% greater than the annual outflow from evapotranspiration. In order to balance inflows and outflows, the net outflow across the boundary of the area is roughly equal in magnitude to the evapotranspiration outflow. This net boundary exchange represents the groundwater outflow on the downgradient side of the site minus the inflow on the upgradient side.

Table 14. Yearly Steady-state Inflows and Outflows from the TVFF Site.

Inflows	Amount (mm·m ⁻² ·yr ⁻¹)
Precipitation	664
Upland Runoff	305
River Recharge (Leakage)	353
Irrigation Inflow	61.6*
Outflows	
Evapotranspiration	406
Baseflow	488
Pond Refill	72
Net Boundary Exchange	417
*The amount shown is the amount over the entire area of the site over the span of 1 year. 400 mm·m ⁻² ·yr ⁻¹ is the amount assumed over the irrigated field only.	

The analytical mass balance results were used to refine the MODFLOW model so that the annual inflows and outflows matched the analytical values. Once the MODFLOW model was calibrated, simulations were run with infiltration ponds of varying sizes. The results of these MODFLOW simulations indicate that increased infiltration from a pond increases the overall volume of the system in the short term, but the lasting effects of additional water diminish within about 2 months following the drying up of the pond. The total volume increase can be directly attributed to infiltration, as less water is input to the system from storage when the infiltration pond is present. Additional water into the system discharges to the river or is removed at the eastern head-dependent boundary in the spring months. The cobble-rich alluvial aquifer transmits water out of the floodplain efficiently and the higher groundwater elevations from the pond water infiltration are not maintained into the late summer months when stored groundwater is desired.

The amount of evapotranspiration from the model domain increases with the addition of an infiltration pond. In the groundwater flow model, more evapotranspiration occurs as pond size increases, but not appreciably. The increased evapotranspiration does not exceed measured PET over the model domain. The simulated ponds were designed to go dry at the end of April when recharge from the uplands north of the site ceases. At this time PET is below its maximum value. If the simulation extended the timeframe in which the ponds had water, losses to evaporation would likely be higher and more noticeable for ponds of larger size.

The analytical water balance computed using a best-fit plane through the head elevations at the observation wells demonstrated that the volume of storage was not only dependent on the volume of aquifer physically available to store water, but also on an accurate value of specific yield for the aquifer medium. This type of idealized model was appropriate at the research site because the model domain was comprised of a gently-sloping, nearly-planar floodplain. The analytical model informed the MODFLOW model regarding total mass balances for measurable quantities at the site, e.g. precipitation, evaporation, and river stage, and the MODFLOW model informed the analytical model regarding specific yield by providing the physical volume of the aquifer (inherent in the volume of the discretized cells) and calibrated values of specific yield necessary for the simulated heads to match the observed heads at the wells. The coupling of the analytical water balance model and MODFLOW groundwater flow model provides the baseline mass balances necessary to enable comparison of the pond model scenario mass balances to the calibrated model.

Future work that addresses the limitations of the groundwater flow model may provide more conclusive answers regarding the quantity and timing of infiltration and discharge. In particular, considering the influence of John Creek and assessing the risk of downgradient flooding would be instructive. Additional model scenarios could investigate using a lowered hydraulic conductivity in the pond to determine if delayed infiltration would affect the timing of discharge into the river or if evaporative losses would negate any gains in groundwater volume. Lastly, continuing to refine the groundwater flow model's calibration against observed heads may provide further insight into the in-situ physical properties of the aquifer materials at the site, including hydraulic conductivity, porosity, and specific yield.

REFERENCES

- Anderson, M.P., Woessner, W.W., and Hunt, R.J., 2015, Applied groundwater modeling: simulation of flow and advective transport: Academic Press, 564 p.
- Bressler, C. T., 1951, The petrology of the Roslyn arkose, central Washington: Pennsylvania State College, University Park, Ph.D. thesis, 147 p.
- Brunner, P., Simmons, C.T., Cook, P.G. and Therrien, R., 2010, Modeling surface water-groundwater interaction with MODFLOW: Some considerations, *Groundwater*, v. 48, no. 2, p. 174–180, <https://doi.org/10.1111/j.1745-6584.2009.00644.x>.
- Chowdhury, F., Gong, J., Rau, G.C. and Timms, W.A., 2022, Multifactor analysis of specific storage estimates and implications for transient groundwater modelling, *Hydrogeology Journal*, v. 30, n. 7, p. 2183-2204, <https://doi.org/10.1007/s10040-022-02535-z>.
- Collins, B.D., Montgomery, D.R., Schanz, S.A. and Larsen, I.J., 2016, Rates and mechanisms of bedrock incision and strath terrace formation in a forested catchment, Cascade Range, Washington, *GSA Bulletin*, v. 128 no. 5/6, p. 926 – 943, <https://doi.org/10.1130/B31340.1>.
- Creech, J., 2003, Teanaway temperature total maximum daily load: detailed implementation plan: Pub. no. 03-10-025, Washington State Department of Ecology, Olympia, WA.
- Eddy, M.P., Bowering, S.A., Umhoefer, P.J., Miller, R.B., McLean, N.M. and Donaghy, E.E., 2016. High-resolution temporal and stratigraphic record of Siletzia’s accretion and triple junction migration from nonmarine sedimentary basins in central and western Washington. *GSA Bulletin*, v. 128, no. 3/4, p. 425-441, <https://doi.org/doi:10.1130/B31335.1>.
- Efetha, A., Dow, T., McKenzie, R.H., Bennett, D.R. and Hohm, R.A., 2009, Effect of irrigation management on yield and water use efficiency of timothy hay in southern Alberta, *Canadian journal of plant science*, v. 89, n. 6, p. 1075–1088 <https://doi.org/10.4141/CJPS09012>.
- Ely, D.M., Bachmann, M.P., and Vaccaro, J.J., 2011, Numerical simulation of groundwater flow for the Yakima River basin aquifer system, Washington: U.S. Geological Survey Scientific Investigations Report 2011-5155, 90 p.
- Fetter, C.W., 2001, Applied Hydrogeology, 4th ed.: Illinois, Waveland Press, 598 p.
- Freeze, R.A. and Cherry, J.A., 1979, *Groundwater*: New Jersey, Prentice Hall, Inc., 604 p.
- Futornick, Z.O., 2015, Using MODFLOW to predict impacts of groundwater pumpage to instream flow: Upper Kittitas County, Washington. [Masters thesis]: Ellensburg, Central Washington University, 127 p.
- Gazis, C. 2020, Effect of large wood restoration on alluvial aquifer storage in Yakima Basin headwater tributaries: Washington State Department of Ecology Quality Assurance Project Plan no. C2100007, 66 p.
- Gendaszek, A.S., Ely, D.M., Hinkle, S.R., Kahle, S.C., and Welch, W.B., 2014, Hydrogeologic framework and groundwater/surface-water interactions of the upper Yakima River Basin, Kittitas County, central Washington: U.S. Geological Survey Scientific Investigations Report 2014–5119, 66 p., doi: 10.3133/sir20145119.
- Ghysels, G., Mutua, S., Veliz, G.B., and Huysmans, M., 2019, A modified approach for modelling river–aquifer interaction of gaining rivers in MODFLOW, including riverbed heterogeneity and river bank seepage, *Hydrogeology Journal*, v. 27, no. 5, p. 1851–1863, <https://doi.org/10.1007/s10040-019-01941-0>.
- Hall, F.R., 1968, Base-flow recessions – A review. *Water resources research*, v. 4, no. 5, p. 973-983, <https://doi.org/10.1029/WR004i005p00973>.

- Haugerud, R.A. and Tabor, R.W., 2009. Geologic map of the North Cascade Range, Washington (p. 29). US Department of the Interior, US Geological Survey.
- Haugerud, R.A., van der Heyden, P., Tabor, R.W., Stacey, J.S., and Zartman, R.E., 1991, Late Cretaceous and early Tertiary plutonism and deformation in the Skagit Gneiss Complex, North Cascade Range, Washington and British Columbia: Geological Society of America Bulletin, v. 103, p. 1297–1307, [https://doi.org/10.1130/0016-7606\(1991\)103<1297:LCAETP>2.3.CO;2](https://doi.org/10.1130/0016-7606(1991)103<1297:LCAETP>2.3.CO;2).
- Henning, L. 2023. Using MODFLOW to Assess Groundwater Storage Enhancement via a Floodplain Infiltration Basin: M.S. Thesis, Central Washington University. <https://digitalcommons.cwu.edu/etd/1873>.
- Hunting, M.T., Bennett, W.A.G., Livingston, V.E. Jr., and Moen, W.S., 1961, Geologic Map of Washington: Washington Division of Mines and Geology, scale 1:500,000.
- Johnson, A.I., 1967, Specific yield: compilation of specific yields for various materials: U.S. Geological Survey Water Supply Paper 1662-D, 80 p., <http://doi.org/10.3133/wsp1662D>.
- Kuang, X., Jiao, J.J., Zheng, C., Cherry, J.A. and Li, H., 2020, A review of specific storage in aquifers, Journal of Hydrology, v. 581, p. 124383, <https://doi.org/10.1016/j.jhydrol.2019.124383>.
- Lautz, L.K. and Siegel, D.I., 2006, Modeling surface and ground water mixing in the hyporheic zone using MODFLOW and MT3D. Advances in Water Resources, v. 29, no. 11, p. 1618–1633, <https://doi.org/10.1016/j.advwatres.2005.12.003>.
- Ly, M., Xu, Z., Yang, Z.L., Lu, H. and Lv, M., 2021, A comprehensive review of specific yield in land surface and groundwater studies. Journal of Advances in Modeling Earth Systems, v. 13, n. 2, p. e2020MS002270, <https://doi.org/10.1029/2020MS002270>.
- Maples, S.R., Fogg, G.E., and Maxwell, R.M., 2019, Modeling managed aquifer recharge processes in a highly heterogeneous, semi-confined aquifer system, Hydrogeology Journal, v. 27, p. 2869 – 2888, doi: 10.1007/s10040-019-02033-9.
- Massuel, S., Perrin, J., Mascré, C., Mohamed, W., Boisson, A. and Ahmed, S., 2014, Managed aquifer recharge in South India: What to expect from small percolation tanks in hard rock?. Journal of Hydrology, no. 512, p. 157–167, <https://doi.org/10.1016/j.jhydrol.2014.02.062>.
- Miller, R.B., Gordon, S.M., Bowring, S.A., Doran, B.A., Michels, Z., Shea, E.K., and Whitney, D.L., 2016, Linking deep and shallow crustal processes during regional transtension in an exhumed continental arc, North Cascades, northwestern Cordillera (USA): Geosphere, v. 12, p. 900–924, <https://doi.org/10.1130/GES01262.1>.
- Miller, R.B., Bryant, K.I., Doran, B., Eddy, M.P., Raviola, F.P., Sylva, N. and Umhoefer, P.J., 2022. Eocene dike orientations across the Washington Cascades in response to a major strike-slip faulting episode and ridge-trench interaction. Geosphere, v. 18, no. 2, p. 697 – 725, <https://doi.org/10.1130/GES02387.1>.
- Natural Resources Conservation Service (NRCS), 2022, United States Department of Agriculture, Web Soil Survey, <http://websoilsurvey.sc.egov.usda.gov/> (accessed April 2022).
- Niswonger, R.G., Panday, S., and Ibaraki, M., 2011, MODFLOW-NWT, A Newton formulation for MODFLOW-2005: U.S. Geological Survey Techniques and Methods 6-A37, 44 p., <https://doi.org/10.3133/tm6A37>.
- Niswonger, R.G., and Prudic, D.E., 2005, Documentation of the Streamflow-Routing (SFR2) Package to include unsaturated flow beneath streams—A modification to SFR1: U.S. Geological Survey Techniques and Methods 6-A13, 50 p.
- Onset Computer Corporation, 2019, HOBOWare Pro (Version 3.7.1) [Software].

- Petralia, J., 2022, The effects of channel incision and land use on surface-water/groundwater interaction in the Teanaway River basin, Washington, USA, Central Washington University, M.S. Thesis, 110 p.
- PRISM Climate Group, Oregon State University, <https://prism.oregonstate.edu>, data created 29 September 2022, accessed 13 October 2022.
- Ringleb, J., Sallwey, J., and Stefan, C., 2016, Assessment of managed aquifer recharge through modeling – a review, *Water*, v. 8, no. 12, p. 579, doi: 10.3390/w8120579.
- Running, S., Mu, Q., Zhao, M., Moreno, A., 2021, MODIS/Terra Net Evapotranspiration Gap-Filled 8-Day L4 Global 500m SIN Grid V061 [Data set]. NASA EOSDIS Land Processes DAAC, <https://doi.org/10.5067/MODIS/MOD16A2GF.061> (accessed March 2023).
- Russo, T.A., Fisher, A.T., and Lockwood, B.S., 2015, Assessment of managed aquifer recharge site suitability using a GIS and modeling, *Groundwater*, v. 53, no. 3, p. 389 – 400, <https://doi.org/10.1111/gwat.12213>.
- Saunders, E.J., 1914, The coal fields of Kittitas County: Washington Geological Survey Bulletin 9, 204 p.
- Schanz, S.A., Montgomery, D.R., Collins, B.D., 2019, Anthropogenic strath terrace formation caused by reduced sediment retention: *National Academy of Sciences*, v. 116, no. 18, p. 8734 – 8739, doi: 10.1073/pnas.1814627116.
- Scherberg, J., Baker, T., Selker, J.S. and Henry, R., 2014, Design of managed aquifer recharge for agricultural and ecological water supply assessed through numerical modeling, *Water resources management*, no. 28, p. 4971a–4984, <https://doi.org/10.1007/s11269-014-0780-2>.
- Scherer, M., 1987, Parameters influencing porosity in sandstones: a model for sandstone porosity prediction, *AAPG bulletin*, v. 71, n. 5, p. 485-491, <https://doi.org/10.1306/94886ED9-1704-11D7-8645000102C1865D>.
- Shah, N., Nachabe, M. and Ross, M., 2007, Extinction depth and evapotranspiration from ground water under selected land covers, *Groundwater*, v. 45, no. 3, p. 329–338, <https://doi.org/10.1111/j.1745-6584.2007.00302.x>.
- Snyder, E.B., and Stanford, J.A., 2001, Review and synthesis of river ecological studies in the Yakima River, Washington, with emphasis on flow and salmon interactions—Final report: Yakima, Wash., U.S. Bureau of Reclamation, August 21, 2001, revised September 20, 2001, 118 p., 1 app.
- Tabor, R.W., Frizzell Jr, V.A., Vance, J.A. and Naeser, C.W., 1984. Ages and stratigraphy of lower and middle Tertiary sedimentary and volcanic rocks of the central Cascades, Washington: Application to the tectonic history of the Straight Creek fault. *Geological Society of America Bulletin*, v. 95, no. 1, p. 26-44, [https://doi.org/10.1130/0016-7606\(1984\)95%3C26:AASOLA%3E2.0.CO;2](https://doi.org/10.1130/0016-7606(1984)95%3C26:AASOLA%3E2.0.CO;2).
- Tabor, R.W., Waitt, R.B., Frizzell, V.A., Swanson, D.A., Byerly, G.R. and Bentley, R.D., 1982, Geologic map of the Wenatchee 1: 100,000 quadrangle, central Washington.
- United States Geological Survey (USGS), 2017, 1/3rd arc-second Digital Elevation Models (DEMs) - USGS National Map 3DEP Downloadable Data Collection: U.S. Geological Survey.
- United States Geological Survey (USGS), 2020, https://www.usgs.gov/mission-areas/water-resources/science/modflow-and-related-programs?qt-science_center_objects=0#qt-science_center_objects. Accessed May 2021.
- Vaccaro, J.J., Jones, M.A., Ely, D.M., Keys, M.E., Olsen, T.D., Welch, W.B., and Cox, S.E., 2009, Hydrogeologic framework of the Yakima River basin aquifer system, Washington: U.S. Geological Survey Scientific Investigations Report 2009–5152, 106 p.

- Vaccaro, J.J. and Olsen, T.D., 2007, Estimates of ground-water recharge to the Yakima River Basin aquifer system, Washington, for predevelopment and current land-use and land-cover conditions. US Geological Survey Scientific Investigations Report, 2007 – 5007, 30 p., <https://pubs.usgs.gov/sir/2007/5007/pdf/sir20075007.pdf>.
- van der Kwast, H. and Menke, K., 2021, QGIS for hydrological applications: recipes for catchment hydrology and water management: Locate Press, 168 p.
- Waterloo Hydrogeologic, 2021, Visual MODFLOW Flex 7.0 (Build 7.0.7187.368950) [Software].
- Woessner, W.W. and Poeter, E.P., 2020, Hydrogeologic properties of earth materials and principles of groundwater flow: Guelph, Ontario, Canada, The Groundwater Project, 205 p.
- Woodard, L.L., Sanford, W. and Reynolds, R.G., 2002, Stratigraphic variability of specific yield within bedrock aquifers of the Denver Basin, Colorado, Rocky Mountain Geology, v. 37, n. 2, p. 229-236, <https://doi.org/10.2113/gsrocky.37.2.229>.
- Zhang, H., Xu, Y. and Kanyerere, T., 2020, A review of the managed aquifer recharge: Historical development, current situation and perspectives, Physics and Chemistry of the Earth, Parts A/B/C, v. 118-119, p. 102887, <https://doi.org/10.1016/j.pce.2020.102887>

3. Evaluation of Soil Moisture and Evapotranspiration at a site on Taneum Creek, Central Washington

INTRODUCTION

This chapter is based on the M.S. thesis research of Edward Vlasenko. Mr. Vlasenko set up soil monitoring sites and an evaporation pan at a site on lower Taneum Creek to collect physical measurements of evapotranspiration (ET) and compared the resulting measurement-based ET estimates to open-source satellite-based measurements of ET (OpenET, 2023). In addition, water samples from Taneum Creek, a side channel, and a beaver pond complex were analyzed for stable isotopes of oxygen and hydrogen. Stable isotope ratios of oxygen and hydrogen in waters change when they undergo evaporation and thus record the extent of evaporation. This chapter presents the results of Mr. Vlasenko's thesis as well as additional monitoring data that was collected after his thesis was completed and the stable isotope data. More details on Mr. Vlasenko's research are available in the thesis itself (Vlasenko, 2023).

Overview and Purpose

Evapotranspiration (ET) is the process by which water is transferred from the land surface and vegetation to the atmosphere through the combined processes of evaporation and transpiration. A notoriously difficult water budget component to quantify, ET plays a critical role in hydrologic cycling in both agricultural and natural settings. Quantifying evapotranspiration rates is important for managing water resources, especially in regions where water availability is limited. It is a major flux in all watersheds, and a necessary parameter for water budget calculations.

Stream restoration efforts that reconnect a channelized river with its floodplain and increase the complexity of water paths are known to also increase groundwater storage in that floodplain. However, these efforts often increase vegetation cover on the floodplain, which in turn removes water through ET. Cottonwood (*Populus fremontii*) trees, in particular, have high transpiration rates and can transfer large amounts of water directly from the saturated zone to the atmosphere during the dry summer months. For example, a study of a cottonwood plantation in Arizona determined transpiration rates of 1.2 m per year (Nagler et al., 2007). As a result, it is not certain whether the combined effects of restoration and ET will have a net positive or negative effect on the water budget, in particular summer streamflow. Previous research suggests that the answer to this question depends on local factors including aquifer size and geometry, stream geomorphology, soil properties, climate and local hydrology. Tague et al. (2008) documented changes to streamflow before and after restoration for Trout Creek in California and determined that streamflow decreased during the snowmelt period due to overbank flow and storage, increased during the recession period, and was the same as pre-restoration during the baseflow in the summer and early fall. A number of models have been developed that compare the water budget of incised and restored streams and show mixed results regarding the impact of restoration on streamflow (e.g., Loheide et al., 2009; Essaid and Hill, 2014).

Evapotranspiration is difficult to measure because it is dependent on a complex set of parameters that vary both spatially and seasonally. Because of its importance in agricultural management, a variety of methods have been developed and refined to calculate evaporation using meteorologic data inputs (e.g., Cordova et al., 2015). Remote sensing methods have been used both

to identify vegetation distribution and to constrain evapotranspiration rates through energy balance (e.g., Burt, 2016). Stable isotopes have also proven useful for determining evaporation rates (e.g. van den Akker et al., 2011; Zanazzi et al., 2020). Finally, direct measurements can be made through evaporation pans, controlled vegetation lysimeters, and sap flow measurements. This project combines several of these techniques to quantify evapotranspiration rates in the Taneum floodplains to assess the magnitude of evapotranspiration in the water budget and how ET is impacted by changes from stream restoration.

Measuring Evapotranspiration

Effective estimation of ET water loss is essential for computing water balances and determining water availability. Historically, a wide variety of empirical and analytical methods have been developed and employed to measure ET, mainly in agricultural settings. Owing to its significance to agricultural production, research into ET within field settings is plentiful and provides a sound basis for quantifying ET. By possessing features and qualities such as relatively flat topography and uniform vegetation, agricultural settings provide a regularity and uniformity not present in a more “natural” setting such as a forest. Additionally, water inputs to the system are generally known, as these represent metered irrigation flows (Subedi and Chavez, 2015; Rana and Katerji, 2000).

ET in “natural” settings is considerably more difficult to measure, as these settings introduce numerous variables that complicate ET estimation. Local environmental factors such as spatial variability in soil profiles, vegetation, and topography influence the amount of water lost from a setting by ET and make it more difficult to quantify.

One common and straight-forward approach is by soil-water balance. Soil-water balance is an indirect measurement method, and is best represented by the simplified equation:

Equation 5. Soil water balance

$$P + I = ET + D \pm \Delta S \quad (5)$$

In this equation, P is precipitation, I is irrigation, ET is evapotranspiration, D is any drainage out of the soil, and ΔS is the change in soil moisture during the measurement interval. Generally, irrigation water supply is known, and precipitation is measurable through the use of rain gauges. For successful application of the equation, drainage must also be measured and soil water content must be measured accurately over a sufficient soil depth.

A similar approach is to employ surface-energy balance, which estimates ET by relating it to energy (heat) transfers between the surface and the atmosphere. This involves accurately measuring incoming and outgoing energy fluxes, including net radiation, sensible heat flux, latent heat flux, and ground heat flux. Surface energy balance is best summarized by the following equation:

Equation 6. Surface energy balance

$$R_n = LE + H + G \quad (6)$$

In this equation, LE refers to latent heat flux, H is the sensible heat flux, G is the soil heat flux, and R_n is net radiation. Net radiation is defined as positive if heat is moving towards the surface (such as during the day, by sunlight), and negative otherwise. All other fluxes are defined as positive if heat is moving away from the surface. Sensible heat flux (H) refers to heat transfer between the ground and the atmosphere by conduction and convection. Soil heat flux (G) is the heat transfer between the surface and deeper soil, primarily by conduction. Within the surface energy balance model, evapotranspiration is represented by the latent heat flux. This is the thermal energy that is absorbed by water at the surface (in soil) as it undergoes a phase change from liquid to gas (evaporates). The Penman-Monteith equation (Allen et al., 1998; Zotarelli et al., 2009), which we used in this study, is a widely used method for calculating ET based on the principles of surface energy balance. The Penman Monteith equation is described in more detail in the Methods section of this chapter.

In recent years, remote-sensing based approaches have become the new standard for measuring ET (e.g., Kalma et al., 2008; McCabe et al., 2019). Remote sensing-based methods for measuring ET use satellite images to estimate the amount of water that is being lost from the land surface. These methods are based on the principle that vegetation absorbs and reflects different wavelengths of radiation (light), and that the amount of absorbed and reflected light is a measure of energy that is related to the amount of water that is being lost through transpiration.

The advantage of remote sensing-based methods for measuring ET is that they can cover large areas and provide spatially explicit estimates of evapotranspiration rates. They are non-invasive and can be used in areas that are difficult to access, such as remote, protected, or mountainous regions. Another advantage is that remote sensing-based methods can be used to monitor evapotranspiration rates over time, allowing for changes in water consumption to be identified and managed.

However, remote sensing-based methods also have some disadvantages. They rely on the availability of satellite data and meteorological data, which may not always be available at the desired spatial or temporal resolution. The accuracy of remote sensing-based estimates can also be affected by cloud cover, atmospheric conditions, and the complexity of the land surface being monitored.

In this study, we compare our ET estimates from field-based measurements to remote-sensing based ET estimates available through the open-source platform OpenET (OpenET, 2023).

Study Site

Taneum Creek is located within Kittitas County in central Washington, approximately 17 km northwest of Ellensburg, WA (Figure 44). The stream flows from west to east and joins the Yakima River at mile 166.1 (Monk, 2009). The total area of the Taneum Creek basin is approximately 215 km² (Jones and Stokes Associates, 1991). Elevation ranges from about 1914 m near Quartz Mountain to 515 m at the Yakima River confluence. Annual precipitation ranges from

>150 cm in the upper Taneum to approximately 25 cm near the Yakima River confluence (Jones and Stokes Associates, 1991).

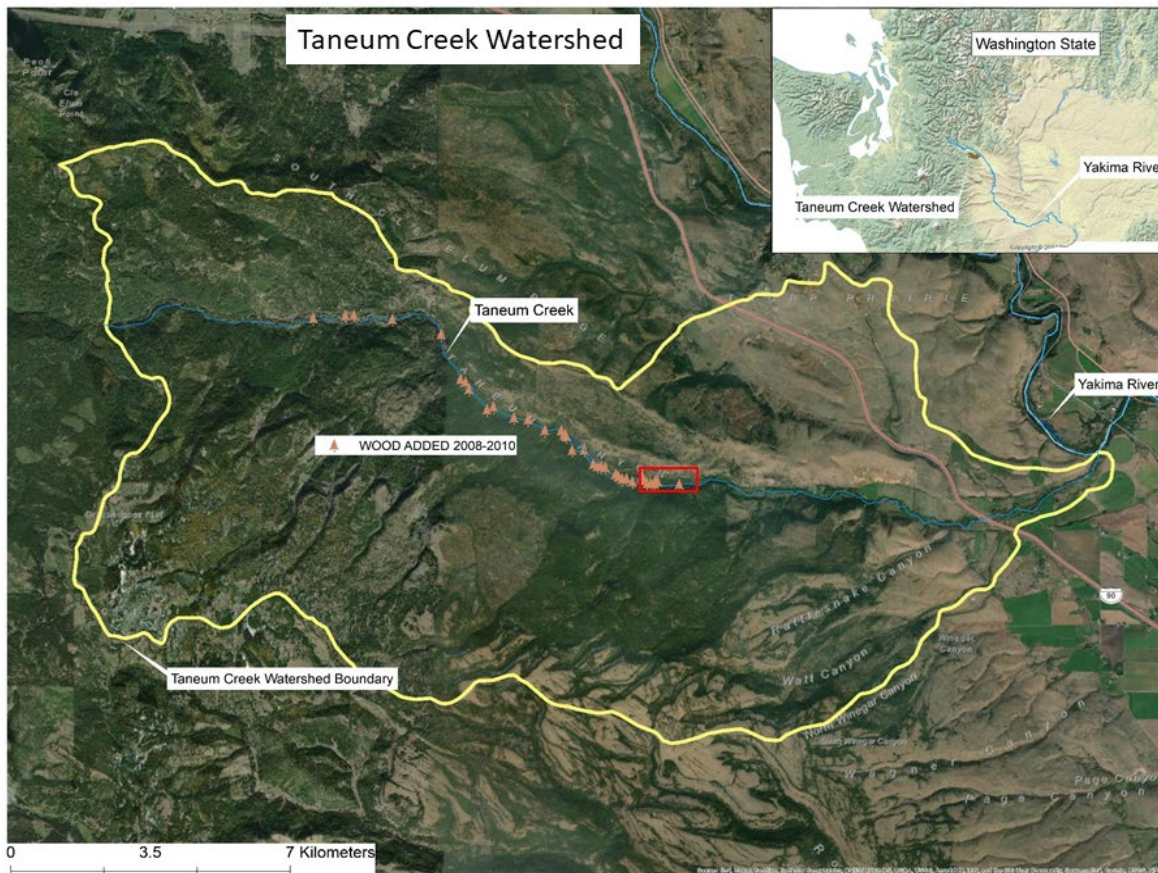


Figure 44. Taneum Creek Watershed Map. The lower watershed boundary of Taneum Creek and the creek itself are highlighted, along with the proximity to the Yakima River. The inset map in the top right corner displays the location of the Taneum Creek watershed and the Yakima River within the broader context of Washington state. Red triangles mark the sites of large wood (LW) additions in the 2008-2010 stream restoration project. Modified from map by Scott Nicolai, Yakama Nation Fisheries.

Logging activities began in the early 20th century, with many old-growth forests being cleared for timber. The practices used were destructive, resulting in erosion of alluvial sediments, and stream incision that extended into bedrock in some areas (Henderson, 1990; Abbe & Montgomery, 1996). In the mid-20th century, mining operations for precious metals were also established in the region, further altering the landscape and introducing new environmental risks. These logging and mining activities included establishment of a railroad line in the Taneum floodplain, by which harvested goods were exported. This railroad line, which served to even further channelize the river, was removed in 1954.

Today, Taneum Creek is used primarily for recreation. The area is popular among outdoor enthusiasts for activities such as hiking, hunting, fishing, and motorbiking. It also plays a critical role in fish ecology, providing habitat for young trout and salmonid fry. Because of this ecological benefit, the Taneum Creek watershed has been the subject of extensive restoration work in recent

years. These efforts include removing diversion dams, building fish passages, and adding large wood to the channel and floodplain. Figure 44 identifies locations of the initial large wood additions in 2008-2010.

On May 15th, 2011, Taneum experienced a large flood event during the spring snowmelt (Figure 45). The discharge of this flood was estimated by Tappel (2012) using a rating curve and flow measurements taken during the event to be 69 -79 m³/s (2,400 to 2,800 cfs). The discharge estimate was approximately 11 - 23 m³/s (400-800 cfs) above the 100-year flood threshold of 57m³/s (2,000 cfs). Most of the logs placed by the Yakama Nation in 2008-2010 mobilized to create large log jams (Tappel, 2012).



Figure 45. Taneum Creek 100-yr flood on May 15th, 2011. Photo was taken near the intake to the Taneum irrigation canal at the downstream end of the watershed. Photo by Paul Tappel, 2011.

The Taneum Creek watershed is underlain by two distinct hydrogeologic bedrock units: basalts of the Columbia River Basalt Group (CRBG) and older bedrock which lies beneath the CRBG flows in the study area and is exposed in the upper reaches of the Taneum watershed (Figure 6; Vaccaro et al., 2009). In the upper reaches, groundwater moves through fracture systems within Paleozoic metamorphic rocks (Ely et al., 2011; Gendaszek et al., 2014). The lower portion of the basin is dominated by the groundwater regime of the CRBG rocks (Vacarro et al., 2009). The alluvial

floodplain aquifer examined in this study overlies these units and/or sedimentary layers within the basalt, collectively called the Ellensburg Formation (Vaccaro et al., 2009).

At Taneum Creek, groundwater and surface water interact, providing a variety of environments for the resident fauna, especially fish. Taneum Creek flows are maintained by a combination of groundwater and surface water recharge. During the summer dry season, the discharge in the creek is driven primarily by groundwater baseflow (Monk, 2009). Characterizing and understanding groundwater-surface water interactions can inform water management environmental and agricultural uses. Both the landscape and the climate are changing, which could impact evapotranspiration, one of the main fluxes of water out of the basin.

METHODS

This study employed extended monitoring of multiple environmental and hydrological parameters to estimate and calculate evapotranspiration. All environmental data were collected at 15-minute time intervals. Daily totals (soil heat flux) and daily averages (all other ET calculation input parameters) of values were derived from the 15-minute-interval time series data.

Environmental Monitoring Field Methods

Aerial Photography

A Ricoh GR II camera installed in a SmartPlanes Freya model drone was used to collect aerial imagery of the study site on four dates: May 2, May 26, June 7, and June 29, 2023. Each flight generated 200-400 photos, which were stitched together into a single orthomosaic using the Agisoft Digital Pro software.

Monitoring Sites

Two monitoring sites were established at the Taneum Creek study area (Figure 46) to collect soil and evaporation data. The sites were chosen to represent locations that represent shaded riparian forest and open meadow end-members within the overall site. The riparian site is surrounded by trees and receives more shade than the meadow site. It will hereafter be referred to as the “riparian site.” The open meadow site is in a grassy area that turns brown by early summer. This will be referred to as the “meadow site.” Figure 47 presents a schematic showing the equipment that was deployed at each site. The equipment is described below.

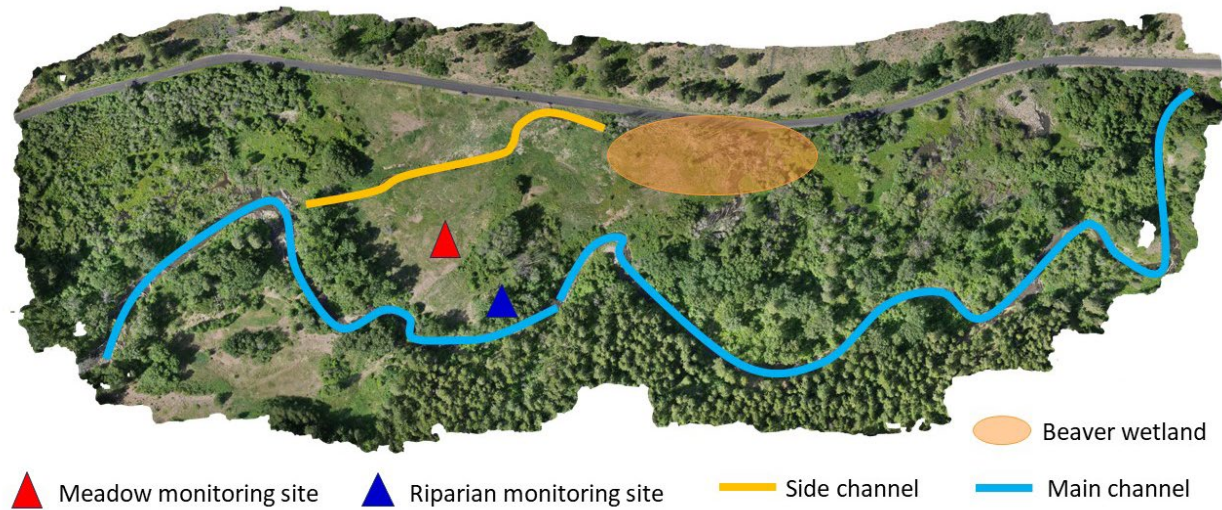


Figure 46. Map of environmental monitoring sites at Taneum Creek study area. The top of the image is bounded by West Taneum Rd and a steep ridge. Labeled with colored triangles, the two environmental monitoring sites were established on the floodplain between the main and side channel of Taneum Creek. The main and side channels are outlined in blue and yellow, respectively, to increase visibility. The side channel feeds a beaver wetland area, which then drains back into the main channel of Taneum Creek at multiple, varying points.

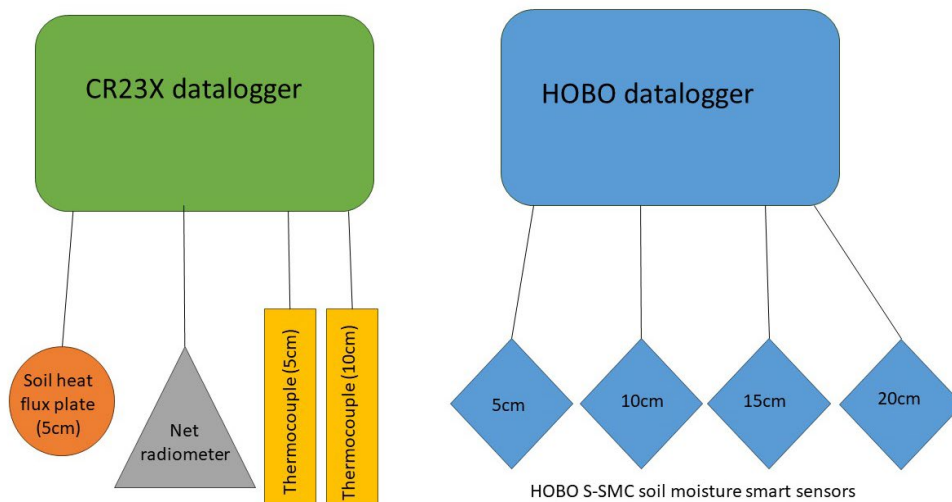


Figure 47. Equipment schematic. This figure provides a summary of all environmental monitoring equipment deployed at the two locations on the Taneum floodplain (Figure 46). All sensors but the net radiometer were buried in the floodplain soil, with their burial depths labeled in the diagram. Connecting lines represent wired connections. A single net radiometer was suspended above the ground at the meadow site by use of a standing ladder and served to measure radiation for both sites.

Evaporation Station

An evaporation station consisting of a NovaLynx 255-200 Class-A evaporation pan with a 255-100 evaporation gauge and 255-704-B datalogger (Figure 48) was deployed at the Taneum riparian monitoring site (Figure 46) to measure pan evaporation. The ground surface was leveled, and the evaporation station was set up on top of a platform consisting of two standard wooden pallets. The pan was filled with water and exposed to the elements to measure evaporation from an open body of water.



Figure 48. Evaporation pan and precipitation gauge. This equipment was installed at the riparian site. The tall white cylinder is the evaporation gauge, which is directly connected to the pan and records its water level. The precipitation gauge is next to the pan (transparent, surrounded by rocks).

During each site visit, evaporation data was downloaded from the datalogger. A manual measurement of pan water level was also taken and compared to the datalogger value. When the water level became low, the pan was replenished with water from the nearby Taneum Creek main channel, and the volume of water used to replenish the pan was recorded.

Due to the nature of the pan model, pan evaporation often represents an overestimation of actual evaporation. A pan coefficient is used to convert pan evaporation rates to corresponding corrected evaporation rates. In this study, the pan coefficient was calculated by the FAO-56 method (Allen et al., 1998) using Equation 7, shown below.

Equation 7. Pan coefficient equation (Allen et al., 1998)

$$K_p = 0.108 - 0.0286 * u_2 + 0.0422 * \ln F + 0.1434 * \ln H - 0.00631 * (\ln F)^2 * \ln H \quad (7)$$

where K_p is the pan coefficient, u_2 is the wind speed at 2 m height (m/s); F is the fetch distance, assumed to be 10 m here; and H is the mean relative humidity (%). Pan coefficients were determined using weather data from a WSU AgWeatherNet station in Thorp, WA (AgWeatherNet, 2023) and ranged from 0.49 to 0.77.

Precipitation gauge

Precipitation at Taneum Creek was measured directly with a standard precipitation gauge set up next to the evaporation station (Figure 48). Precipitation was measured and recorded at the time of each field site visit, a sample was taken for isotopic analysis, and then the gauge was emptied.

Soil heat flux plates

Two HFP01 Huskeflux heat flux plates were used to quantify soil heat flux in the Taneum meadow. Both plates were wired to their own CR23X dataloggers. The flux plates were buried at the two different sites, riparian and meadow. Each plate was installed at the standard 5.0 cm depth.

Soil moisture probes

Four S-SMC-M005 EC5 Soil Moisture Smart Sensors were wired to HOBO dataloggers. Similar to the soil heat flux plates, the sensors were buried at both the meadow and the riparian site. Sensors were installed at 5 cm, 10 cm, 15 cm, and 20 cm depth.

Thermocouples

Two thermocouples were wired to each CR23X datalogger to track soil temperature. One thermocouple was installed at 10 cm depth, and the other at 5 cm depth.

Net radiometer

An net radiometer manufactured by Radiation and Energy Balance Systems, Inc. was connected to a CR23X datalogger, and deployed along with the other environmental monitoring equipment at the Meadow monitoring site. The net radiometer was connected to a 1-m pipe, and attached to a ladder, in order to suspend the device above the height of the tall grass, and away from

any shadows. Tent stakes were used to secure the ladder-radiometer setup in the frequent high wind conditions present at the field site. The radiometer measures radiation in mV and is calibrated for a linear conversion to W/m² with the following calibration factors: 8.74 for positive measurements, 10.75 for negative measurements. In the first three weeks of measurements, there were multiple data gaps, sometimes for several hours, always during the daytime. When daily averages were calculated, these gaps were filled with the average value of the four measurements on either side of the data gap. Although an approximation, this prevented a systematic bias toward nighttime measurements.

Calculation of Evapotranspiration using Penman-Monteith Method

Reference ET for the Taneum field site was calculated empirically using the FAO-56 version of the Penman-Monteith equation (Allen et al., 1998; Zotarelli et al., 2009). The Penman-Monteith equation represents a refined, widely used method for calculating reference evapotranspiration in mm/day based on the principles of surface energy balance. The equation combines various meteorological parameters to estimate daily potential evapotranspiration in a given setting. A summary of the equation and all input parameters can be seen below in Equation 8 and Table 15. Among the inputs, the soil heat flux density and radiation were measurements made at our sites. Additional weather data was obtained from Washington State University’s AgWeatherNet (AWN), for the Thorp weather station (AgWeatherNet, 2023).

Equation 8. Penman-Monteith Equation (Allen et al., 2005; Zotarelli et al., 2009)

$$ET_o = \frac{0.408\Delta(R_n - G) + \gamma \frac{c_n}{T + 273} u_2 (e_s - e_a)}{\Delta + \gamma(1 + C_d u_2)} \tag{8}$$

Table 15. Summary of Penman-Monteith equation input parameters

Variable	Name	Units	Data source*
ET _o	Reference evapotranspiration	mm/day	calculated
Δ	Slope of the saturation vapor pressure-temperature curve	kPa/°C	AgWeatherNet
R _n	Net radiation at the crop surface	MJ/m ² /day	measured, meadow site
G	Soil heat flux density	MJ/m ² /day	measured, both sites
g	Psychrometric constant	kPa/°C	AgWeatherNet
T	Mean daily air temperature at 2m height	°C	AgWeatherNet
u ₂	Mean daily wind speed at 2m height	m/s	AgWeatherNet
e _s	Saturation vapor pressure	kPa	AgWeatherNet
e _a	Actual vapor pressure	kPa	AgWeatherNet

Variable	Name	Units	Data source*
C_n	Numerator constant for reference crop type		900*
C_d	Denominator constant for reference crop type		0.34*

*data sources were measurements from this study and AgWeatherNet (2023). Crop constants are from Allen et al. (2005). Description of parameter calculations is given in Zotarelli et al. (2009)

A numerator constant (C_n), of 900 and the denominator constant (C_d) of 0.34 were used. These are the short reference crop constants (Allen et al., 2005; Zotarelli et al., 2009) and were chosen because they might represent the dominant meadow vegetation of the study area and yield the lowest evapotranspiration estimates.

Stable Isotope Sampling and Analysis

Water samples were collected every 1-2 weeks during two summers from August 11 – October 3, 2022 and March 29 - June 28, 2023, with less frequent sampling during the intervening winter. Sampling locations are shown in Figure 49. Five locations were sampled every time: Taneum Creek, the evaporation pan (not during winter and early spring), the side channel, and two locations in the beaver ponds. In addition, six other beaver pond locations were sampled once to see how much

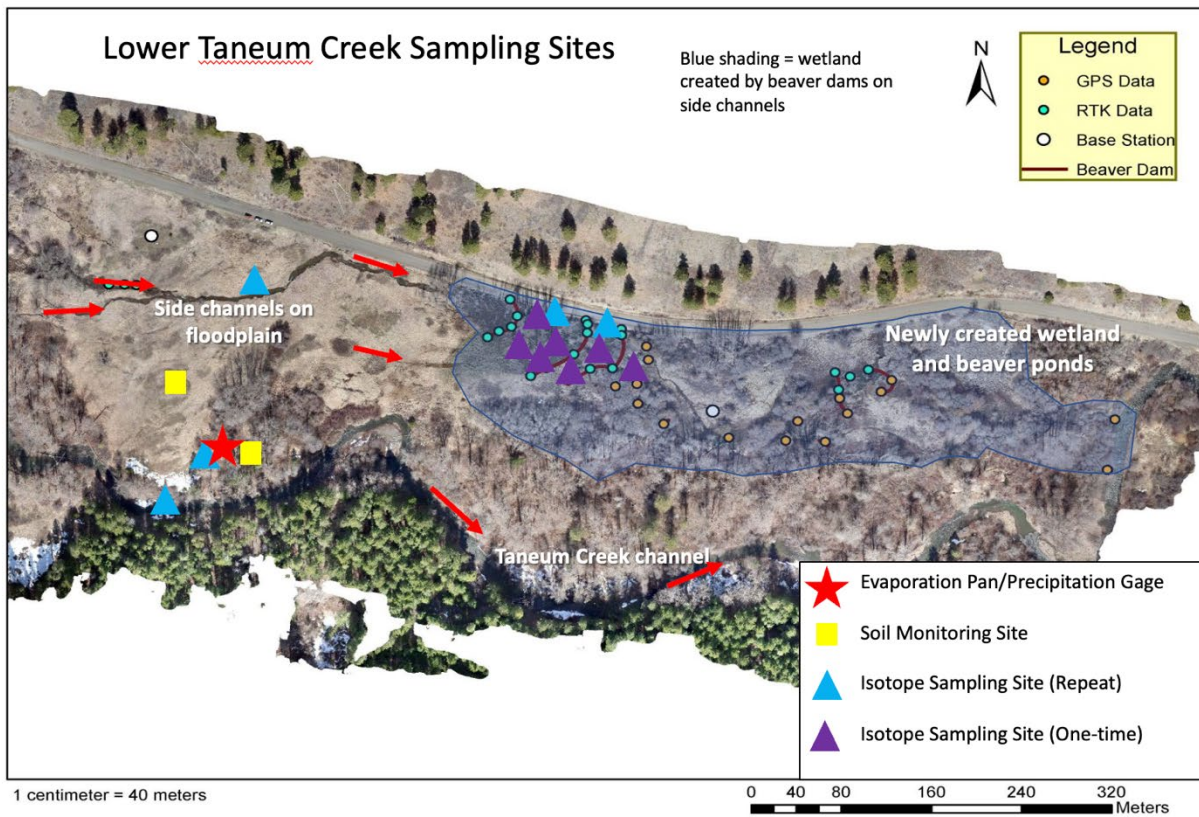


Figure 49. Lower Taneum Creek Isotope Sampling Sites.

isotopic variability existed in the beaver pond complex. Samples were collected by hand from a well-mixed location in 30 ml polypropylene bottles and capped tightly. In the laboratory, samples were filtered and analyzed with a Picarro L2130-I Isotopic H₂O Analyzer. Isotope ratios are reported in the standard δ -notation.¹ Uncertainties for this method are 0.1 per mil for $\delta^{18}\text{O}$ and 1 per mil for δD .

QUALITATIVE AERIAL IMAGERY ANALYSIS

Analysis of aerial photos is useful for quickly identifying trends in vegetation and water level. Composite aerial photos of the study site for the dates of May 2nd, May 26th, June 7th, and June 29th, 2023 can be found in Appendix A. In the aerial imagery, the main channel of Taneum Creek can be seen meandering, flowing west to east (left to right in the composite images; Figures 47 and 49). At the first sharp bend, some of the streamflow cuts through the channel walls, escaping and flowing out onto the floodplain. This forms a side channel which feeds a downstream beaver wetland, where water seems to slow down and pool. Numerous fallen logs and dam structures can be seen in this beaver wetland area (Appendix A; Figure 49). On the north side, the wetland is bounded by the road, which the beavers have used as one of the retaining walls for their flooded wetland area.

There are two main trends seen in the aerial imagery of the study site (Table 16; Appendix A). The first is a pattern of increasing greenness. In the May 2nd imagery, the meadow is completely brown and yellow. The only greenness in the photo comes from evergreen trees. By May 26th, grass produces a patchy green and yellow-brown mosaic across the meadow. Shrubs and non-evergreen trees that were dormant at the beginning of May have turned green. This suggests a re-initiation of transpiration as plants begin growing and photosynthesizing again. The greenness increases into June, when it appears to peak.

Table 16. Summary of Aerial Imagery Interpretations.

Site	May 2	May 26	June 7	June 26
Beaver wetland	Flooded	Draining	Half capacity	Half capacity
Side channel	Two channels	One channel	One channel	One channel
Meadow	Yellow	Patchy green	Green	Green

The second trend visible in the aerial photography is a declining water level. Peak discharge at Taneum Creek is snowmelt-dependent and thus occurs in April. In the May 2nd imagery, the recent presence of floodwaters is apparent. At this time, the side channel is multi-threaded, and water seems to be trapped and ponded in several locations across the floodplain. Filled by floodwaters, the beaver wetland is at its greatest extent. By May 26th, discharge has reduced sufficiently that flow is confined to a single side channel. A corresponding slight water-level decline can be seen in the beaver wetland, as its waters are supplied by the side channel. The water level in the beaver wetland continues to decline into June.

¹ $\delta = \frac{(R_{smp} - R_{std})}{R_{std}} \times 1000$, where smp is the sample, std is a standard and R is the isotope ratio, $\frac{^{18}\text{O}}{^{16}\text{O}}$ for $\delta^{18}\text{O}$ and $\frac{\text{D}}{\text{H}}$ for δD . The standard for water analyses is Vienna Standard Mean Ocean Water (V-SMOW).

SOLAR RADIATION

Solar radiation is one of the main driving factors for evapotranspiration, both in providing sunlight for plant photosynthesis and in transmitting energy to warm the environment. In the Penman-Monteith equation net solar radiation is a dominant term in most settings. In this study, net solar radiation was measured using a radiometer that was set up on a ladder in the Meadow site, a relatively sunny location in the study area. In Figure 50, our measured data is compared to net solar

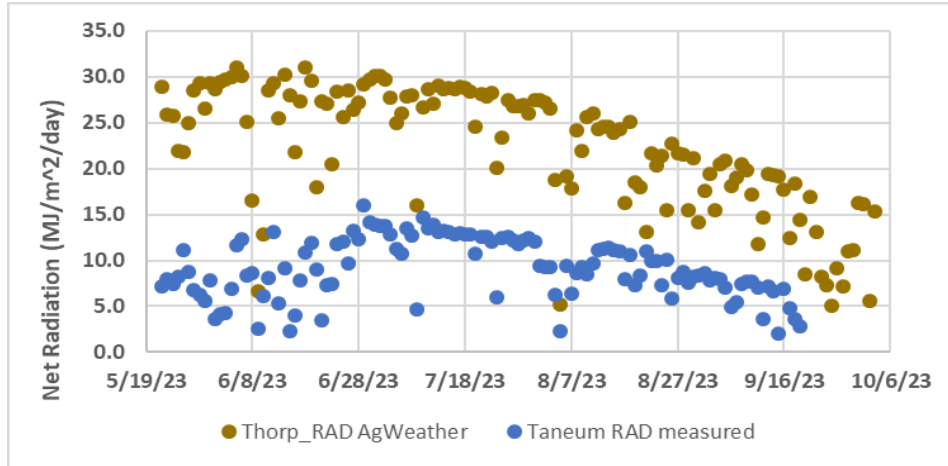


Figure 50. Net solar radiation measured at the Taneum Meadow site and at an AgWeather station in Thorp, WA (AgWeatherNet, 2023).

radiation from AgWeatherNet (2023) for a site in Thorp, WA. Although the data trends are similar, the Taneum site data is 4 to 7 times lower than the Thorp data. It is possible that some of this discrepancy is due to an inaccurate calibration for one or both of the radiometers. However, it is likely that much of the difference is because the Taneum site is in a valley and does not receive sunlight for several additional hours in the morning and the evening. In contrast, the Thorp AgWeatherNet site is in a field close to the Yakima River, far from any trees or hills that block sunlight.

VARIATION IN SOIL PROPERTIES IN TANEUM STUDY AREA

The two monitoring locations at the Taneum site are close, approximately 50 meters apart, but were chosen to represent a relatively wet location in the riparian vegetation (Riparian site) and a relatively dry site, a section of the meadow which turns brown earlier in the summer (Meadow site). Thus measurements at these two sites should capture much of the range of characteristics.

Figures 51 and 52 show soil temperature and soil moisture at the two Taneum monitoring sites. In Figure 51, the daily mean air temperature, computed as the geometric mean of the maximum and minimum temperature, for the Thorp AgWeatherNet site is shown on each graph for reference. The Meadow site has soil temperatures above or equal to the Thorp AgWeather temperatures while the Riparian site has temperatures that are approximately 5°C lower. One might expect that the Meadow site would also have drier soil. In fact, the soil there is only drier at 5 cm depth in the late summer. The deeper soils, 10-20 cm, at the Meadow site have a higher moisture content than those

at the Riparian site. They do not show the same response to precipitation as the shallower soil or any of the depths at the Riparian site.

The two sites differ in soil depth and composition, particularly grain size. Though no quantitative grain size analysis was conducted, sediment at the riparian location was observed to be noticeably coarser during equipment installation, ranging from fine sand to gravel. In contrast, the meadow sediment is much finer, ranging from clay to coarse sand. This variability in soil composition may have an influence on this unexpected moisture trend.

The meadow monitoring location noticeably lacks vegetation. There are numerous patches across the Taneum floodplain that possess much less vegetation than the surrounding area. The

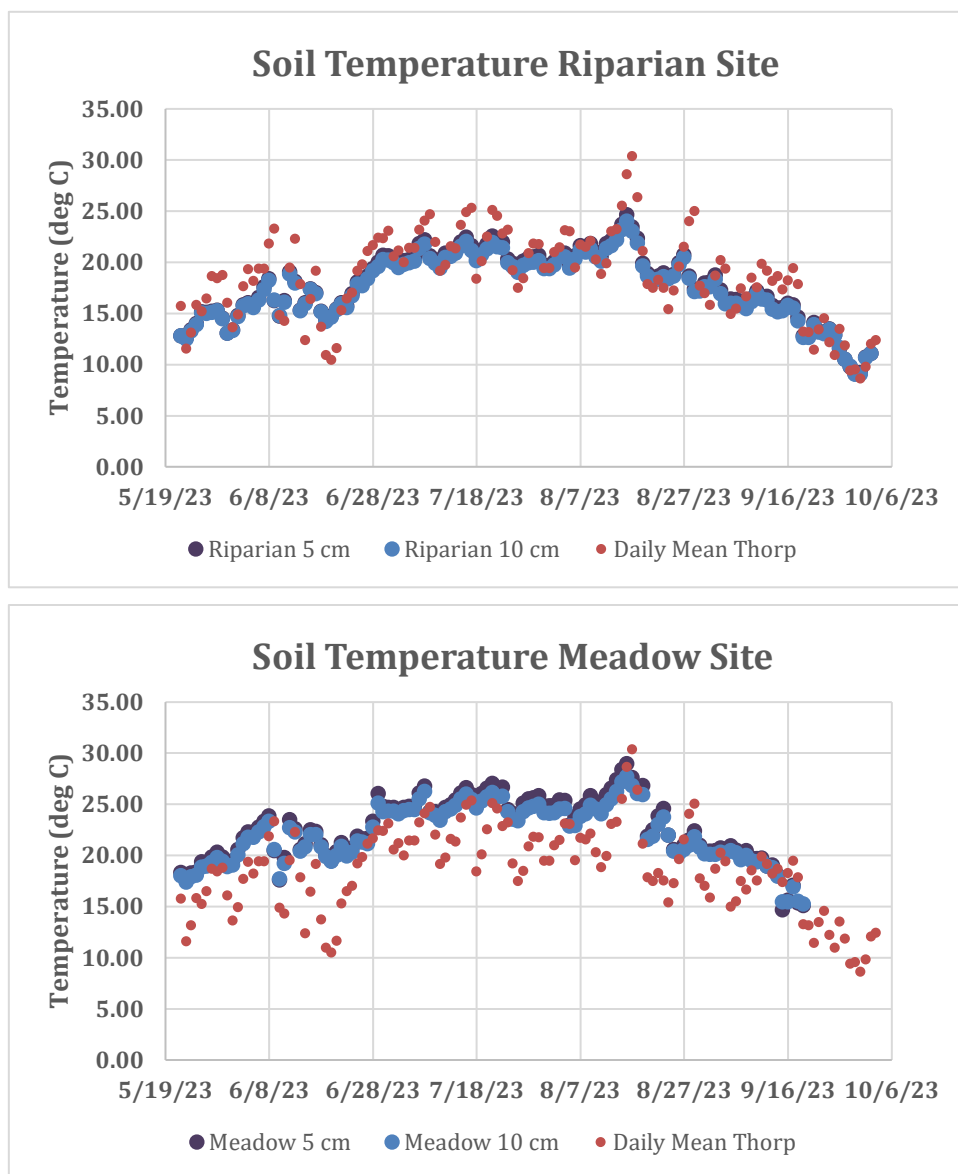


Figure 51. Daily average soil temperatures at two Taneum sites and daily mean temperatures at Thorp AgWeatherNet station. Soil temperatures were measured at 5 and 10 cm depth. For the Riparian site, they are nearly identical.

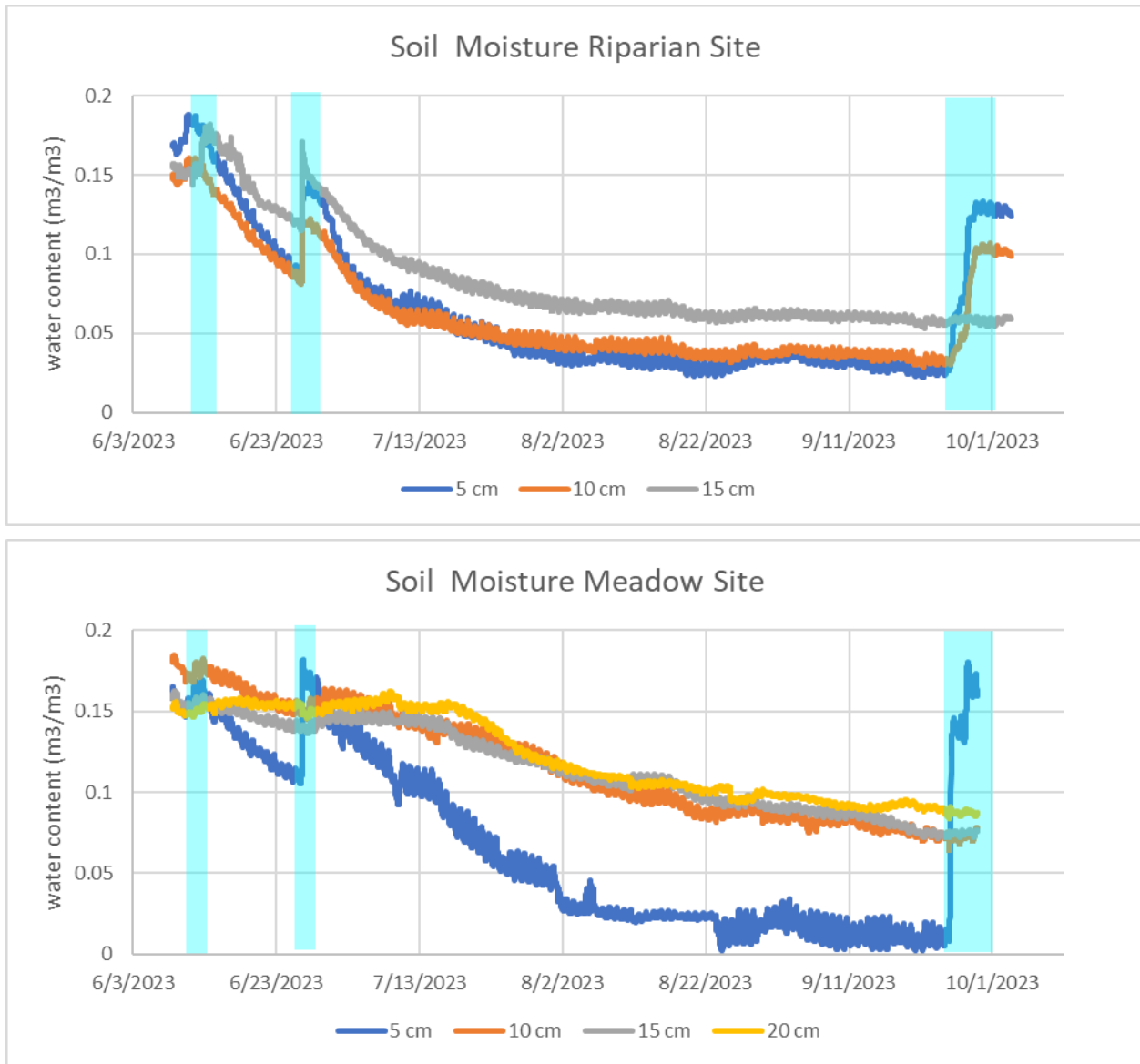


Figure 52. Soil moisture measurements at two Taneum sites. Measurements for three depths are shown (5, 10, 15 cm) for the Riparian site and four depths (5, 10, 15, 20 cm) for the Meadow site. The light blue shaded strips highlight precipitation events.

meadow monitoring location was established in one of these relatively clear patches of ground. This lack of flora may limit evapotranspiration from the shallow soil at the site to just soil evaporation.

The moisture lost from the top 15-20 cm of soil column at the two sites can be summed over the periods between precipitation events to determine the total amount of water lost from that part of the soil column over the observation period. Table 17 presents the results of this calculation. The total water lost from the upper 20 cm of soil is 0.3 to 0.5 mm between June 11 and June 25 or 0.003 to 0.005 mm/day. This is a small fraction of the precipitation that occurred during that period, approximately 8 mm. It is likely that the majority of that moisture is retained in shallow soil, including grass roots in the upper 5 cm, and consumed by plants or evaporated. It is evident from

the soil moisture curves (Figure 52) that this moisture is removed rapidly in the first two weeks, particularly from the shallow soil, and then at decreasing rates over the following month.

Table 17. Calculated moisture lost from upper 20 cm of soil at Taneum sites.

	Riparian	Meadow
June 11 – June 25		
moisture lost* (mm)	0.19	0.6
Rate of moisture loss (mm/day)	0.014	0.005
June 27 – September 24		
moisture lost* (mm)	0.28	0.27
Rate of moisture loss (mm/day)	0.003	0.003
Total		
moisture lost* (mm)	0.47	0.33
Rate of moisture loss (mm/day)	0.005	0.003

*assumes soil densities between 1.2 for 0 – 5 cm depth and 1.5 g/cm³ for 5 – 20 cm depth. Moisture depth profiles is approximated as a step function.

Soil heat flux, G , is the only directly measured Penman-Monteith equation input parameter that varies between the Riparian and Meadow monitoring sites (see Equation 6). The relatively dry meadow monitoring site is surrounded by almost exclusively grass, whereas the relatively wet riparian location represents a mix of vegetation, including grass, bushes, and deciduous and evergreen trees. The two sites are in close proximity to each other, less than 50 m apart. Thus we make the assumption that they are subject to approximately the same weather conditions, though there is likely some variability due to the difference in vegetation and cover between the two sites. Besides soil heat flux, weather-based parameters serve as all the other input variables in the Penman-Monteith equation. As a result, any variation in calculated ET values between the two sites should mirror soil heat flux differences.

Daily soil heat fluxes during the entire study period can be seen in Figure 53. There are a number of differences between the two sites, which are discussed in detail in Vlasenko (2023). But to the first order, the two sites are very similar in both magnitude and weekly trends of heat flux. They fluctuate most strongly in May and June and then tend to decline from approximately 1 MJ/m²/day to 0 MJ/m²/day by mid-September.

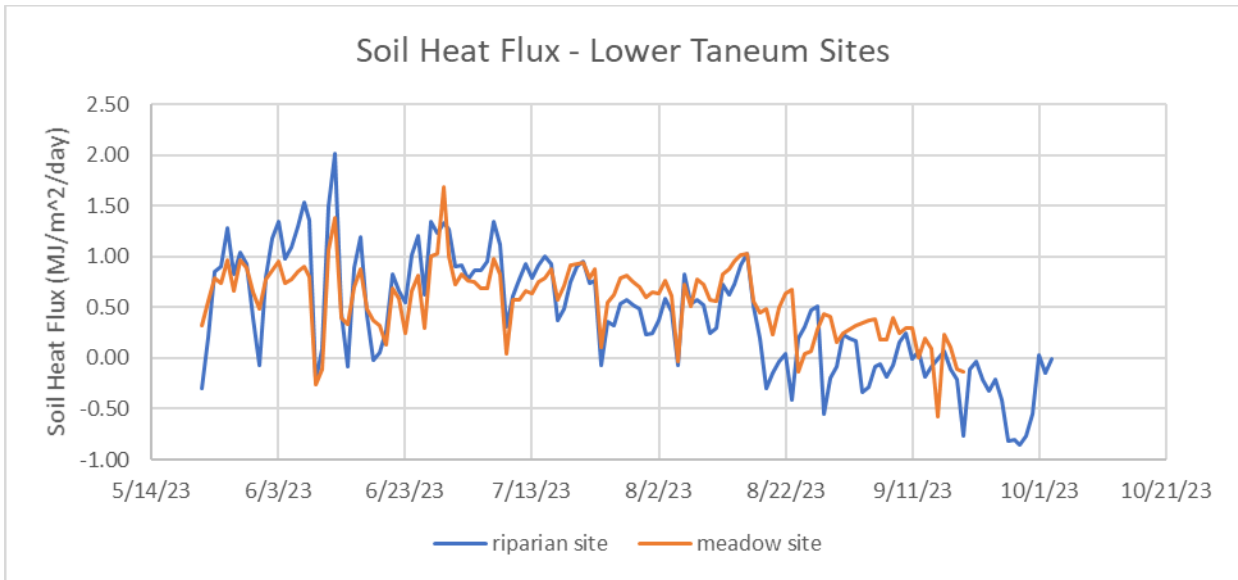


Figure 53. Daily soil heat flux averages at two Taneum sites.

EVAPORATION TRENDS

Evaporation pan measurements are a common method of quantifying evaporation. Evaporation pans generally overestimate actual evaporation, because they are relatively shallow and can be heated from the sides and bottom as well as the top, so evaporation rates are corrected using a pan coefficient (Allen et al., 1998). Derived from local wind speed and relative humidity data, an average pan coefficient over the measurement period was 0.62. Daily evaporation rates, corrected with pan coefficients, are shown in Figure 54. The measured evaporation rate in late June through mid-August fluctuated around approximately 1 mm/day, followed by an abrupt drop in late August and a more gradual decline into the fall. It should be pointed out that these evaporation rates are

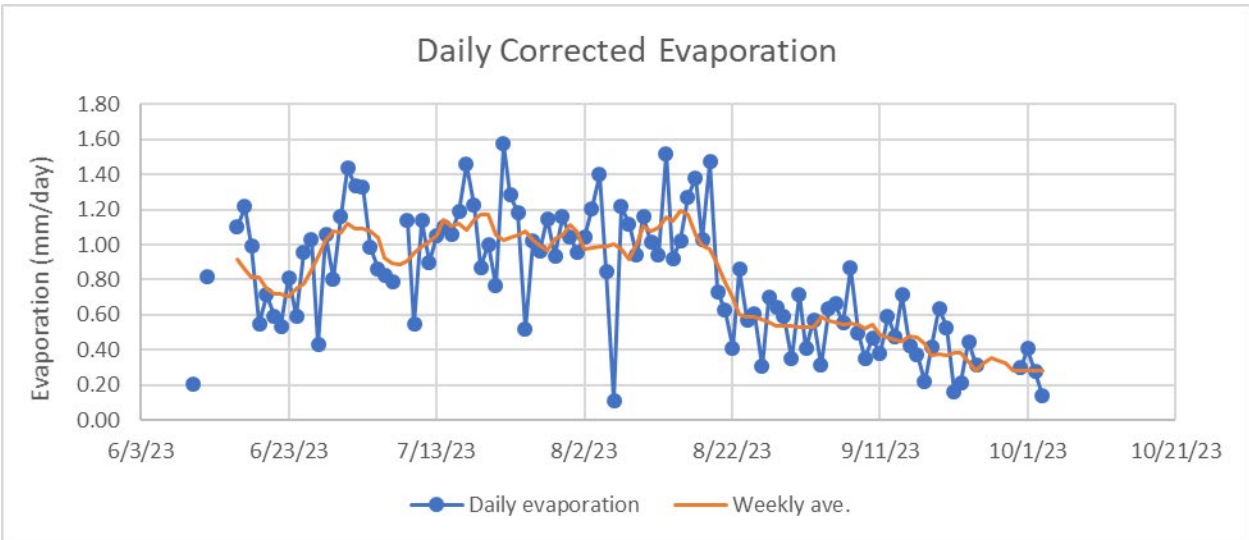


Figure 54. Daily evaporation rates at the Taneum study area. Values are based on pan evaporation rates corrected with a pan coefficient (Allen et al., 1998). Blue dots are daily rates, red line is weekly average.

essentially potential evaporation rates which would be achieved from a free water surface. Evaporation of this magnitude is not achieved in the majority of the study area because evaporation is limited by soil moisture and precipitation amounts. However, evaporation of this magnitude might be expected in the beaver ponds and the wetlands surrounding them.

SOIL-HEAT-FLUX BASED DETERMINATIONS OF EVAPOTRANSPIRATION AND COMPARISON WITH SATELLITE-BASED ESTIMATES

Using the measured soil heat flux and net solar radiation at the environmental monitoring sites, ET rates were calculated using a FAO-56 form of the Penman-Monteith calculation adapted from Zotarelli et al. (2010). This calculated ET, call a “reference ET”, also incorporates two crop-related constants, C_n and C_d , and meteorological data (wind speed, temperature, humidity). The daily measured input values to the Penman-Monteith equation (Equation 8) used in our calculations can be found in Appendix B.

On most days, daily ET between the two equipment sites is very similar and ET curves for the two sites overlap almost completely (Figure F). On Figure 55, the Taneum ET rates are compared to ET values obtained from OpenET (2023) for a 4.3-hectare parcel chosen to represent the entire floodplain at the study site and to the evaporation rates calculated from pan evaporation. The OpenET platform can calculate ET values using a variety of established models/equations. The curve shown in Figure 55 is an ensemble of different models, which has been filtered to remove outlier values prior to averaging.

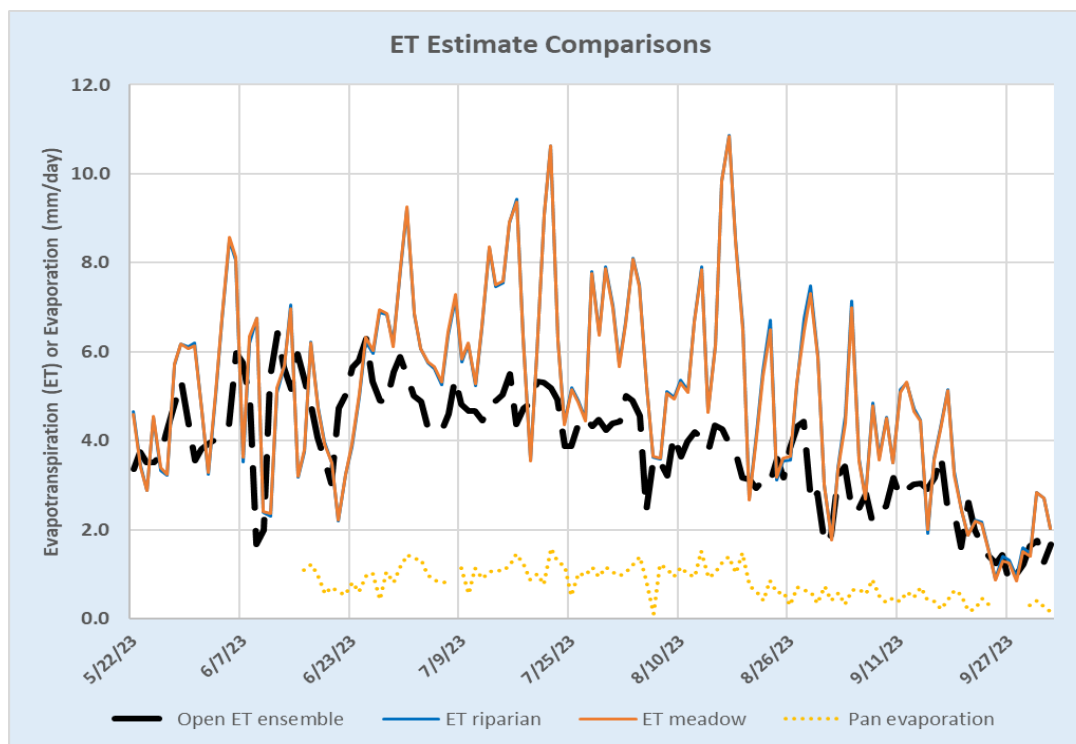


Figure 55. Calculated ET and evaporation rates at Taneum site. Shown are soil-heat-flux based ET rates for two Taneum sites (orange and blue solid lines), ensemble of satellite-based ET rates (dashed black line) from OpenET (2023), and evaporation rates from pan measurements (dotted yellow line).

The soil-heat-flux based ET estimates are significantly higher than the remote-sensing based estimates, particularly in the months of July and August. The median values, shown in a box-and-whisker diagram in Figure 56, is 5.1 mm/day for the soil-based measurements versus 4.1 mm/day for OpenET. The soil-heat-flux based determinations also have a greater variability and fluctuate more strongly from day to day than the OpenET values. The greatest differences between the two ET estimates occurs on days with high mean temperature. In fact, there is a moderate correlation between the difference in the two estimates and daily mean temperature (Figure 57).

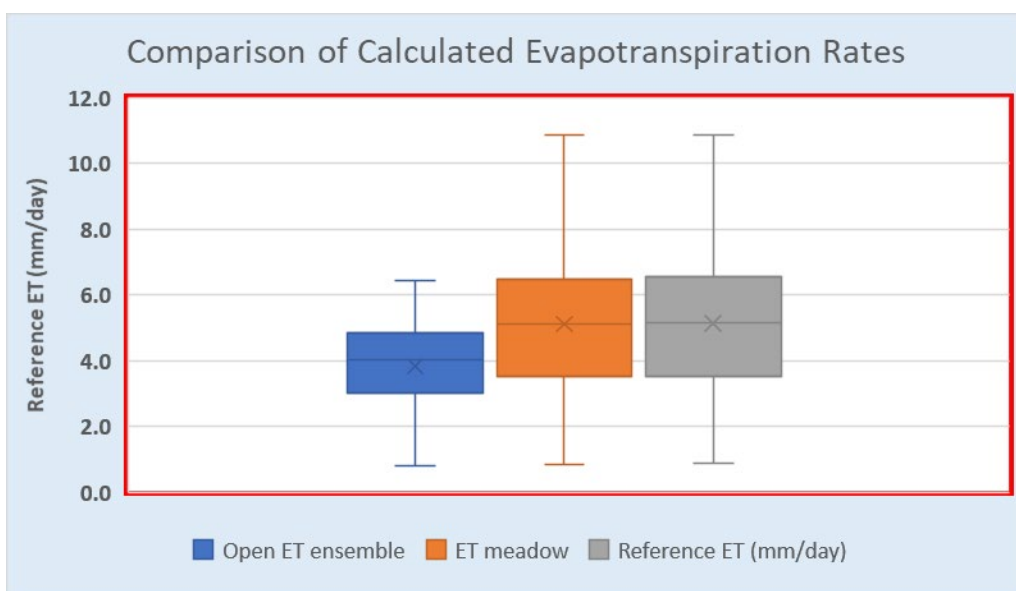


Figure 56. Box and whisker plots showing distributions of ET values for OpenET and field-measurement-based estimates.

In exploring the discrepancy between the soil-heat-flux and satellite-based estimates of ET, we considered the role of two inputs to the Penman-Monteith equation that were not well constrained: wind velocity and crop constants. The wind velocities used in our calculations were from the Thorp AgWeatherNet station, which is located in Thorp near the Yakima River, generally the windiest part of Kittitas Valley. In contrast, the Taneum site is within the Taneum Creek canyon. Although wind is sometimes channeled down the canyon, it is often less windy than the exposed site in Thorp. As such, we recalculated the soil-heat-flux based estimates with 70% lower mean wind speeds. The resultant ET values matched the OpenET values much more closely (Figure 58).

We used two crop constants in the modified Penman-Monteith equation, one in the numerator, C_n , and one in the denominator, C_d (Equation 8). The reference values suggested by Zotarelli et al. (2010) are 900 (C_n) and 0.34 (C_d) for short reference crops and 1600 (C_n) and 0.38 (C_d) for tall reference crops. In our ET calculations, we used the short reference crop values, both because our sites were dominated by grasses and because those constants yielded lower ET values. To test if still lower crop values might yield ET values more similar to OpenET values, C_n of 600 and C_d of 0.32 were used in a calculation. The results, shown in Figure 58, are also more similar to OpenET than the results with the short crop constants. However, the adjusted crop factor curve still tends to have a greater range and more large fluctuations than either the 70% wind speed or the OpenET estimates.

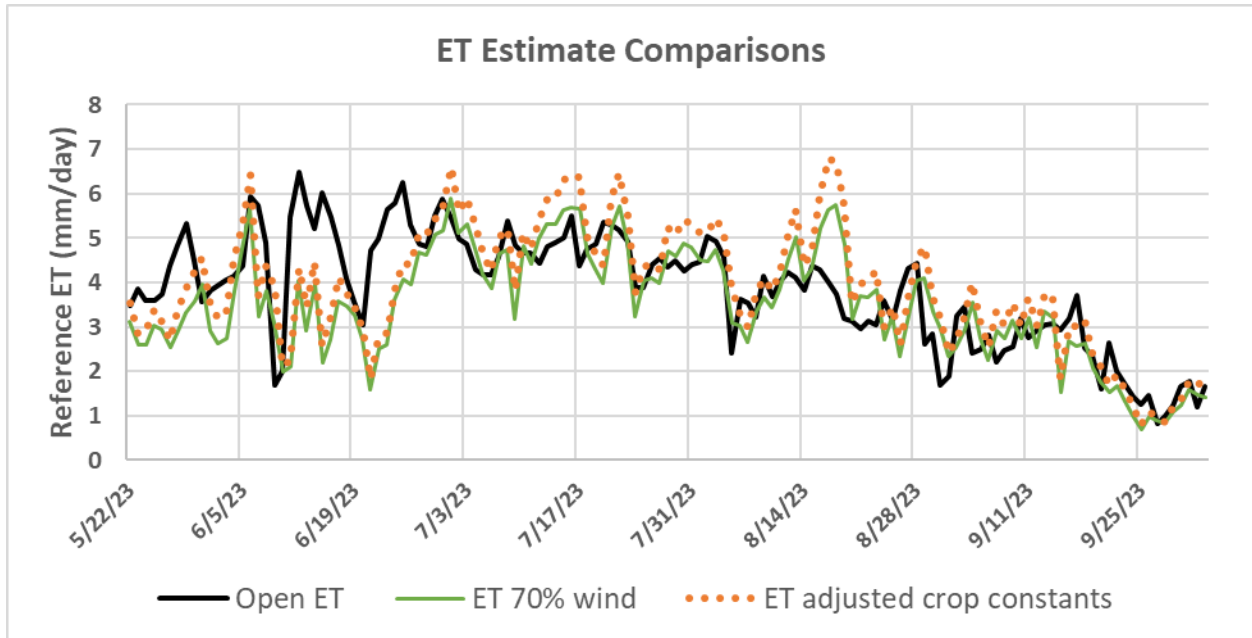


Figure 57. Comparison of ET values for OpenET and two modified soil-heat-flux calculations. Solid black line is OpenET daily values (as in Figure 55); solid green line is soil-heat-flux calculation with wind speed at 70% of the AgWeatherNet values for Thorp; orange dotted line is soil-heat-flux calculation with lower crop constants of $C_n = 600$ and $C_d = 0.32$.

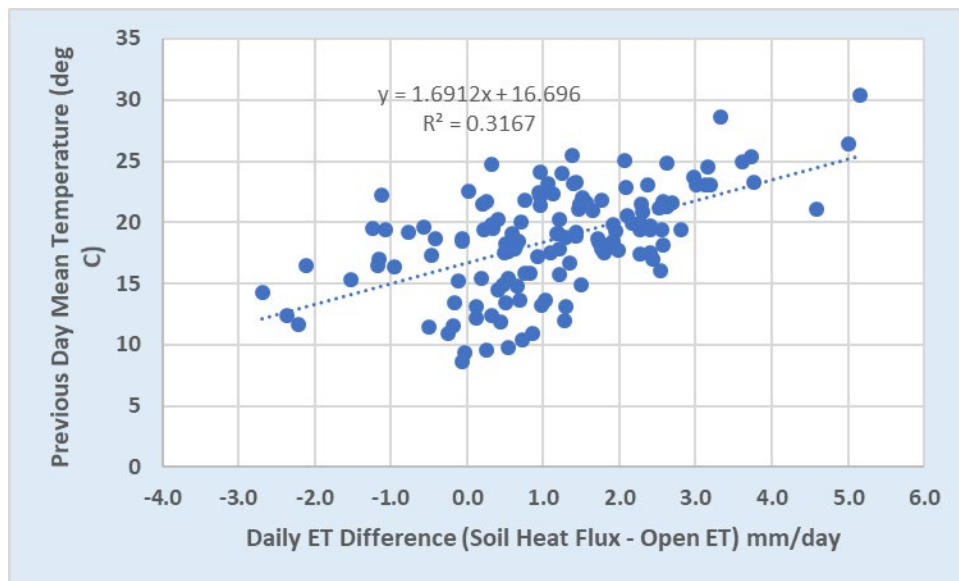


Figure 58. Difference in calculated ET methods vs. daily temperature. The difference between the ET calculated from field measurements of soil heat flux and the ET calculated using Open ET increases with temperature at the site.

STABLE ISOTOPE EVIDENCE FOR EVAPORATION AND GROUNDWATER INPUT

Stable isotopes of oxygen and hydrogen are useful for studying a number of hydrologic processes including evaporation and mixing between isotopically distinct water bodies, in particular surface water-groundwater interaction. The evaporation process preferentially removes water molecules with the lighter isotopes of oxygen (^{16}O) and hydrogen (^1H), leaving behind water with greater amounts of the heavier isotopes (^{18}O and D). As a result, these water body will become more enriched in the heavy isotopes as it undergoes evaporation. This evaporative enrichment is described by mass balance equations, which have been used to determining evaporation rates in lakes and other standing water bodies (e.g. van den Akker et al., 2011; Zanazzi et al., 2020 and references therein).

When isotopically distinct water bodies mix, the water mixture will have an isotopic composition that is the weighted average of the mixing end members. In many cases, surface water is isotopically distinct from the resident groundwater in the region. Thus, when surface water enters an aquifer and mixes with the groundwater there, the interaction will be recorded in the isotopic composition of the mixture. In the Yakima River basin, resident groundwater is usually isotopically lighter (lower $\delta^{18}\text{O}$ and δD) than Yakima River and irrigation water and a number of studies have defined regions of surface water infiltration based on this distinct surface water signature (e.g. Taylor and Gazis, 2016; Sleeper, 2020).

In this study, water was collected from two Taneum Creek channels, multiple locations in a complex of beaver ponds and dams, and an evaporation pan between August 11, 2022 and June 28, 2023. The measured $\delta^{18}\text{O}$ for these samples is shown in Figure 59. The evaporation pan samples show a clear evaporative ^{18}O enrichment for both of the summers when it was installed. One would expect a similar enrichment, but less pronounced, in standing water bodies such as lakes and ponds. With the exception of one sample, the beaver pond samples appear to be very similar isotopically to Taneum Creek. Because they are likely undergoing evaporation, this isotopic similarity implies that water residence time in the beaver ponds is short and water that has been enriched isotopically by evaporation is rapidly carried away from the ponds.

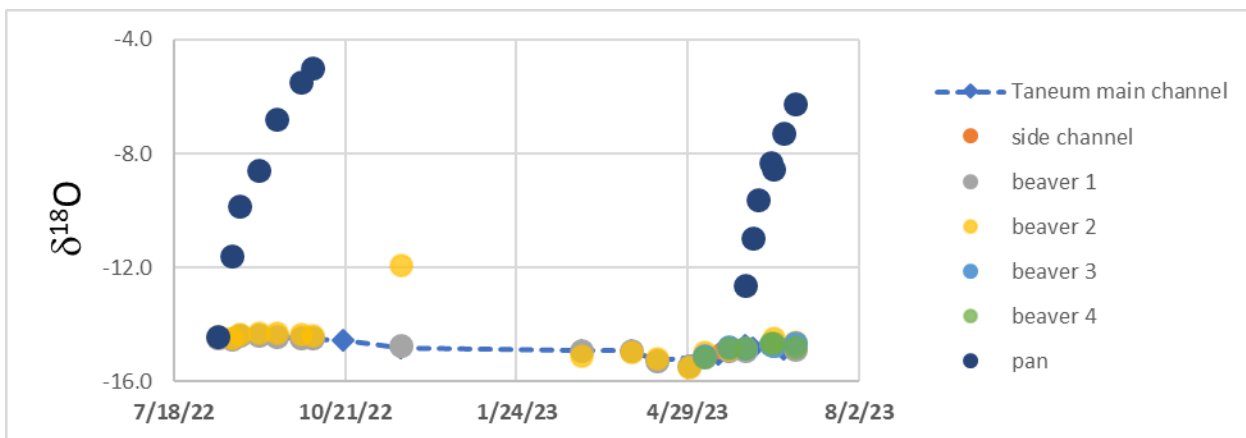


Figure 59. Oxygen isotope compositions of Taneum site water samples from the channels, evaporation pan and beaver ponds. Beaver 1-4 represent different beaver pond locations from which samples were all collected on the same day.

Although the beaver pond samples are isotopically similar to Taneum Creek, there are some subtle differences, which can be seen in Figure 59. In this plot, the difference in hydrogen isotopic composition between the beaver pond samples and Taneum Creek is plotted versus the sampling date. A number of beaver pond samples, particularly in late summer 2022, show a slight enrichment in D relative to Taneum Creek, likely the result of evaporation. However, many of beaver pond samples that were collected in 2023 have isotopic compositions that are lighter than the Taneum main channel, indicating that they have mixed with isotopically lighter water (Figure 60). In that

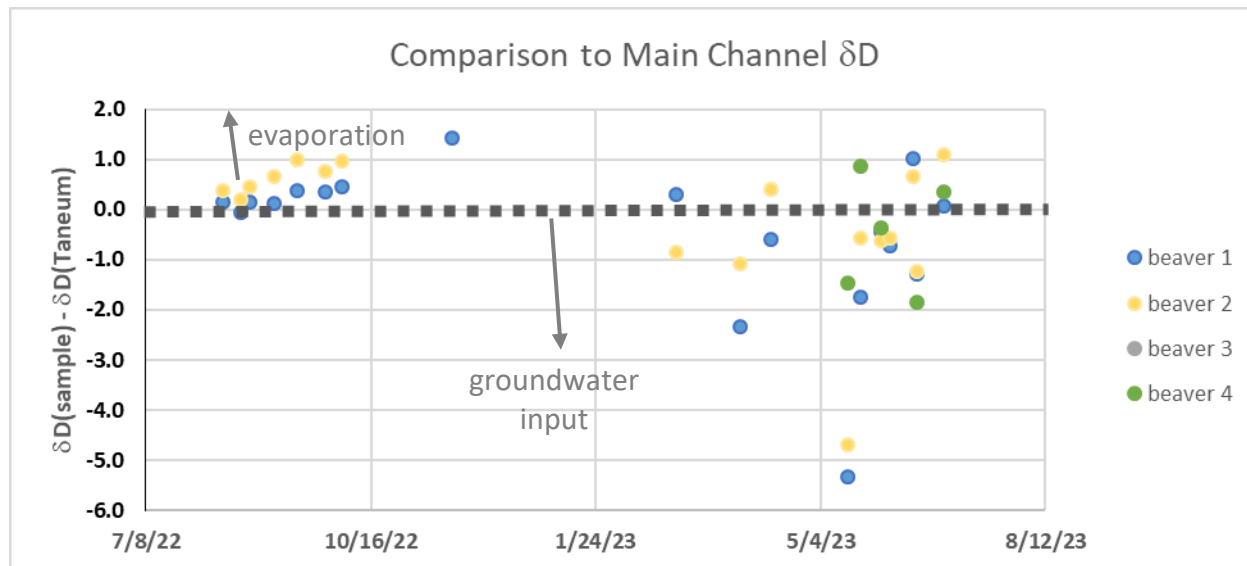


Figure 60. Difference in hydrogen isotope composition between beaver ponds and Taneum Creek samples. Beaver 1-4 represent different beaver pond locations that were all collected on the same day. The dashed black line is the value of samples that are isotopically identical to the Taneum Creek main channel.

there is no obvious surface source for this isotopically lighter water, we conclude that there is some input of groundwater to the beaver ponds during that time, from March to June, 2023. This groundwater could be derived from local snow, which tends to be light isotopically or it could be from a deeper aquifer.

CHAPTER 3 CONCLUSIONS

Taneum Creek is a tributary in the upper Yakima River basin, located in central Washington state in the rainshadow of the Cascade Mountains. Extensive restoration efforts on Taneum Creek, primarily through large wood emplacement, have greatly increased channel-floodplain connectivity and are returning the hydrology and geomorphology to a more “natural” state. This has had beneficial impacts on the wildlife in the area, especially spawning fish. Since restoration, beavers have colonized the area, further altering surface and groundwater flows at the study site. In general, the increased connectivity and beaver activity has led to a greening of the floodplain and increased recharge of the floodplain aquifer through side channels and overbank flows (Fixler, 2022). However, the increased vegetation growth can in turn remove water from the floodplain aquifer at a greater rate through ET, and the net impact of restoration on aquifer storage depends on this balance. This study aimed to quantify ET water loss from Taneum Creek and its floodplain during the dry season, when stream flows are maintained by groundwater baseflow.

For this study, two monitoring sites were established in the lower Taneum floodplain, representing the relatively moist riparian zone and the drier meadow nearby. Soil heat flux and radiation measurements at those sites, combined with weather data from a nearby station were used to determine ET rates, which were compared to estimates based on remote sensing data. Soil moisture and evaporation were also monitored at the Taneum sites.

This study provides a range of estimates for important water budget components for the Taneum floodplain aquifer, summarized in Table 18 and Figure 61. The flux values (precipitation, ET, evaporation, transpiration) represent the totals (in m) for June 11 to September 24, 2023. Our calculated ET based on soil heat flux is nearly identical for the two sites at Taneum and is significantly higher than the ET estimate produced by OpenET (2023), which calculates daily values based on satellite data. The discrepancy between the two ET calculations may be because we used wind speed data from a nearby weather station that is less protected than the Taneum study area. However, there are a number of other parameters and assumptions that go into both estimates that might also cause systematic error.

Table 18. Estimates of Water Budget Components for Taneum Floodplain Aquifer

Parameter	Low Estimate	High Estimate
Floodplain Storage Available*	0.18 m	0.46 m
Precipitation**	0.008 m	
Evapotranspiration**	<i>OpenET</i> 0.43 m	<i>Soil-heat-flux</i> 0.56
Evaporation**	<i>Soil moisture loss</i> 0.0005 m	<i>Evaporation pan</i> 0.085 m
Transpiration***	0.34 m	0.56 m

*Floodplain storage estimate from Chapter 1 Table 7 and Polizzi (2023), using available thickness and porosity of 0.3.

**Flux estimates are based on measurements (precipitation, evaporation) and Penman-Monteith calculation (ET) and represent the total amount between June 11 and September 24, 2023.

***Transpiration is calculated from ET – evaporation. Low estimate uses lower ET (OpenET) and higher evaporation (pan); high estimate uses higher ET and lower evaporation.

Regardless of which estimate is used, it is evident that these ET values, between 0.4 and 0.6 meters in uniform thickness, represent a large outflow of water from the Taneum floodplain. Soil moisture values indicate that ET outflows from the unsaturated zone represent a negligible amount of this total loss. Evaporation pan measurements, which give potential losses from beaver ponds, Taneum channels and marshy zones, are also small compared to total ET, implying that much of the ET outflows are due to plant transpiration of moisture derived from the floodplain aquifer.

Estimated ET over this four-month period removes a volume of water similar to or larger than the estimated volume of storage available in the portion of the shallow floodplain aquifer above the elevation of the Taneum Creek channel bed (Chapter 1 Table 7; Polizzi, 2023). Thus, although

river restoration has many ecological benefits, it is likely that any groundwater storage gained by increased floodplain inundation from the river may well be lost through increased vegetation and ET.

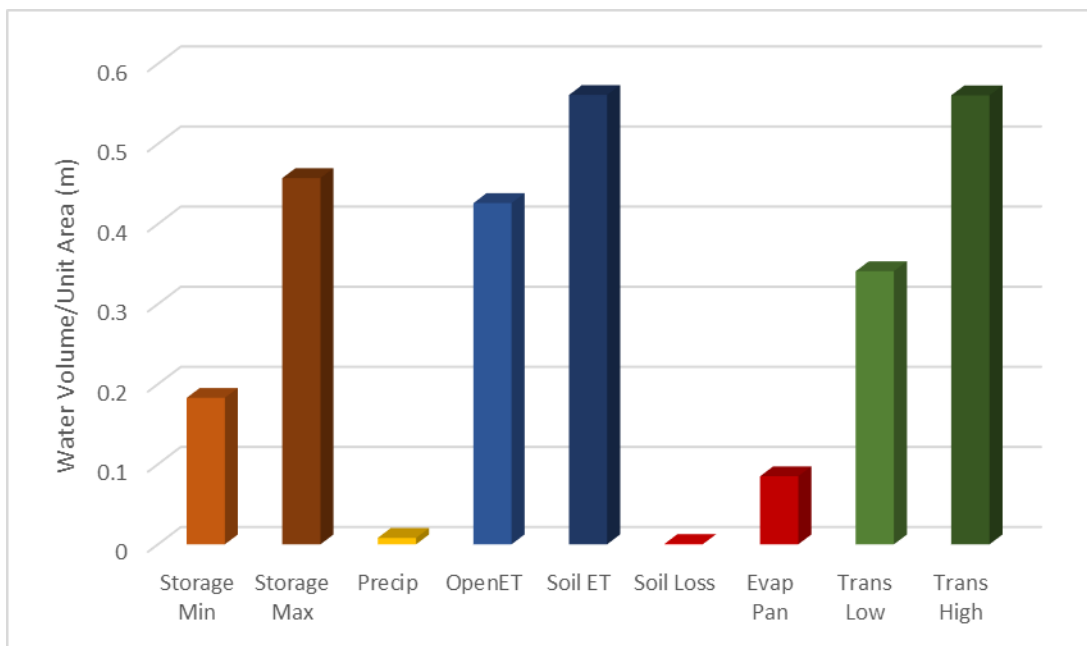


Figure 61. Magnitude of fluxes and available storage at Taneum Creek site. Explanations of each category are in Table 18.

Stable isotope data for waters from Taneum Creek and locations in the beaver pond complex further elucidate flows into and out of the system. Beaver pond isotopic values indicate that water residence times in the beaver ponds are short such that water passes quickly through the system. Furthermore, isotopic signatures of some beaver pond samples from spring 2023 suggest that there is some influx of groundwater into the alluvial aquifer and the beaver ponds. The source of this groundwater is not known and would be a good target of future investigations.

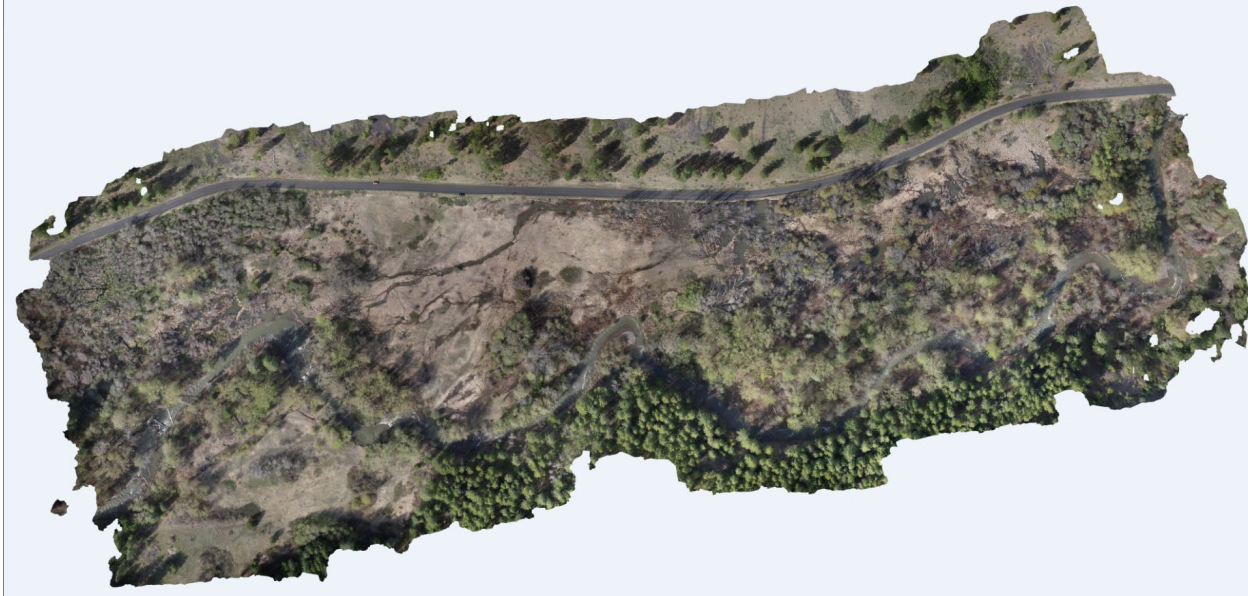
REFERENCES

- Abbe, T.B. and Montgomery, D.R., 1996, Large woody debris jams, channel hydraulics and habitat formation in large rivers, *Regulated Rivers: Research and Management*, no 2-3, p. 201-221.
- AgWeatherNet. Site 30, Thorp: <https://weather.wsu.edu/>, accessed June, 2023.
- Allen, R. G., Walter, I. A., Elliot, R. L., Howell, T.A., Itenfisu, D., Jensen, M. E. and Snyder, R., 2005, The ASCE standardized reference evapotranspiration equation, ASCE and American Society of Civil Engineers.
- Allen, R.G.; Pereira, L.S.; Raes, D.; Smith, M. Crop evapotranspiration: guidelines for computing crop water requirements. Rome: FAO, 1998. 301p. Irrigation and Drainage Paper, 56.
- Córdova, M., Carrillo-Rojas, G., Crespo, P., Wilcox, B., and Célleri, R., 2015. Evaluation of the Penman-Monteith (FAO 56 PM) Method for Calculating Reference Evapotranspiration Using Limited Data. *Mountain Research and Development*, 35(3):230-239 DOI: 10.1659/MRD-JOURNAL-D-14-0024.1.
- Ely, D.M., Bachmann, M.P., and Vaccaro, J.J., 2011, Numerical simulation of groundwater flow for the Yakima River basin aquifer system, Washington: U.S. Geological Survey Scientific Investigations Report 2011-5155, 90 p.
- Essaid, H.I., Hill, B.R., 2014. Watershed-scale modeling of streamflow change in incised montane meadows. *Water Resources Research* 50 (3) DOI: [10.1002/2013WR014420](https://doi.org/10.1002/2013WR014420)
- Fixler, S., 2022, Decadal-Scale Effects of Large Wood Restoration on Channel Morphology and Groundwater Connectivity, Taneum Creek, WA: M.S. Thesis, Central Washington University. <https://digitalcommons.cwu.edu/etd/1783>.
- Gendaszek, A.S., Ely, D.M., Hinkle, S.R., Kahle, S.C., and Welch, W.B., 2014, Hydrogeologic framework and groundwater/surface-water interactions of the upper Yakima River Basin, Kittitas County, central Washington: U.S. Geological Survey Scientific Investigations Report 2014 5119, 66 p., <http://dx.doi.org/10.3133/sir20145119>.
- Henderson, E.M., 1990, The Pine Tree Express: A history of the Cascade Lumber Company's pine hauling railroad in Kittitas County, Washington, 1916-1946
- Henning, L. 2023. Using MODFLOW to Assess Groundwater Storage Enhancement via a Floodplain Infiltration Basin: M.S. Thesis, Central Washington University. <https://digitalcommons.cwu.edu/etd/1873>.
- Jones and Stokes Associates, 1991, Watershed characteristics and conditions inventory; Taneum Creek and Tacoma Creek watersheds. Prepared for Washington Department of Natural Resources, p. 61.
- Loheide SP, Deitchman RS, Cooper DJ, Wolf EC, Hammersmark CT, Lundquist JD. 2009. A framework for understanding the hydroecology of impacted wet meadows in the Sierra Nevada and Cascade Ranges, California, USA. *Hydrogeology Journal* 17 (1): 229–246 DOI: [10.1007/s10040-008-0380-4](https://doi.org/10.1007/s10040-008-0380-4).
- McCabe, M.F., Miralles, D.G., Holmes, T.R.H., and Fisher, J.B., 2019, Advances in the remote sensing of terrestrial evaporation: *Remote Sensing*, v. 11, p. 1138, doi: 10.3390/rs11091138.
- Monk, P., 2009, Taneum Creek Study: The Bruton-KRD Water Exchange Project. Bureau of Reclamation Open-File Report, p. 1-26
- Nagler, P., Jetton, A., Fleming, J., Didan, K., Glenn, E., Erker, J., Morino, K., Milliken, J., Gloss, S., 2007, Evapotranspiration in cottonwood (*Populus fremontii*) restoration plantation estimated by sap flow and remote sensing methods. *Agricultural and Forest Meteorology* 144: 95-110 DOI: 10.1016/j.agrformet.2007.02.002.

- OpenET, <https://openetdata.org/>, accessed July 2023.
- Polizzi, E., 2023, Floodplain Aquifer Storage Capacity in Upper Yakima River Tributaries, Kittitas County, WA: M.S. Thesis, Central Washington University. <https://digitalcommons.cwu.edu/etd/1872>.
- Rana, G., and Katerji, N., 2000, Measurement and estimation of actual evapotranspiration in the field under Mediterranean climate: A review. *European Journal of Agronomy*, v. 13(2-3), p. 125-153. doi:10.1016/s1161-0301(00)00070-8.
- Sleeper, S. 2020. A Geochemical Assessment of Potential Groundwater Storage Locations within the Yakima River Basin. MS Thesis, Central Washington University. <https://digitalcommons.cwu.edu/etd/1372>
- Subedi, A., and Chávez, J.L., 2015, Crop evapotranspiration (ET) estimation models: A review and discussion of the applicability and limitations of ET methods: *Journal of Agricultural Science*, v. 7, doi: 10.5539/jas.v7n6p50.
- Tague C, Valentine S, Kotchen M. 2008. Effect of geomorphic channel restoration on streamflow and groundwater in a snowmelt-dominated watershed. *Water Resources Research* 44 (10): n/a-n/a DOI: [10.1029/2007WR006418](https://doi.org/10.1029/2007WR006418)
- Tappel, P., 2012, Consideration of Large Wood Placed in Taneum Creek by the Yakima Indian Nation, with Respect to Flood Damages to Private Property in Mid-May 2011. Fisheries Engineers, Inc Open-File Report, p. 1-8.
- Taylor S. and Gazis C.A., 2014. A geochemical study of the impact of irrigation on groundwater in the Upper Yakima River Basin, Washington, USA: *Environmental Geology*, v. 72, p 1569-1587.
- Toth, S, 1995, In Support of the Habitat Conservation Plan on Forested Lands Owned by Plum Creek Timber Company, L.P. in the I-90 Corridor of the Central Cascades Mountain Range, Washington, 1995. Technical Report #11.
- Vaccaro, J.J. and Olsen, T.D., 2007, Estimates of ground-water recharge to the Yakima River Basin aquifer system, Washington, for predevelopment and current land-use and land-cover conditions. US Geological Survey Scientific Investigations Report, 2007 – 5007, 30 p., <https://pubs.usgs.gov/sir/2007/5007/pdf/sir20075007.pdf>.
- [van den Akker](#) J, [Simmons](#) CT, and [Hutson](#) JL. 2011. Use of Stable Isotopes Deuterium and Oxygen-18 to Derive Evaporation from Flood Irrigation on the Basis of Pan Evaporation Techniques. *Journal of Irrigation and Drainage Engineering* [137 \(12\)](#) DOI: [10.1061/\(ASCE\)IR.1943-4774.0000361](https://doi.org/10.1061/(ASCE)IR.1943-4774.0000361).
- Vlasenko, E., 2023, Estimating Evapotranspiration and Analyzing Soil Moisture and Heat Flux Parameters at Taneum Creek, Central Washington: M.S. Thesis, Central Washington University. <https://digitalcommons.cwu.edu/etd/1897>.
- Zanazzi A, Wang W, Peterson H and Emerman SH. 2020. Using Stable Isotopes to Determine the Water Balance of Utah Lake (Utah, USA). *Hydrology* 7 (88) DOI:[10.3390/hydrology7040088](https://doi.org/10.3390/hydrology7040088)
- Zotarelli, L., Dukes, M.D., Romero, C.C., Migliaccio, K.W., and Morgan, K.T., 2009, Step by step calculation of the penman-monteith evapotranspiration (FAO-56 Method), https://www.agraria.unirc.it/documentazione/materiale_didattico/1462_2016_412_24509.pdf (accessed June 2023).

Appendix A. Composite Aerial Imagery of Taneum Creek

These images were used in the analysis of evapotranspiration at Taneum Creek, as described in Chapter 3 of this report.



May 2nd, 2023



May 26th, 2023



June 7th, 2023



June 29th, 2023

Appendix B. Environmental Measurements and Weather Data for Taneum Creek Study Area

Table B1. Daily Averages of Soil Moisture Measurements for Taneum Sites (in m³/m³)

Date	Riparian 2	Riparian 4	Riparian 6	Meadow 2	Meadow 4	Meadow 6	Meadow 8
6/9/23	0.168	0.147	0.153	0.152	0.178	0.156	0.150
6/10/23	0.180	0.154	0.151	0.153	0.172	0.153	0.148
6/11/23	0.183	0.158	0.152	0.159	0.173	0.154	0.149
6/12/23	0.178	0.154	0.161	0.162	0.177	0.156	0.151
6/13/23	0.169	0.147	0.178	0.156	0.175	0.155	0.153
6/14/23	0.160	0.140	0.173	0.149	0.172	0.153	0.153
6/15/23	0.153	0.134	0.166	0.148	0.170	0.152	0.155
6/16/23	0.147	0.130	0.165	0.142	0.169	0.151	0.156
6/17/23	0.139	0.124	0.161	0.136	0.168	0.151	0.156
6/18/23	0.130	0.117	0.149	0.132	0.164	0.149	0.156
6/19/23	0.122	0.111	0.142	0.128	0.160	0.147	0.155
6/20/23	0.116	0.107	0.134	0.125	0.158	0.145	0.154
6/21/23	0.111	0.103	0.131	0.123	0.157	0.144	0.154
6/22/23	0.105	0.099	0.129	0.118	0.156	0.144	0.154
6/23/23	0.099	0.095	0.127	0.115	0.153	0.142	0.154
6/24/23	0.094	0.091	0.124	0.113	0.152	0.141	0.154
6/25/23	0.089	0.087	0.121	0.111	0.152	0.141	0.154
6/26/23	0.103	0.097	0.135	0.134	0.150	0.140	0.152
6/27/23	0.142	0.120	0.150	0.169	0.150	0.139	0.148
6/28/23	0.139	0.116	0.144	0.163	0.153	0.142	0.149
6/29/23	0.132	0.112	0.140	0.157	0.155	0.145	0.150
6/30/23	0.121	0.105	0.135	0.147	0.158	0.146	0.153
7/1/23	0.109	0.098	0.129	0.140	0.158	0.146	0.154
7/2/23	0.098	0.090	0.124	0.139	0.158	0.146	0.154
7/3/23	0.090	0.084	0.118	0.137	0.156	0.146	0.154
7/4/23	0.084	0.079	0.113	0.133	0.155	0.146	0.155
7/5/23	0.080	0.074	0.109	0.128	0.154	0.146	0.156
7/6/23	0.077	0.071	0.105	0.125	0.153	0.145	0.156
7/7/23	0.075	0.069	0.103	0.122	0.152	0.146	0.157
7/8/23	0.071	0.067	0.100	0.117	0.151	0.146	0.159
7/9/23	0.067	0.063	0.097	0.104	0.147	0.144	0.159
7/10/23	0.068	0.061	0.095	0.107	0.146	0.145	0.154
7/11/23	0.068	0.059	0.094	0.107	0.144	0.144	0.153
7/12/23	0.068	0.060	0.092	0.106	0.143	0.144	0.152
7/13/23	0.066	0.059	0.091	0.105	0.141	0.144	0.152
7/14/23	0.065	0.059	0.089	0.104	0.137	0.143	0.152
7/15/23	0.062	0.058	0.087	0.100	0.138	0.142	0.152
7/16/23	0.059	0.057	0.086	0.092	0.140	0.141	0.153
7/17/23	0.056	0.055	0.084	0.085	0.139	0.137	0.154
7/18/23	0.054	0.053	0.082	0.080	0.137	0.133	0.151
7/19/23	0.052	0.053	0.080	0.077	0.136	0.131	0.149
7/20/23	0.051	0.052	0.079	0.074	0.136	0.130	0.147
7/21/23	0.051	0.052	0.079	0.070	0.135	0.129	0.145
7/22/23	0.049	0.051	0.077	0.065	0.133	0.128	0.142

Date	Riparian 2	Riparian 4	Riparian 6	Meadow 2	Meadow 4	Meadow 6	Meadow 8
7/23/23	0.048	0.049	0.076	0.062	0.132	0.126	0.138
7/24/23	0.046	0.048	0.074	0.056	0.129	0.124	0.135
7/25/23	0.045	0.047	0.074	0.054	0.127	0.123	0.131
7/26/23	0.040	0.046	0.072	0.054	0.125	0.122	0.128
7/27/23	0.040	0.046	0.072	0.053	0.125	0.121	0.125
7/28/23	0.040	0.046	0.071	0.052	0.124	0.121	0.123
7/29/23	0.039	0.046	0.071	0.050	0.123	0.120	0.122
7/30/23	0.039	0.045	0.070	0.048	0.120	0.119	0.120
7/31/23	0.037	0.044	0.069	0.047	0.118	0.117	0.118
8/1/23	0.036	0.043	0.068	0.037	0.115	0.115	0.118
8/2/23	0.035	0.043	0.068	0.029	0.112	0.113	0.116
8/3/23	0.035	0.043	0.068	0.029	0.110	0.112	0.115
8/4/23	0.033	0.042	0.067	0.027	0.109	0.111	0.113
8/5/23	0.032	0.041	0.066	0.032	0.106	0.109	0.112
8/6/23	0.035	0.041	0.067	0.032	0.104	0.107	0.111
8/7/23	0.036	0.043	0.067	0.025	0.103	0.107	0.111
8/8/23	0.036	0.043	0.067	0.025	0.102	0.106	0.110
8/9/23	0.035	0.043	0.067	0.025	0.101	0.106	0.110
8/10/23	0.034	0.042	0.066	0.024	0.100	0.105	0.109
8/11/23	0.033	0.041	0.065	0.023	0.099	0.106	0.107
8/12/23	0.033	0.041	0.065	0.022	0.098	0.109	0.105
8/13/23	0.032	0.041	0.065	0.023	0.097	0.108	0.105
8/14/23	0.032	0.041	0.065	0.024	0.097	0.108	0.105
8/15/23	0.032	0.041	0.066	0.024	0.098	0.108	0.106
8/16/23	0.032	0.042	0.066	0.024	0.098	0.107	0.106
8/17/23	0.032	0.040	0.065	0.024	0.096	0.105	0.106
8/18/23	0.030	0.039	0.064	0.024	0.094	0.104	0.105
8/19/23	0.028	0.037	0.062	0.023	0.090	0.100	0.104
8/20/23	0.027	0.036	0.061	0.023	0.088	0.098	0.102
8/21/23	0.027	0.036	0.061	0.024	0.086	0.096	0.102
8/22/23	0.027	0.036	0.061	0.024	0.086	0.096	0.101
8/23/23	0.028	0.036	0.060	0.018	0.087	0.095	0.102
8/24/23	0.028	0.036	0.060	0.011	0.088	0.094	0.103
8/25/23	0.029	0.035	0.060	0.012	0.089	0.094	0.099
8/26/23	0.031	0.036	0.061	0.015	0.090	0.094	0.095
8/27/23	0.033	0.038	0.062	0.016	0.090	0.095	0.096
8/28/23	0.034	0.039	0.062	0.015	0.091	0.095	0.097
8/29/23	0.034	0.037	0.062	0.016	0.089	0.093	0.099
8/30/23	0.033	0.036	0.061	0.020	0.085	0.091	0.100
8/31/23	0.034	0.037	0.061	0.022	0.084	0.090	0.098
9/1/23	0.035	0.038	0.062	0.023	0.085	0.090	0.098
9/2/23	0.035	0.039	0.062	0.022	0.085	0.090	0.098
9/3/23	0.036	0.040	0.063	0.021	0.086	0.091	0.098
9/4/23	0.035	0.039	0.062	0.017	0.083	0.090	0.097
9/5/23	0.033	0.038	0.061	0.016	0.079	0.089	0.096
9/6/23	0.033	0.038	0.061	0.015	0.082	0.088	0.095
9/7/23	0.032	0.037	0.061	0.014	0.084	0.088	0.094
9/8/23	0.032	0.037	0.061	0.013	0.084	0.087	0.093
9/9/23	0.032	0.037	0.060	0.012	0.084	0.087	0.092

Date	Riparian 2	Riparian 4	Riparian 6	Meadow 2	Meadow 4	Meadow 6	Meadow 8
9/10/23	0.032	0.037	0.061	0.012	0.084	0.087	0.092
9/11/23	0.032	0.038	0.061	0.011	0.083	0.087	0.092
9/12/23	0.030	0.037	0.061	0.011	0.081	0.086	0.091
9/13/23	0.030	0.037	0.061	0.013	0.080	0.086	0.091
9/14/23	0.029	0.036	0.060	0.011	0.079	0.084	0.091
9/15/23	0.029	0.036	0.059	0.011	0.079	0.083	0.091
9/16/23	0.029	0.035	0.059	0.011	0.079	0.082	0.092
9/17/23	0.029	0.036	0.060	0.011	0.078	0.081	0.093
9/18/23	0.028	0.035	0.060	0.012	0.077	0.079	0.094
9/19/23	0.027	0.034	0.059	0.010	0.076	0.077	0.094
9/20/23	0.025	0.032	0.057	0.007	0.074	0.076	0.092
9/21/23	0.025	0.032	0.057	0.010	0.074	0.074	0.090
9/22/23	0.027	0.033	0.058	0.011	0.075	0.075	0.091
9/23/23	0.026	0.033	0.057	0.010	0.073	0.074	0.090
9/24/23	0.026	0.032	0.057	0.010	0.073	0.074	0.087
9/25/23	0.047	0.035	0.059	0.115	0.072	0.075	0.088
9/26/23	0.067	0.045	0.059	0.138	0.072	0.074	0.087
9/27/23	0.098	0.064	0.059	0.160	0.073	0.075	0.088
9/28/23	0.126	0.097	0.059	0.164	0.074	0.075	0.087
9/29/23	0.130	0.104	0.058				
9/30/23	0.128	0.103	0.057				
10/1/23	0.127	0.102	0.058				
10/2/23	0.127	0.102	0.059				

Table B2. Daily Averages for other measured parameters: Evaporation, Net Solar Radiation, Soil Heat Flux and Soil Temperature

Date	Evaporation Rate <i>mm/day</i>	Net Solar Radiation <i>MJ/m²/day</i>	Soil Heat Flux Riparian <i>MJ/m²/day</i>	Soil Heat Flux Meadow <i>MJ/m²/day</i>	Riparian Soil 5 cm <i>T (°C)</i>	Riparian Soil 10 cm <i>T (°C)</i>	Meadow Soil 5 cm <i>T (°C)</i>	Meadow Soil 10 cm <i>T (°C)</i>
5/22/23		7.11	-0.296	0.320	12.8	12.8	18.3	18.0
5/23/23		7.92	0.213	0.559	12.6	12.5	17.7	17.4
5/24/23		7.48	0.858	0.786	13.4	13.3	18.3	17.9
5/25/23		8.18	0.901	0.736	14.0	13.9	18.4	18.0
5/26/23		11.13	1.288	0.968	15.1	15.0	19.3	18.8
5/27/23		8.71	0.828	0.659	15.1	15.0	19.3	18.9
5/28/23		6.73	1.048	0.965	15.2	15.1	19.8	19.3
5/29/23		6.19	0.923	0.892	15.3	15.2	20.3	19.8
5/30/23		5.62	0.404	0.653	14.5	14.5	19.8	19.4
5/31/23		7.88	-0.071	0.482	13.0	13.0	19.2	18.8
6/1/23		3.61	0.809	0.774	13.4	13.3	19.5	19.0
6/2/23		4.08	1.187	0.870	14.8	14.7	20.5	20.0
6/3/23		4.33	1.350	0.950	15.8	15.7	21.7	21.1
6/4/23		6.89	0.985	0.740	16.0	15.9	22.3	21.7
6/5/23		11.66	1.088	0.775	15.8	15.6	22.2	21.7
6/6/23		12.26	1.292	0.850	16.5	16.3	22.7	22.2
6/7/23		8.39	1.538	0.900	17.6	17.3	23.3	22.8
6/8/23		8.57	1.363	0.809	18.4	18.2	23.8	23.3
6/9/23		2.60	-0.223	-0.255	16.2	16.3	20.4	20.5
6/10/23	0.2	6.12	0.089	-0.103	14.7	14.8	17.6	17.6
6/11/23		8.07	1.504	1.066	16.2	16.1	19.7	19.2
6/12/23	0.8	13.13	2.015	1.387	19.1	18.9	23.4	22.7
6/13/23		5.28	0.452	0.401	18.1	18.0	22.5	22.2
6/14/23		9.12	-0.083	0.332	15.3	15.3	20.5	20.4
6/15/23		2.35	0.897	0.704	16.0	15.9	21.1	20.8
6/16/23	1.1	3.96	1.199	0.878	17.4	17.3	22.4	22.0
6/17/23	1.2	7.86	0.418	0.481	17.0	16.9	22.3	22.0
6/18/23	1.0	10.83	-0.015	0.370	15.2	15.1	21.0	20.8
6/19/23	0.5	11.89	0.060	0.322	14.3	14.2	19.9	19.8
6/20/23	0.7	9.07	0.277	0.126	14.7	14.6	19.5	19.4
6/21/23	0.6	3.48	0.828	0.694	15.4	15.4	20.3	19.9
6/22/23	0.5	7.30	0.659	0.588	16.0	15.9	21.2	20.9
6/23/23	0.8	7.50	0.551	0.248	15.7	15.6	20.1	19.9
6/24/23	0.6	11.84	1.022	0.666	16.9	16.7	20.7	20.3
6/25/23	1.0	12.05	1.213	0.812	18.1	17.9	21.8	21.3
6/26/23	1.0	9.63	0.626	0.303	17.9	17.7	21.6	21.3
6/27/23	0.4	13.30	1.343	1.002	18.6	18.4	21.6	21.1
6/28/23	1.1	12.33	1.230	1.033	19.4	19.1	23.3	22.7
6/29/23	0.8	15.98	1.333	1.684	20.0	19.6	26.0	25.1
6/30/23	1.2	14.19	1.271	1.004	20.7	20.2	24.7	24.2
7/1/23	1.4	13.96	0.902	0.721	20.6	20.2	24.6	24.3
7/2/23	1.3	13.74	0.920	0.822	20.4	20.0	24.7	24.3
7/3/23	1.3	13.72	0.771	0.765	19.9	19.5	24.3	24.0
7/4/23	1.0	12.86	0.865	0.756	20.1	19.8	24.7	24.3
7/5/23	0.9	11.32	0.861	0.694	20.3	19.9	24.8	24.5
7/6/23	0.8	10.78	0.960	0.690	20.4	20.1	24.8	24.4
7/7/23	0.8	13.46	1.340	0.981	21.8	21.4	26.1	25.5
7/8/23		12.66	1.113	0.823	22.2	21.8	26.7	26.2

Date	Evaporation Rate mm/day	Net Solar Radiation MJ/m ² /day	Soil Heat Flux Riparian MJ/m ² /day	Soil Heat Flux Meadow MJ/m ² /day	Riparian Soil 5 cm T (°C)	Riparian Soil 10 cm T (°C)	Meadow Soil 5 cm T (°C)	Meadow Soil 10 cm T (°C)
7/9/23	1.1	4.72	0.309	0.044	20.6	20.3	24.2	24.1
7/10/23	0.5	14.73	0.613	0.569	20.3	19.9	24.3	23.8
7/11/23	1.1	13.43	0.781	0.580	19.8	19.4	23.7	23.4
7/12/23	0.9	13.87	0.926	0.658	20.9	20.5	24.6	24.2
7/13/23	1.1	13.17	0.784	0.641	21.0	20.6	24.9	24.5
7/14/23	1.1	13.20	0.912	0.754	21.3	20.9	25.4	24.9
7/15/23	1.1	13.12	1.008	0.791	22.0	21.5	26.0	25.5
7/16/23	1.2	12.78	0.927	0.873	22.5	22.0	26.6	25.9
7/17/23	1.5	12.95	0.366	0.575	21.6	21.1	25.9	25.4
7/18/23	1.2	12.87	0.481	0.716	20.6	20.2	25.1	24.6
7/19/23	0.9	12.88	0.757	0.919	21.2	20.8	26.0	25.3
7/20/23	1.0	10.72	0.907	0.924	21.8	21.3	26.5	25.7
7/21/23	0.8	12.56	0.949	0.941	22.5	21.9	27.0	26.1
7/22/23	1.6	12.56	0.733	0.793	22.1	21.5	26.4	25.7
7/23/23	1.3	12.05	0.763	0.877	22.0	21.4	26.6	25.7
7/24/23	1.2	5.96	-0.075	0.103	20.3	20.0	24.4	24.2
7/25/23	0.5	12.46	0.364	0.552	19.9	19.6	24.1	23.5
7/26/23	1.0	12.52	0.321	0.623	19.4	19.0	24.0	23.4
7/27/23	1.0	12.17	0.538	0.789	20.1	19.7	25.1	24.2
7/28/23	1.1	11.80	0.576	0.815	20.4	19.9	25.5	24.6
7/29/23	0.9	12.18	0.520	0.751	20.5	20.0	25.6	24.8
7/30/23	1.2	12.44	0.481	0.705	20.7	20.2	25.8	25.0
7/31/23	1.0	12.11	0.229	0.599	19.7	19.4	24.8	24.1
8/1/23	1.0	9.39	0.249	0.648	19.6	19.4	24.8	24.1
8/2/23	1.0	9.29	0.368	0.643	20.0	19.8	24.9	24.1
8/3/23	1.2	9.28	0.590	0.768	20.9	20.5	25.4	24.5
8/4/23	1.4	6.22	0.464	0.606	20.9	20.5	25.3	24.6
8/5/23	0.8	2.24	-0.070	-0.034	19.8	19.4	23.0	22.8
8/6/23	0.1	9.42	0.828	0.727	20.6	20.3	23.8	22.9
8/7/23	1.2	6.42	0.532	0.509	21.6	21.2	24.5	23.8
8/8/23	1.1	8.64	0.578	0.780	21.5	21.0	24.9	24.0
8/9/23	0.9	9.27	0.519	0.730	21.8	21.3	25.8	24.9
8/10/23	1.2	8.52	0.241	0.577	21.0	20.5	25.2	24.5
8/11/23	1.0	9.70	0.292	0.562	20.6	20.1	24.7	24.0
8/12/23	0.9	11.13	0.725	0.830	21.8	21.3	25.9	24.9
8/13/23	1.5	11.22	0.627	0.880	22.1	21.6	26.5	25.5
8/14/23	0.9	11.38	0.722	0.952	22.7	22.2	27.3	26.2
8/15/23	1.0	11.06	0.922	1.015	23.7	23.2	28.4	27.1
8/16/23	1.3	10.96	1.033	1.026	24.6	24.0	28.9	27.7
8/17/23	1.4	7.96	0.516	0.567	23.5	23.0	27.6	26.8
8/18/23	1.0	10.63	0.189	0.451	22.4	21.9	26.6	26.0
8/19/23	1.5	7.28	-0.303	0.488	19.9	19.6	26.8	25.9
8/20/23	0.7	8.38	-0.143	0.231	18.9	18.6	21.8	21.5
8/21/23	0.6	11.02	-0.027	0.502	18.4	18.3	22.5	21.8
8/22/23	0.4	9.98	0.043	0.632	18.6	18.3	23.8	23.0
8/23/23	0.9	9.93	-0.415	0.675	19.0	18.6	24.5	23.7
8/24/23	0.6	7.34	0.197	-0.140	18.6	18.4	21.9	21.9
8/25/23	0.6	10.12	0.309	0.045	18.8	18.6	20.5	20.4
8/26/23	0.3	5.92	0.478	0.073	19.9	19.7	20.3	20.2
8/27/23	0.7	8.13	0.508	0.280	20.7	20.5	20.9	20.5

Date	Evaporation Rate <i>mm/day</i>	Net Solar Radiation <i>MJ/m²/day</i>	Soil Heat Flux Riparian <i>MJ/m²/day</i>	Soil Heat Flux Meadow <i>MJ/m²/day</i>	Riparian Soil 5 cm <i>T (°C)</i>	Riparian Soil 10 cm <i>T (°C)</i>	Meadow Soil 5 cm <i>T (°C)</i>	Meadow Soil 10 cm <i>T (°C)</i>
8/28/23	0.6	8.79	-0.551	0.437	18.6	18.4	21.5	21.0
8/29/23	0.6	7.59	-0.194	0.409	17.4	17.1	22.4	21.8
8/30/23	0.3	8.29	-0.089	0.160	17.4	17.2	21.0	20.7
8/31/23	0.7	8.30	0.233	0.247	17.9	17.6	20.4	20.1
9/1/23	0.4	8.62	0.196	0.287	18.1	17.6	20.4	20.1
9/2/23	0.6	7.79	0.175	0.326	18.7	18.3	20.4	20.0
9/3/23	0.3	8.04	-0.333	0.344	17.3	16.9	20.7	20.3
9/4/23	0.6	8.03	-0.283	0.369	16.4	15.9	20.6	20.2
9/5/23	0.7	7.02	-0.080	0.379	16.4	16.0	20.9	20.4
9/6/23	0.6	4.89	-0.052	0.185	16.3	16.0	20.5	20.2
9/7/23	0.9	5.52	-0.178	0.181	16.2	15.8	19.8	19.5
9/8/23	0.5	7.42	-0.072	0.393	15.9	15.5	20.4	19.9
9/9/23	0.4	7.66	0.161	0.247	16.5	16.1	19.7	19.4
9/10/23	0.5	7.73	0.247	0.298	17.2	16.9	19.7	19.3
9/11/23	0.4	7.09	-0.008	0.301	16.7	16.4	19.7	19.4
9/12/23	0.6	3.65	0.073	0.004	16.7	16.3	18.9	18.9
9/13/23	0.5	7.14	-0.187	0.198	15.8	15.4	19.0	18.8
9/14/23	0.7	6.68	-0.077	0.100	15.5	15.2	18.0	17.9
9/15/23	0.4	2.07	-0.003	-0.574	15.6	15.3	14.7	15.4
9/16/23	0.4	6.96	0.070	0.228	16.0	15.8	15.6	15.4
9/17/23	0.2	4.81	-0.111	0.102	15.8	15.5	17.0	16.9
9/18/23	0.4	3.57	-0.211	-0.103	14.6	14.3	15.3	15.5
9/19/23	0.6	2.81	-0.769	-0.136	12.8	12.6	15.1	15.2
9/20/23	0.5	2.24	-0.113		12.9	12.6	0.076	0.092
9/21/23	0.2	4.50	-0.033		14.1	13.9	0.074	0.090
9/22/23	0.2	3.48	-0.215		13.3	13.2	0.075	0.091
9/23/23	0.4	2.19	-0.317		13.1	13.0	0.074	0.090
9/24/23	0.3	1.95	-0.212		13.5	13.4	0.074	0.087
9/25/23		1.34	-0.416		12.9	12.8	0.075	0.088
9/26/23		2.43	-0.818		11.5	11.6	0.074	0.087
9/27/23		1.89	-0.807		10.5	10.5	0.075	0.088
9/28/23		2.91	-0.854		9.8	9.8	0.075	0.087
9/29/23		2.93	-0.767		9.1	9.0		
9/30/23	0.3	4.31	-0.552		9.2	9.0		
10/1/23	0.4	4.26	0.031		10.7	10.6		
10/2/23	0.3	1.50	-0.146		11.1	11.1		
10/3/23	0.1	4.08	-0.009					

Table B3. Weather Data from Thorp Weather Station (AgWeatherNet, 2023)

Date	Min T °C	Max T °C	Mean T °C	Ave. Relative Humidity at 2 m %	Ave. Wind Speed at 2 m m/s	Daily Precipitation mm	Net Solar Radiation MJ/m ² /day
5/22/23	7.8	15.3	11.6	59.2	8.2	0	28.9
5/23/23	6.8	19.4	13.1	57.3	8.0	0	25.9
5/24/23	9.4	22.2	15.8	54.9	5.0	0	25.8
5/25/23	8.3	22.1	15.2	61.4	4.3	0	22.0
5/26/23	9.1	23.8	16.4	63.2	2.9	0	21.8
5/27/23	12.7	24.6	18.6	51.8	2.8	0	25.0
5/28/23	12.0	24.8	18.4	50.6	4.9	0	28.5
5/29/23	12.1	25.4	18.8	46.6	6.6	0	29.3
5/30/23	10.4	21.7	16.0	45.2	7.5	0	26.6
5/31/23	9.4	17.8	13.6	44.8	8.6	0	29.4
6/1/23	7.4	22.4	14.9	44.3	9.4	0	28.7
6/2/23	9.9	25.3	17.6	46	5.0	0	29.4
6/3/23	11.1	27.6	19.3	37.3	5.0	0	29.7
6/4/23	12.1	24.2	18.2	41	5.1	0	29.9
6/5/23	11.1	27.7	19.4	32.1	8.0	0	31.1
6/6/23	9.1	29.7	19.4	38	7.2	0	30.1
6/7/23	11.8	31.9	21.8	37.9	2.9	0	25.1
6/8/23	17.2	29.4	23.3	41.7	3.3	0	16.5
6/9/23	12.6	17.1	14.8	79.7	5.2	0.8	6.6
6/10/23	10.9	17.6	14.3	72	6.1	4.1	12.9
6/11/23	11.3	27.7	19.5	60.1	6.3	0	28.6
6/12/23	14.2	30.4	22.3	53.3	4.4	0	29.4
6/13/23	11.3	24.3	17.8	52.7	4.8	0	25.5
6/14/23	7.6	17.1	12.4	53.6	8.4	0	30.2
6/15/23	9.7	23.1	16.4	47.6	9.0	0	28.0
6/16/23	13.4	24.9	19.1	52.7	6.4	0	21.8
6/17/23	8.4	19.0	13.7	55.9	6.6	0	27.4
6/18/23	6.9	14.9	10.9	55.6	7.3	0	31.1
6/19/23	6.0	14.9	10.4	57.1	8.0	0	29.6
6/20/23	8.5	14.7	11.6	63.8	7.7	0	18.0
6/21/23	9.2	21.4	15.3	55.7	5.7	0	27.4
6/22/23	9.2	23.7	16.5	58.8	3.5	0	27.1
6/23/23	8.4	25.6	17.0	55.5	3.3	0	20.5
6/24/23	13.0	25.3	19.2	47.4	3.7	0	28.3
6/25/23	11.8	27.8	19.8	47.7	4.5	0	25.6
6/26/23	15.3	26.8	21.1	52.9	4.4	0	28.5
6/27/23	15.2	28.1	21.6	55.3	5.0	0	26.4
6/28/23	15.2	29.7	22.4	53.7	5.3	0	27.2
6/29/23	15.4	29.3	22.4	46.2	4.0	0	29.1
6/30/23	16.7	29.5	23.1	44.5	5.5	0	29.7
7/1/23	16.3	24.8	20.6	43.6	6.8	0	30.1
7/2/23	14.6	27.7	21.2	35.1	6.9	0	30.1
7/3/23	11.0	28.9	20.0	32.7	4.6	0	29.7
7/4/23	12.7	30.1	21.4	39.6	3.1	0	27.7
7/5/23	13.3	29.6	21.4	42.1	3.0	0	25.0
7/6/23	14.8	31.6	23.2	42.1	2.7	0	26.0
7/7/23	16.1	32.1	24.1	46.4	2.9	0	27.9

Date	Min T °C	Max T °C	Mean T °C	Ave. Relative Humidity at 2 m %	Ave. Wind Speed at 2 m m/s	Daily Precipitation mm	Net Solar Radiation MJ/m ² /day
7/8/23	16.6	32.8	24.7	49.0	3.6	0	28.0
7/9/23	17.2	26.8	22.0	55.4	4.9	0	16.0
7/10/23	14.6	23.7	19.1	57.9	5.9	2.3	26.7
7/11/23	13.6	25.8	19.7	54.9	6.3	0	28.7
7/12/23	15.3	27.9	21.6	50.3	6.3	0	27.1
7/13/23	14.9	27.8	21.3	45.7	7.2	0	29.1
7/14/23	15.8	31.6	23.7	41.9	6.4	0	28.6
7/15/23	15.5	34.3	24.9	34.1	4.6	0	28.7
7/16/23	17.9	32.7	25.3	36.8	4.4	0	28.7
7/17/23	15.0	21.8	18.4	50.6	6.4	0	28.9
7/18/23	12.2	27.9	20.1	46.8	8.5	0	28.8
7/19/23	13.7	31.3	22.5	45.0	3.3	0	28.3
7/20/23	16.0	34.2	25.1	42.9	3.0	0	24.6
7/21/23	18.7	30.4	24.6	39.9	4.0	0	28.1
7/22/23	16.4	29.2	22.8	43.3	7.2	0	27.9
7/23/23	14.6	31.8	23.2	46.0	6.1	0	28.3
7/24/23	14.8	23.6	19.2	57.2	4.8	0	20.1
7/25/23	13.4	21.6	17.5	56	5.9	0	23.4
7/26/23	10.8	26.1	18.4	49.6	6.1	0	27.5
7/27/23	14.0	27.7	20.9	47.4	4.1	0	26.9
7/28/23	14.3	29.3	21.8	47.9	5.1	0	26.8
7/29/23	15.6	27.9	21.8	50.0	4.1	0	26.9
7/30/23	14.7	24.1	19.4	49.5	6.0	0	26.0
7/31/23	11.8	27.1	19.4	45.4	7.4	0	27.4
8/1/23	12.8	29.2	21.0	38.3	5.5	0	27.5
8/2/23	13.6	29.3	21.4	37.7	4.8	0	27.2
8/3/23	16.2	30.0	23.1	39.0	5.8	0	26.6
8/4/23	17.2	28.8	23.0	38.1	6.1	0	18.7
8/5/23	17.1	21.8	19.5	66.5	4.6	0.5	5.2
8/6/23	15.6	27.8	21.7	62.9	4.7	0	19.2
8/7/23	17.3	25.8	21.5	56.7	4.4	0	17.8
8/8/23	15.9	28.3	22.1	54.7	4.8	0	24.2
8/9/23	16.6	24.0	20.3	57.2	4.2	0	21.9
8/10/23	13.8	23.8	18.8	53.2	6.1	0	25.7
8/11/23	13.9	25.9	19.9	47.7	6.2	0	26.0
8/12/23	17.1	29.0	23.0	44.4	6.7	0	24.3
8/13/23	14.9	31.6	23.3	49.4	6.3	0	24.6
8/14/23	16.6	34.4	25.5	44.6	3.1	0	24.5
8/15/23	18.8	38.4	28.6	41.6	2.8	0	23.9
8/16/23	23.5	37.2	30.4	30.7	4.2	0	24.3
8/17/23	18.8	33.9	26.4	37.8	4.9	0	16.2
8/18/23	15.6	26.7	21.1	33.1	5.8	0	25.0
8/19/23	10.4	25.2	17.8	45.5	7.0	0	18.6
8/20/23	9.2	25.7	17.5	43	3.0	0	17.9
8/21/23	11.2	25.3	18.3	48.6	2.6	0	13.2
8/22/23	12.2	22.8	17.5	50.0	3.6	0	21.7
8/23/23	9.6	21.2	15.4	56.8	6.3	0	20.4
8/24/23	8.9	25.6	17.2	55.1	4.6	0	21.4

Date	Min T °C	Max T °C	Mean T °C	Ave. Relative Humidity at 2 m %	Ave. Wind Speed at 2 m m/s	Daily Precipitation mm	Net Solar Radiation MJ/m ² /day
8/25/23	13.2	25.9	19.6	55.3	2.9	0.5	15.5
8/26/23	13.1	29.9	21.5	50.9	2.7	0	22.7
8/27/23	14.8	33.2	24.0	45.0	3.0	0	21.7
8/28/23	16.4	33.6	25.0	50.1	3.2	0	21.6
8/29/23	14.6	20.8	17.7	62.5	4.5	0	15.5
8/30/23	13.8	20.2	17.0	61.2	10.4	0	21.1
8/31/23	11.6	20.1	15.8	68.9	7.5	0	14.1
9/1/23	12.9	24.4	18.7	65.9	2.4	0	17.6
9/2/23	11.9	28.4	20.2	57.3	2.4	0	19.4
9/3/23	14.3	24.4	19.4	56.7	2.6	0	15.4
9/4/23	9.9	19.9	14.9	58.4	6.8	0	20.5
9/5/23	9.2	21.7	15.5	58.2	6.8	0	20.9
9/6/23	11.3	23.6	17.4	52.9	4.7	0	18.1
9/7/23	10.3	23.0	16.6	57.9	5.0	0	19.0
9/8/23	11.5	25.4	18.5	54.7	3.8	0	20.4
9/9/23	8.0	27.1	17.5	53.2	3.7	0	19.9
9/10/23	11.1	28.6	19.8	47.2	2.7	0	17.2
9/11/23	15.2	23.1	19.1	54.6	3.4	0	11.8
9/12/23	13.5	22.8	18.2	59.0	6.4	0	14.7
9/13/23	13.3	24.0	18.6	53.8	6.2	0	19.5
9/14/23	8.3	26.4	17.4	57.3	5.4	0	19.3
9/15/23	8.2	28.3	18.2	49.7	2.6	0	19.2
9/16/23	9.1	29.8	19.4	47.8	2.3	0	17.7
9/17/23	14.6	21.1	17.8	46.7	2.6	0	12.4
9/18/23	10.1	16.3	13.2	54.6	5.2	0	18.4
9/19/23	8.4	17.9	13.1	53.3	6.9	0	14.4
9/20/23	7.8	15.1	11.4	66.9	5.8	0	8.5
9/21/23	6.2	20.7	13.4	58.5	4.6	0	17.0
9/22/23	8.1	20.9	14.5	59.8	3.0	0	13.1
9/23/23	7.0	17.4	12.2	65.0	2.5	0	8.3
9/24/23	6.2	15.6	10.9	77.4	2.5	1.3	7.3
9/25/23	10.7	16.2	13.5	82.7	2.0	7.6	5.1
9/26/23	7.3	16.3	11.8	78.7	2.1	1.3	9.2
9/27/23	6.1	12.7	9.4	86.7	2.1	2.3	7.1
9/28/23	5.7	13.3	9.5	74.5	2.2	0	11.0
9/29/23	3.2	14.0	8.6	76.4	3.1	0	11.1
9/30/23	2.2	17.3	9.8	67.7	2.3	0	16.3
10/1/23	4.2	19.8	12.0	61.7	4.2	0	16.1
10/2/23	8.9	15.8	12.4	68.3	4.2	0	5.7
10/3/23	11.5	18.1	14.8	63.9	3.8	0	15.4

Table B4. Stable Isotope Data for Taneum Creek Study

Date	main channel $\delta^{18}\text{O}$	main channel δD	side channel $\delta^{18}\text{O}$	side channel δD	beaver pond 1 $\delta^{18}\text{O}$	beaver pond 1 δD	beaver pond 2 $\delta^{18}\text{O}$	beaver pond 2 δD	beaver pond 3 $\delta^{18}\text{O}$	beaver pond 3 δD	beaver pond 4 $\delta^{18}\text{O}$	beaver pond 4 δD	evap pan $\delta^{18}\text{O}$	evap pan δD
8/11/22	-14.48	-106.5	-14.47	-106.4	-14.45	-106.4	-14.41	-106.1					-14.42	-106.2
8/19/22	-14.50	-106.7	-14.49	-106.5	-14.52	-106.7	-14.47	-106.5					-11.60	-94.4
8/23/22	-14.40	-106.3	-14.44	-106.4	-14.37	-106.2	-14.32	-105.9					-9.84	-87.5
9/3/22	-14.38	-106.3	-14.41	-106.4	-14.39	-106.2	-14.27	-105.6					-8.57	-81.2
9/13/22	-14.44	-106.8	-14.45	-106.8	-14.41	-106.4	-14.27	-105.8					-6.80	-73.1
9/26/22	-14.47	-106.9	-14.45	-106.9	-14.45	-106.6	-14.34	-106.2					-5.50	-65.7
10/3/22	-14.53	-107.3	-14.48	-107.2	-14.47	-106.9	-14.36	-106.4					-4.99	-62.9
10/20/22	-14.56	-108.1												
11/21/22	-14.81	-109.5	-14.65	-108.9	-14.74	-108.08	-11.90	-91.6						
3/1/23	-14.93	-110.2	-14.94	-110.1	-14.92	-109.87	-15.07	-111.0						
3/29/23	-14.90	-109.8	-14.98	-110.8	-14.91	-112.15	-14.98	-110.9						
4/12/23	-15.27	-113.0	-15.23	-112.9	-15.29	-113.56	-15.17	-112.6						
5/16/23	-15.03	-109.6	-15.47	-114.3	-15.45	-114.97	-15.48	-114.3	-15.09	-110.8	-15.15	-111.1		
5/22/23	-14.98	-109.5	-15.13	-111.4	-15.14	-111.20	-14.94	-110.0	-14.80	-108.7	-14.83	-108.6		
5/31/23	-14.73	-108.7	-14.94	-108.6	-14.91	-109.20	-14.89	-109.4	-14.82	-109.0	-14.83	-109.1	-12.61	-99.4
6/4/23	-14.83	-108.6	-14.90	-109.2	-14.90	-109.31	-14.81	-109.2					-10.97	-93.0
6/7/23													-9.63	-88.5
6/14/23	-14.75	-109.1	-14.87	-109.3	-14.69	-108.07	-14.65	-108.4	-14.69	-108.4	-14.63	-106.7	-8.31	-80.2
6/16/23	-14.67	-106.7	-14.75	-108.3	-14.72	-107.99	-14.45	-107.9	-14.73	-108.7	-14.66	-108.5	-8.53	-81.1
6/21/23	-14.85	-107.7	-14.86	-109.2									-7.28	-75.4
6/28/23	-14.86	-108.8	-14.92	-108.9	-14.86	-108.72	-14.58	-107.7	-14.66	-107.9	-14.78	-108.4	-6.23	-71.1